Optimization and Control of Water Conveyance/Storage Systems

1998

Koichi Unami

Optimization and Control of Water Conveyance/Storage Systems

1998

Koichi Unami

Contents

Notations

The following symbols are used in this thesis.

A = cross-sectional area
$\mathbf{A}$ = discretized vector for A
$\hat{A}$ = state matrix in controller K_R
A_X = $A_0 + B_2F$
A_Y = $A_0 + LC_2$
A_0 = state matrix in generalized plant
a = opening area of gate
a_i = $i-$th decay coefficient
B = incidence matrix
$\hat{B}$ = control distribution matrix in controller K_R
B_F = stabilizing matrix for B
B_1 = disturbance distribution matrix in generalized plant
B_2 = control distribution matrix in generalized plant
b = algebraic equation to prescribe the boundary condition
$\tilde{b}$ = specified boundary value
C = solute concentration
$\mathcal{C}$ = spatial position of channel bed
$\hat{C}$ = observation output matrix in controller K_R
C_A = constant in convergence condition of the Newton-Raphson method
C_B = constant in convergence condition of the Newton-Raphson method
C_C = constant in convergence condition of the Newton-Raphson method
C_d = discharge coefficient
C_h = numerical solution to solute transport equation
C_I = interpolated C
C_q = solute concentration which q has
C_0 = constant in convergence condition of the Newton-Raphson method
C_1 = error output matrix in generalized plant
C_0^∞ = function space

C_2 = observation output matrix in generalized plant
c = dissipation parameter
c_k = constant in the 4-point Gauss quadrature rule
D = the diffusion tensor
$\mathcal{D}$ = wetted part of cross-section
$\mathtt{D}$ = determinant
D_x = dispersion coefficient
d = stochastic component of virtual inflow discharge
$\mathbf{d}$ = the drift vector
d_i = $i-$th component of $\mathbf{d}$
d_{ij} = $ij-$component of D
diag = diagonal matrix
E = left hand side of the first algebraic Riccati inequality
$\mathbf{e}$ = unitary vector to prescribe boundary condition
$\mathbf{e}^{\perp}$ = unitary vector perpendicular to $\mathbf{e}$
F = stabilizing matrix for B_2
$\mathbf{F}$ = flux vector
F_M = flux of momentum
$\mathbf{f}$ = friction force
$\boldsymbol{f}$ = nonlinear function vector
f_i = component of load vector
G = generator
$\mathcal{G}$ = any subset of $\mathbb{R}^{N_N}$
G_a = allowable storage domain
G_{ij} = matrix of compatible dimension
G_s = allowable surface profile domain
G_0 = nominal generator
g = gravitational acceleration
$\mathbf{H}$ = transformed coordinate system
H^1 = Sobolev space
H_0^1 = completion of C_0^∞ in H^1
h = water depth
$\mathbf{h}$ = discretized vector for h and also stochastic variable in Markov process model
$\mathbf{h}_0$ = steady surface profile
$\mathbf{h}^+$ = $\mathbf{h}$ at t^+
h_i = $i-$th component of $\mathbf{h}$ which is equal to $i-$th nodal value of h
h_d = water depth at the downstream node

h_i^l = nodal values of h at x_i^l

h_i^r = nodal values of h at x_i^r

h_u = water depth at the upstream node

$h_{0_i}^k$ = $i-$th component of $\mathbf{h}$ deviated from $\mathbf{h}_0$ under the $k-$th stochastic event

I = n_s-dimensional unit matrix

I_n = n-dimensional unit matrix

$J(\mathbf{u})$ = functional to be minimized

$J_R(u)$ = functional to be maximized

J_S = reliability of surface profile

J_S^* = lower bound of J_S

K_C = anti wind-up controller

K_G = feed-forward controller

K_R = feed-back controller

k_i = $i-$th load coefficient

L = detecting matrix for C_2

l_i = lower bound of interval

$M = 1 + \frac{1}{\hat{\lambda}} \left(\int_\Omega \left(\frac{Q}{AD_x} \right)^2 dx \right)^{\frac{1}{2}}$

M_s = number of elements of Λ_s

M_q = number of turnouts

$\mathbf{M}$ = mass vector of discretized continuity equations

m_s = number of control structures

N_E = number of elements

N_N = number of nodes

N_B = number of boundary nodes

$\mathbf{n}$ = Manning's roughness coefficient

$\mathbf{n}$ = outward unit normal vector

n_s = number of pools

o = infinitesimal

P = transition probability

$\mathcal{P}$ = boundary of $\mathcal{D}$

Pe_i = local Peclet number

p = probability density function

$\mathbf{p}$ = pressure

Q = discharge

$\mathbf{Q}$ = discretized vector for Q

$Q^{(k)}$ = transformation matrix in Householder tridiagonalization

Q_i = $i-$th component of $\mathbf{Q}$ which is equal to $i-$th elemental value of Q
$\tilde{\mathbf{Q}}$ = extended $\mathbf{Q}$
q = unit-width lateral discharge
$\mathbf{q}$ = discretized vector for q
$\boldsymbol{q}$ = external disturbance vector
q_j = lateral discharge at $j-$th turnout
R = hydraulic radius
$\mathbb{R}^n$ = $n-$dimensional real Euclidean space
r = radius in the polar coordinate system
r_i = upper bound of interval
r_0 = divergence free part of $\dfrac{Q}{AD_x}$
r_1 = divergence part of $\dfrac{Q}{AD_x}$
$\boldsymbol{r}$ = reference vector
S = symmetric matrix
$S^{(k)}$ = transformed matrix in Householder tridiagonalization
S_f = friction slope
S_M = source of momentum
$\mathbf{S}$ = source vector
$\mathcal{S}$ = boundary of $\mathcal{V}$
s = frequency
$s_{i,j}$ = ij component of S
$\mathbf{s}_k$ = vector in Householder tridiagonalization
T = terminal time
T_e = examination period
t = time
t_f = specified final time
t_i = specified initial time
t_{ij} = $ij-$component of transformation matrix
$t_{i,j}$ = time at the $j-$th stage of the $i-$th series of data
t^+ = time which is greater than t
$\mathbf{U}$ = conserved vector
U_{ad} = set of admissible control
U_k = orthogonal matrix
u = deterministic component of virtual inflow discharge
$\mathbf{u}$ = control variable
$\boldsymbol{u}$ = control variable vector

$\mathbf{u}_{ad}$ = admissible control variable
$\mathbf{u}^{\epsilon}$ = perturbed control variable
$\boldsymbol{u}_1$ = nominal control variable vector
$\mathcal{V}$ = test domain
V_h = finite dimensional space of piecewise linear functions
$\mathbf{v}$ = absolute velocity of water
$\mathbf{v}_i^{(k)}$ = estimate of eigenvector
$\mathbf{v}_s$ = proper velocity of $\mathcal{S}$
W = contribution factor
W_D = orthogonal matrix
W_1 = the first row of W
W_2 = the second rows of W
$\boldsymbol{w}_1$ = first block of input disturbance vector
$\boldsymbol{w}_2$ = second block of input disturbance vector
$\boldsymbol{w}_3$ = third block of input disturbance vector
w_k = constant in the 4-point Gauss quadrature rule
w_i^y = $i-$th constant weight to scale $\boldsymbol{y}$ as $\boldsymbol{z}_3$
X = storage
$\mathbf{X}$ = state variable vector
X_c = current storage
X_h = finite dimensional space of piecewise constant functions
$X_{i,j}$ = X at $t_{i,j}$
$X_{\max}$ = allowable maximum storage
$X_{\min}$ = allowable minimum storage
X_∞ = solution to the first algebraic Riccati inequality
x = local curvilinear abscissa
$\mathbf{x}$ = the tangential vector of $\mathcal{C}$ in $\mathbb{R}^3$
$\boldsymbol{x}$ = unknown independent variable vector
x_i^l = inferior of Ω_i^e
x_i^r = superior of Ω_i^e
x_q = the spatial point on which the turnout T-5 is located
$\boldsymbol{x}^{(k)}$ = $k-$th approximation to $\boldsymbol{x}$
x_1 = upper bound of $\mathcal{V}$ on x
x_2 = lower bounds of $\mathcal{V}$ on x
Y_∞ = solution to the second algebraic Riccati inequality
y = reservoir reliability
$\mathbf{y}$ = state variable

$\boldsymbol{y}$ = observation output vector
$\mathbf{y}_T$ = targeted value of $\mathbf{y}$ in a steady state
$\mathbf{y}_0$ = specified initial value of $\mathbf{y}$
$\bar{y}$ = targeted value of $\mathbf{e}^{\perp} \cdot \mathbf{y}$
$\bar{\mathbf{y}}$ = targeted value of $\mathbf{y}$
z = vertical axis
$\mathbf{z}$ = vertical upward unit vector
z_b = elevation of channel bed
$\boldsymbol{z}_1$ = first block of error signal vector
$\boldsymbol{z}_2$ = second block of error signal vector
$\boldsymbol{z}_3$ = third block of error signal vector
α = velocity-distribution coefficient
α_k = scalar in Householder tridiagonalization
α_q = relaxation parameter
β = bilinear form
β' = normalized bilinear form
β_i = non-diagonal component of tridiagonal matrix
β^e_{ik} = contribution from $\Omega_{\kappa_{ik}}$ to $i-$th node
Γ = boundary of Ω
$\mathit{\Gamma}$ = gamma function
Γ_1 = first boundary of WB model
Γ_2 = second boundary of WB model
Δ^a_i = deviation parameter for a_i
$\Delta^{\mathbf{H}}$ = Laplace operator in the $\mathbf{H}-$coordinate system
$\Delta\mathbf{h}^a$ = allowable deviation vector
Δh^a_i = $i-$th component of $\Delta\mathbf{h}^a$
Δ^k_i = deviation parameter for k_i
Δq_j = absolute value of deviation of q_j
Δt = temporal integration interval
Δt_0 = time increment
Δ^u_i = deviation parameter for the $i-$th component of $\boldsymbol{u}$
Δx_i = measure of Ω^e_i
$\Delta\eta$ = difference between the water levels that bounds gate
$\hat{\delta}$ = Dirac's delta function
δ_i = diagonal component of tridiagonal matrix
δJ_B = contribution of $\mathbf{u}$ on the boundary to $\delta J(\mathbf{u})$
δJ_D = contribution of $\mathbf{u}$ in the domain to $\delta J(\mathbf{u})$

δJ_I = contribution of $\mathbf{u}$ at the initial time to $\delta J(\mathbf{u})$

$\mathcal{J}_k$ = Jacobian matrix

δJ_T = contribution of $\mathbf{y}$ at the terminal time to $\delta J(\mathbf{u})$

δJ_Γ = contribution of $\mathbf{y}$ on the boundary to $\delta J(\mathbf{u})$

δJ_Ω = contribution of $\mathbf{y}$ in the domain to $\delta J(\mathbf{u})$

ϵ_j = $C - C_h$ at $j-$th node

ε = positive real number

η = elevation of water surface

η_u = elevation of upstream water surface

η_d = elevation of downstream water surface

Θ = implicit parameter

θ_d = linkage parameter

θ_{ij}^r = angle between Ω_i^e and $\Omega_{\kappa_{ij}^r}^e$

θ_{ij}^l = angle between Ω_i^e and $\Omega_{\kappa_{ij}^l}^e$

θ_s = submergency

θ_w = down-windiness

κ_{ij} = element number of $j-$th element connected to the $i-$th node

κ_{ij}^l = element number of the $j-$th element connected to x_i^l

κ_{ij}^r = element number of the $j-$th element connected to x_i^r

$\Lambda_k(\lambda')$ = diagonal matrix for λ'

Λ_s = set of indices i and j

λ = adjoint variable for the FPPDE

$\boldsymbol{\lambda}$ = adjoint variable for open channel unsteady flow equations

λ' = any real number

$\hat{\lambda}$ = $\inf_{\psi \in H_0^1, \psi \neq 0} \frac{\|\psi\|_V}{\left(\int_\Omega \psi^2 dx\right)^{\frac{1}{2}}}$

λ_i^D = $i-$th eigenvalue of D

λ_1 = the first component of $\boldsymbol{\lambda}$

λ_2 = the second component of $\boldsymbol{\lambda}$

λ_{2i} = λ_2 value in Ω_i^e

λ_{2i}^l = estimated value of λ_2 at x_i^l

λ_{2i}^r = estimated value of λ_2 at x_i^r

μ = $1 - \frac{1}{\hat{\lambda}} \left(\int_\Omega r_1^2 dx\right)^{\frac{1}{2}}$

ν_i = number of elements connected to the $i-$th node

ν_i^l = the number of elements connected to x_i^l

ν_i^r = the number of elements connected to x_i^r

$\boldsymbol{\Xi}$ = vector function of $\mathbf{h}$ and $\tilde{\mathbf{Q}}$

ϖ = probability density function for reservoir reliability
ρ = density of water
ϱ = positive real number
σ_k = scalar in Householder tridiagonalization
τ = scaled time
Φ = unknown vector in the heat equation
$\mathbf{\Phi}$ = load vector
ϕ_i = Sturm sequence
φ = source term due to friction force which a hydraulic structure causes
$\mathbf{\Psi}$ = vector function of $\mathbf{h}$ and $\tilde{\mathbf{Q}}$
ψ = weighting function
ψ_i^C = weighting function for solute transport equation
ψ_i^V = i-th basis of V_h
ψ_i^X = i-th basis of X_h
Ω = domain
Ω_i^e = i-th element
Ω_0 = any domain which contains the origin
$\mathbf{0}$ = null vector

Prefix

δ = right hand derivative with respect to ε

Superscript

ε = value when $\mathbf{u}^\varepsilon$ is chosen as the control variable

Subscripts

$+$ = time after Δt
$*$ = time between t and t^+

List of Tables

List of Figures

Acknowledgments

The author would like to acknowledge with deep gratitude the considerable guidance he has received from Dr. Toshihiko Kawachi, Professor of Water Resources Engineering, Graduate School of Agricultural Science, Kyoto University, in the preparation of this dissertation.

Also much appreciated are the helpful comments received from the members of his Dissertation Committee, Professor Dr. Shigeyasu Aoyama and Professor Dr. Toru Mitsuno.

The author is much indebted to his earlier supervisors the late Professor Dr. Isao Minami and Professor Dr. Takashi Hasegawa.

Thanks are due to the co-researchers, Associate Professor Dr. Hiroshi Itagaki at Gifu University, Associate Professor Hiroshi Okumura at Kinki University, Associate Professor Takeo Maruyama at Mukogawa Women's University, Dr. Macarius Yangyuoru at Ghana University, Instructor Ken Hiramatsu at Kyoto University, Mr. Muhammad Munir Babar at Kyoto University, Mr. Ken-ichi Kawakatsu at the Osaka Prefectural Government, and Mr. Shigeki Nakanishi at the Ministry of Agriculture, Forestry and Fishery. The author also extends his thanks to all the members of Water Resources Engineering Laboratory including Dr. Hantae Kim, Mr. Muhammad Abul Fazal, the former and the current students, and the secretary Mrs. Yukiko Oki.

The author is grateful to the Yasugawa land improvement association and the Chu-Shikou Regional Agricultural Administration Office for providing the data.

Chapter 1

Introduction

1.1 Background

Water resources engineering plays a significant role in achieving prosperity of human society. Flood mitigation, land drainage, sewerage, are necessary means to protect life and property from being damaged. Irrigation technologies, from simple water harvesting to modern piped distribution system, make a major contribution to food production, establishing sustainable use of limited fresh water resources. Hydroelectric-power and navigation are examples of the utilization of water for beneficial purposes. However, even if infrastructures such as dams, canals, and hydroelectric plants are complete, mismanagement of them may cause serious disaster. Importance of systematic management of water resources is now increasing with the rapid development of human activities.

Recent drastic advance in information technology enables theoretical and practical approach to management of stock and flow of water. Hydraulic and hydrological investigation of phenomena on a mathematical basis is materialized with the help of a computer. It is remarked that there are two aspects in the computer-aided water resources engineering; one is "modeling", and the other one is "controlling".

Modeling problems in water resources engineering include hydrodynamical modeling of water in motion, statistical modeling of water under uncertainty, and then numerical modeling of these mathematical models. Since water is regarded as continuous medium, a mathematical model is described in terms of partial differential equations (PDEs). A hydrodynamical model may comprise equations of continuity and motion such as Euler's equations, whereas a statistical model may be given as a Fokker-Planck partial differential equation (FPPDE) which represents a Markov process (Ito [37]). Such PDEs require accompanying algebraic equations to represent initial conditions, and external and/or internal boundary conditions so as to constitute a complete system. Then, the system represents a water resources system in a mathematical sense. An approximate solution

to the PDEs with the algebraic equations is obtained using a numerical model that is implemented in a computer. A numerical model discretizes unknown functions or function spaces for unknowns into finite dimensional ones. Stability and accuracy of the numerical model depend on the discretization scheme, which should be suitable for the nature of the PDEs to be solved. Discretized PDEs turn algebraic equations which may be nonlinear. Nonlinear algebraic equations are solved using the Newton-Raphson method. However, the Newton-Raphson method requires certain functional regularity (See Appendix A), which is often violated without a special smoothing technique.

Controlling water resources means formulating an optimal control problem on a mathematical model as mentioned above. An optimal control problem in general comprises the following components (Lions [57]).

1. A control variable constrained in a set of admissible control.

2. A state variable which is given for a chosen control variable as the solution to an equation which describes the model of the controlled system.

3. An observation variable of the state variable.

4. A functional of the observation variable.

The problem is to search a control variable that minimizes or maximizes the functional. The control variable in a water resources system is to determine operational strategy of hydraulic structures. The state variable is given by the unknowns of the mathematical model. The observation variable is taken as a function of the state variable and/or the control variable. The functional is the performance index to evaluate how much the behavior of the observation variable is suitable for an engineering purpose. Once an optimal control problem is formulated, conditions to optimize the control variable are investigated. The conditions may be given by inequalities. An optimization procedure is developed to search the control variable to satisfy the conditions and is mainly implemented by computer.

1.2 Purpose and structure of this thesis

This thesis focuses on water conveyance systems and water storage systems from among various water resources systems. These two systems are considered as generalization of canals and dams in an irrigation system, respectively. Thus, primary application in the real world shall be to design and management of large area irrigation systems which need stable supply of water, but other problems in water resources engineering can be discussed in the same framework.

In order to approach the water conveyance/storage systems, open channels in terms of hydraulics and reservoirs under stochastic environment are intensively researched. Clarification of mathematical rationales of open channel flows and reservoir storages, especially when they are controlled under human will, is the main objective. Numerical techniques are elaborated to simulate states of the systems, to present optimization procedures, and to design optimizing controllers.

Succeeding chapters are organized as follows.

Chapter 2 introduces a mathematical model of open channel unsteady flows and presents a numerical model which is applicable to channels of network type. Governing PDEs, which are derived from physical conservation laws, are discretized using the finite element method and the finite volume method. General principle to introduce hydraulic structures such as sudden transition and gate is demonstratively shown. In addition to that numerical model for open channel unsteady flows, a scheme is proposed to solve the solute transport equation which governs water quality in open channels. This scheme compatively uses the finite element method and the finite volume method so as to be applicable to any parabolic PDE such as FPPDE in Chapter 5. Although the numerical techniques developed in this chapter aim to be calculation tools in other chapters, combining the different two methods into one model is a novel approach in computational hydraulics.

Chapter 3 considers optimal control problems of open channel flows in the framework of variational calculus. The observation variable is supposed to be the state variable, and the functional to be minimized is of quadratic type. A minimum principle in a general form is given using an adjoint system of the governing PDEs system of open channel flows. Gate stroking problems, which are to design external and/or internal boundary conditions such as gate motions to produce a predetermined flow, are approached.

In contrast with Chapter 3 whose object is restricted to deterministic process, Chapter 4 deals with open channels under stochastic environment. A statistical model of stochastic process in open channels is presented as FPPDE for multiple variable (Risken [79]), and applied to designing optimal surface profile, taking a reliability as the functional.

Chapter 5 considers reliability of a single reservoir. The mathematical model of the reservoir reliability is given as the FPPDE with one variable. An optimal control problem is formulated so as to maximize the reservoir reliability. A maximum principle is obtained in a similar manner to Chapter 3. Coefficients in FPPDE are determined from data observed at existing reservoirs, and strategies of release discharges are optimized.

Chapter 6 is devoted to design of linear controllers which are applicable to open channel networks as well as reservoirs. In the preceding chapters, open-loop control systems which drive control variables without feed-back are used. The control system in this chapter includes linear controllers to feed-back observed quantities and is oriented toward

automatic control. The modern control theory is employed to construct a robust control system, which has not yet been established in water resources engineering. A virtual mathematical model where the observation vector is an error signal vector is considered instead of a physical model as in the preceding chapters. The functional is taken as an H_∞ norm, or the least upper bound of the maximum singular value on the imaginary axis, of a generalized plant in the frequency domain, and the controllers are designed using the algebraic design method.

Chapter 7 gives conclusions to summarize this thesis.

Thus, Chapters 2 through 6 are related with each other by key words as shown in Figure 1.1.

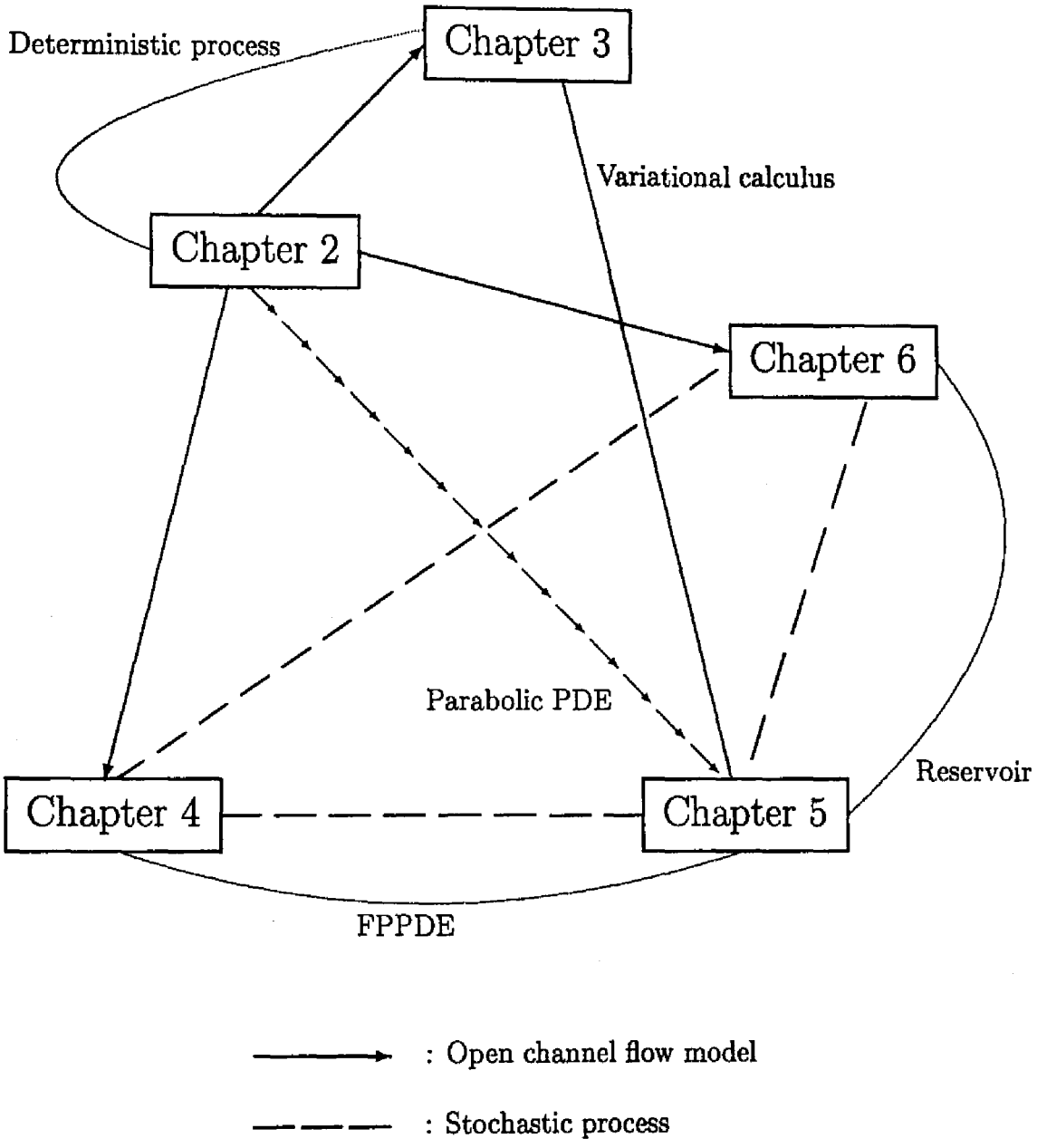

Figure 1.1: Structure of this thesis and relating key words

Chapter 2

Modeling of Open Channel Flows

2.1 Introduction

Modeling of flows in an open channel network with hydraulic structures is an indispensable approach to water conveyance systems. A system of PDEs which describe the conservation laws of mass and momentum in continuous fluid is widely used as a mathematical model of flowing water. One-dimensional (1D) models are applied to conveyance systems where water flows along courses. In a 1D model, the PDEs system represents states of unknowns such as flow depth and discharge in time and space, whereas hydraulic structures may be incorporated as external or internal boundary conditions which algebraic equations prescribe.

Numerical models are developed to obtain an approximate solution to the PDEs system with the algebraic equations. Many numerical schemes have been developed to discretize the PDEs system, which is hyperbolic and nonlinear. Lax and Wendroff [53] investigate finite difference schemes to capture discontinuity in a solution. The characteristic speeds are carefully considered in the finite volume method to represent transcritical flows (García-Navarro *et al.* [27]; Meselhe and Holly Jr. [63]; Meselhe *et al.* [64]) or dam break flows (Jha *et al.* [38]; Jha *et al.* [39]; Jin and Fread [40]). Finite element schemes based on the weak formulation of the PDEs also require special numerical technique to avoid oscillations as discussed by Anastasiadou-Partheniu and Terzidis [6], Hicks and Steffler [34], Alam and Bhuiyan [3], Muñoz-Carpena [68], and Choi and García [18]. Equalizing boundary values at junctions, the above discretization schemes are applicable to a channel network when it is simply connected so that any couple of points is connected along only one path (Misra *et al.* [66]; Choi and Molinas [17]; Nguyen and Kawano [72]; Blandford and Ormsbee [10] Naidu *et al.* [69]), but difficulty arises in a multiply connected channel network which has a couple of points that is connected along more than one path. Nguyen and Kawano [73] develop an iterative algorithm to combine simply connected

channel networks into a multiply connected channel network. Joliffe [41] proposes an implicit finite difference scheme to handle multiply connected channels as a single unit. The Abbott-Ionescu scheme (Abbott and Basco [1]), whose numerical solution method is given by Kutija [52], is a versatile one which evaluates water depth and discharge at different points.

The algebraic equations which govern flow-discharge relationships of hydraulic structures are incorporated into numerical models of the PDEs system as external or internal boundaries (Husain *et al.* [36]; Swain and Chin [85]; Kawachi and Itagaki [45]). However, such models are often unstable because functional regularity that the Newton-Raphson method, which is used for solving nonlinear algebraic equations, requires.

In the numerical model presented here, the following innovations are included to handle multiply connected channel networks with hydraulic structures (Kawachi *et al.* [49]).

1. A finite element scheme is used for the continuity equation, whereas a finite volume scheme is used for the momentum equation.

2. Linkage parameters are introduced to modify the dynamic equations fulfilling functional regularity at hydraulic structures.

Upwind technique considering the characteristic speed is not employed in the discretization procedure of the PDEs because it is assumed that flows are dominantly subcritical in water conveyance systems to be considered. However, this assumption may be violated at a finite number of points where hydraulic structures, and such points are handled as internal boundaries. Transitions and gates are especially focused on from among the hydraulic structures.

In addition to the flow modeling, a discretization scheme for solute transport equations is proposed to analyze water quality in open channel networks. The scheme compatibly uses the finite element method and the finite volume method to be applicable to general parabolic PDEs including the governing equation of the reservoir reliability discussed in Chapter 5.

2.2 Governing equations of open channel flows

Unsteady flow in open channels are governed by continuity and dynamic equations.

A course of water which flows on the terrestrial surface is defined as the following mathematical model after Afif [2], as shown in Figure 2.1.

1. A curve C is given in $\mathbb{R}^3$, 3-dimensional real Euclidean space, to represent the spatial position of the channel bed on which water flows. The local curvilinear abscissa x

is established along $\mathcal{C}$, and the tangential vector of $\mathcal{C}$ in $\mathbb{R}^3$ is denoted by $\mathbf{x}$. The vertical z-axis is taken originated at a horizontal datum.

2. The geometry of the vertical cross-section of the course is given at each point of $\mathcal{C}$. The wetted part of the cross-section is denoted by $\mathcal{D}$, which is a time dependent 2-dimensional bounded domain. The measure of $\mathcal{D}$ is the wetted cross-sectional area, which is denoted by A. Since a z-value determines an A-value at a point of $\mathcal{C}$, A is given as $A(z)$, which is a monotone increasing function of z.

3. The water depth h is defined by the vertical distance from $\mathcal{C}$ to the free surface, which is the upper edge of $\mathcal{D}$.

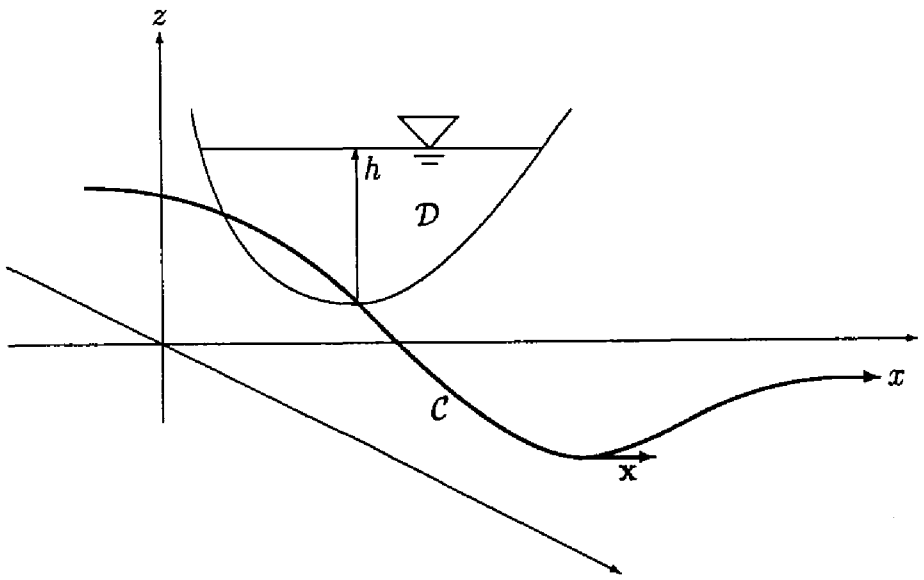

Figure 2.1: Definition sketch of water course

The governing equations of open channel flows are derived from the physical conservation laws, which are applied to a test domain $\mathcal{V}$. The test domain $\mathcal{V}$, shown in Figure 2.2, is defined as

$$\mathcal{V} = (x_1, x_2) \times \mathcal{D} \tag{2.1}$$

where $x_1 < x_2$, and subscripts 1 and 2 are used for referring to the x_1 and the x_2 sections, respectively.

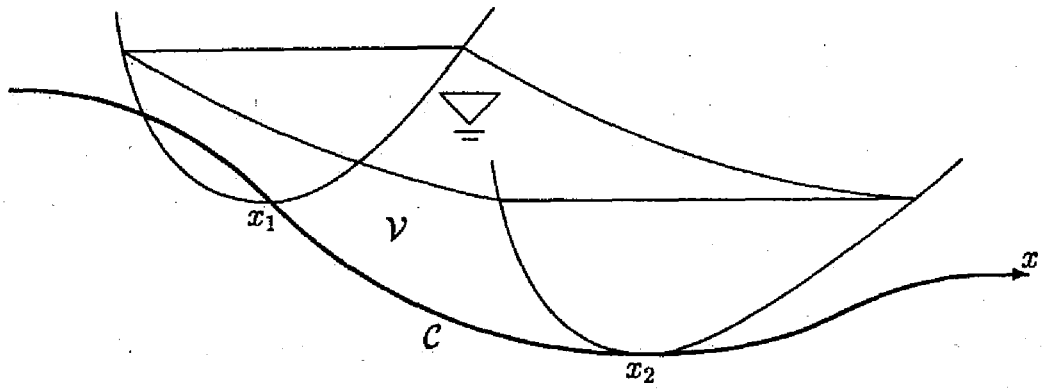

Figure 2.2: Test domain $\mathcal{V}$

2.2.1 Continuity equation

The conservation law of mass states that the temporal variation of the mass of the water contained in $\mathcal{V}$ is equal to the total mass flux entering into $\mathcal{V}$. Since the relative velocity of the water entering into $\mathcal{V}$ is given by the difference between the absolute velocity of water and the proper velocity of the boundary of $\mathcal{V}$, the conservation law of mass is represented as

$$\frac{d}{dt}\int_{\mathcal{V}} \rho d\mathcal{V} = -\int_{\mathcal{S}} \rho(\mathbf{v} - \mathbf{v}_s)\cdot \mathbf{n} d\mathcal{S} \tag{2.2}$$

where t = time, ρ = density of water which is taken as a constant, $\mathcal{S}$ = boundary of $\mathcal{V}$, $\mathbf{v}$ = absolute velocity of water, $\mathbf{v}_s$ = proper velocity of $\mathcal{S}$, and $\mathbf{n}$ = outward unit normal vector. Note that $\mathbf{v}_s$ vanishes on $\mathcal{S}$ except the free surface where $\mathbf{v}_s = \mathbf{v}$ and that $\mathbf{n}$ is equal to $-\mathbf{x}$ and $\mathbf{x}$ on $\mathcal{D}_1$ and $\mathcal{D}_2$, respectively. Assuming that the density ρ is a constant, the left hand side of Eqn.(2.2) is rewritten as

$$\frac{d}{dt}\int_{\mathcal{V}} \rho d\mathcal{V} = \rho\frac{d}{dt}\int_{x_1}^{x_2}\left(\int_{\mathcal{D}} d\mathcal{D}\right) dx = \rho\int_{x_1}^{x_2}\left(\frac{\partial A}{\partial t}\right) dx \tag{2.3}$$

whereas the right hand side is reduced to

$$-\int_S \rho(\mathbf{v}-\mathbf{v}_s)\cdot\mathbf{n}dS = -\rho(Q_2-Q_1)+\rho\int_{x_1}^{x_2} q\,dx = -\rho\int_{x_1}^{x_2}\left(\frac{\partial Q}{\partial x}-q\right)dx \tag{2.4}$$

where Q = discharge defined as

$$Q=\int_{\mathcal{D}}\mathbf{v}\cdot\mathbf{x}d\mathcal{D} \tag{2.5}$$

and q = lateral discharge per unit-width given by

$$q=\int_{\mathcal{P}}\mathbf{v}\cdot\mathbf{n}d\mathcal{P} \tag{2.6}$$

where $\mathcal{P}$ = boundary of $\mathcal{D}$. Since the conservation law of mass holds for arbitrary x_1 and x_2, the continuity equation

$$\frac{\partial A}{\partial t}+\frac{\partial Q}{\partial x}=q \tag{2.7}$$

holds at any point of $\mathcal{C}$.

2.2.2 Momentum equation

Next, the conservation law of momentum is applied to the same $\mathcal{V}$ to obtain the equation of motion. The temporal variation of the total momentum contained in $\mathcal{V}$ is equalized to the sum of the total momentum flux entering into $\mathcal{V}$, the contact force acting on $\mathcal{S}$, and the inertial force acting in $\mathcal{V}$. Assuming that the contact force consists of the pressure force and the friction force, the conservation law of momentum is represented as

$$\frac{d}{dt}\int_{\mathcal{V}}\rho\mathbf{v}d\mathcal{V} = -\int_S\rho(\mathbf{v}-\mathbf{v}_s)\cdot\mathbf{n}\,\mathbf{v}\,dS-\int_S\mathbf{p}\,\mathbf{n}\,dS+\int_S\mathbf{f}\,dS-\int_{\mathcal{V}}\rho g\,\mathbf{z}\,d\mathcal{V} \tag{2.8}$$

where $\mathbf{p}$ = pressure, $\mathbf{f}$ = friction force, g = gravitational acceleration, and $\mathbf{z}$ = vertical upward unit vector. Each term of Eqn.(2.8) is rewritten as

$$\frac{d}{dt}\int_{\mathcal{V}}\rho\mathbf{v}d\mathcal{V}=\rho\frac{d}{dt}\int_{x_1}^{x_2}\left(\int_{\mathcal{D}}\mathbf{v}d\mathcal{D}\right)dx=\rho\int_{x_1}^{x_2}\left(\frac{\partial}{\partial t}\int_{\mathcal{D}}\mathbf{v}d\mathcal{D}\right)dx \tag{2.9}$$

$$-\int_S\rho(\mathbf{v}-\mathbf{v}_s)\cdot\mathbf{n}\,\mathbf{v}\,dS$$

$$= -\int_{\mathcal{D}_2} \rho(\mathbf{v}\cdot\mathbf{n}_2)\mathbf{v}d\mathcal{D} - \int_{\mathcal{D}_1} \rho(\mathbf{v}\cdot\mathbf{n}_1)\mathbf{v}d\mathcal{D} - \int_{x_1}^{x_2}\left(\int_{\mathcal{D}} \rho(\mathbf{v}\cdot\mathbf{n})\,\mathbf{v}\,d\mathcal{D}\right)dx$$

$$= -\rho\int_{\mathcal{D}_2} v\mathbf{v}d\mathcal{D} + \rho\int_{\mathcal{D}_1} v\mathbf{v}d\mathcal{D} - \rho\int_{x_1}^{x_2}\left(\int_{\mathcal{D}} \mathbf{v}\cdot\mathbf{n}\,\mathbf{v}\,d\mathcal{D}\right)dx$$

$$= -\rho\int_{x_1}^{x_2}\left(\frac{\partial}{\partial x}\int_{\mathcal{D}} v\mathbf{v}\,d\mathcal{D} + \int_{\mathcal{D}} \mathbf{v}\cdot\mathbf{n}\,\mathbf{v}\,d\mathcal{D}\right)dx \tag{2.10}$$

$$-\int_{\mathcal{S}} \mathrm{p}\,\mathbf{n}\,d\mathcal{S} = -\int_{\mathcal{V}} \nabla\mathrm{p}\,d\mathcal{V} = -\int_{x_1}^{x_2}\left(\int_{\mathcal{D}} \nabla\mathrm{p}\,d\mathcal{D}\right)dx \tag{2.11}$$

$$\int_{\mathcal{S}} \mathbf{f}\,d\mathcal{S} = \int_{x_1}^{x_2}\left(\int_{\mathcal{P}} \mathbf{f}d\mathcal{P}\right)dx \tag{2.12}$$

$$-\int_{\mathcal{V}} \rho g\,\mathbf{z}\,d\mathcal{V} = -\rho\int_{x_1}^{x_2}\left(\int_{\mathcal{D}} g\,\mathbf{z}d\mathcal{D}\right)dx = -\rho\int_{x_1}^{x_2} gA\,\mathbf{z}\,dx \tag{2.13}$$

where $v = \mathbf{v}\cdot\mathbf{x}$, and the flow direction of the lateral discharge q is assumed perpendicular to $\mathcal{C}$. Thus, the momentum equation in vector form

$$\frac{\partial}{\partial t}\int_{\mathcal{D}} \mathbf{v}d\mathcal{D} + \frac{\partial}{\partial x}\int_{\mathcal{D}} v\mathbf{v}d\mathcal{D} + \frac{1}{\rho}\int_{\mathcal{D}} \nabla\mathrm{p}\,d\mathcal{D} - \frac{1}{\rho}\int_{\mathcal{P}} \mathbf{f}d\mathcal{P} + gAz = 0 \tag{2.14}$$

where $\mathbf{0}$ = null vector, holds at any point of $\mathcal{C}$. In order to obtain a scalar equation, Eqn.(2.14) is projected onto the flow direction assuming that the pressure distribution is hydrostatic. This is achieved by taking the scalar product between Eqn.(2.14) and $\mathbf{x}$, which is reduced for each term as

$$\frac{\partial}{\partial t}\int_{\mathcal{D}} \mathbf{v}d\mathcal{D}\cdot\mathbf{x} = \frac{\partial}{\partial t}\int_{\mathcal{D}} \mathbf{v}\cdot\mathbf{x}d\mathcal{D} = \frac{\partial Q}{\partial t} \tag{2.15}$$

$$\frac{\partial}{\partial x}\int_{\mathcal{D}} v\mathbf{v}d\mathcal{D}\cdot\mathbf{x} = \frac{\partial}{\partial x}\int_{\mathcal{D}} v(\mathbf{v}\cdot\mathbf{x})d\mathcal{D} - \int_{\mathcal{D}} v\mathbf{v}d\mathcal{D}\cdot\frac{\partial\mathbf{x}}{\partial x}$$

$$= \frac{\partial}{\partial x}\int_{\mathcal{D}} v^2 d\mathcal{D} - \int_{\mathcal{D}} v^2\mathbf{x}\cdot\frac{\partial\mathbf{x}}{\partial x}d\mathcal{D} = \frac{\partial}{\partial x}\left(\frac{\alpha Q^2}{A}\right) \tag{2.16}$$

$$\frac{1}{\rho}\int_{\mathcal{D}} \nabla\mathrm{p}\,d\mathcal{D}\cdot\mathbf{x} = g\int_{\mathcal{D}} \nabla(\eta - z)\cdot\mathbf{x}d\mathcal{D} = gA\left(\frac{\partial\eta}{\partial x} - \frac{\partial z_b}{\partial x}\right) = gA\frac{\partial h}{\partial x} \tag{2.17}$$

$$\frac{1}{\rho}\int_{\mathcal{P}} \mathbf{f} d\mathcal{P} \cdot \mathbf{x} = \varphi - gAS_f \tag{2.18}$$

$$gA\mathbf{z} \cdot \mathbf{x} = gA\frac{\partial z_b}{\partial x} \tag{2.19}$$

where α = velocity-distribution coefficient, z_b = elevation of channel bed, $\eta = z_b + h$ = elevation of water surface, φ = source term due to friction force which a hydraulic structure, if any, causes, and S_f = friction slope which is given by

$$S_f = S_f(h, Q) = \frac{\mathrm{n}^2 Q|Q|}{A^2 R^{4/3}} \tag{2.20}$$

where n = Manning's roughness coefficient, and R = hydraulic radius. Finally, the momentum equation in scalar form is obtained as

$$\frac{\partial Q}{\partial t} + \frac{\partial}{\partial x}\left(\frac{\alpha Q^2}{A}\right) + gA\frac{\partial h}{\partial x} + gA\frac{\partial z_b}{\partial x} + gAS_f = \varphi \tag{2.21}$$

which is rewritten as the conservative form

$$\frac{\partial Q}{\partial t} + \frac{\partial F_M}{\partial x} + S_M = \varphi \tag{2.22}$$

where F_M and S_M = flux and source of momentum given by

$$F_M = F_M(h, Q) = \frac{\alpha Q^2}{A(h)} + g\int_0^h A(z)dz \tag{2.23}$$

and

$$S_M = S_M(h, Q) = -g\int_0^h \frac{\partial A(z)}{\partial x}dz + gA(h)\frac{\partial z_b}{\partial x} + gA(h)S_f(h, Q) \tag{2.24}$$

respectively.

Determining A, F_M, and S_M uniquely, h and Q are taken as the unknown functions to be found. Thus, Eqns.(2.7) and (2.22), the governing equations of open channel flows, consist a hyperbolic PDE system of the first order in two different independent variables.

2.2.3 Initial and boundary conditions

Generally speaking, the solution to a differential equation is not uniquely determined by the equation itself. The solution to an ordinary differential equation depends on arbitrary constants, which can often be taken as the initial values of the unknown function and its derivatives because the number of them should be equal to the order of the differential equation. The situation is similar for simultaneous PDEs such as the governing equations of open channel flows deduced above. The solution will depend on a number of arbitrary functions.

Let the open channel network to be considered be a locally 1D open set which shall be referred to as the domain Ω. If the domain Ω is of infinite extent, a problem to solve the governing equations so that the unknown function takes specified value at the initial moment of time is known as a generalized Cauchy problem. The specified condition is called the initial condition or the Cauchy data. However, in engineering practice, the domain Ω may be of finite extent with the boundary Γ where the values of unknowns are prescribed at any moment of time. The prescribed condition is called the boundary condition and may be expressed as

$$b(h, Q)|_{\Gamma} = \tilde{b} \tag{2.25}$$

where b = algebraic equation to prescribe the boundary condition, $\tilde{b}$ = specified boundary value.

2.3 Discretization of governing equations

A numerical model of Eqns.(2.7) and (2.22) is obtained by means of the finite element method and the finite volume method. For the sake of simplicity, the lateral discharge flowing into or out of the stream is assumed to vanish almost everywhere in the channel and is given by a linear combination of Dirac's delta functions whose sources are located on finite number of spatial points.

The channel network to be analyzed is divided into N_E elements by N_N nodes, so that any singular point falls on one of the nodes. The number of boundary nodes are denoted by N_B. Given such a division, two finite dimensional spaces V_h and X_h are defined. V_h is the N_N-dimensional space whose generic $i-$th basis ψ_i^V is given by

$$\psi_i^V = \begin{cases} 1 & (\text{ at the } i-\text{th node}) \\ 0 & (\text{ at other nodes}) \\ \text{linearly interpolated} & (\text{in elements}) \end{cases} \tag{2.26}$$

as shown in Figure 2.3, whereas X_h is the N_E-dimensional space whose generic $i-$th basis ψ_i^X is given by

$$\psi_i^X = \begin{cases} 1 & (\text{ in the } i-\text{th element}) \\ 0 & (\text{ in other elements}) \end{cases} \tag{2.27}$$

as shown in Figure 2.4.

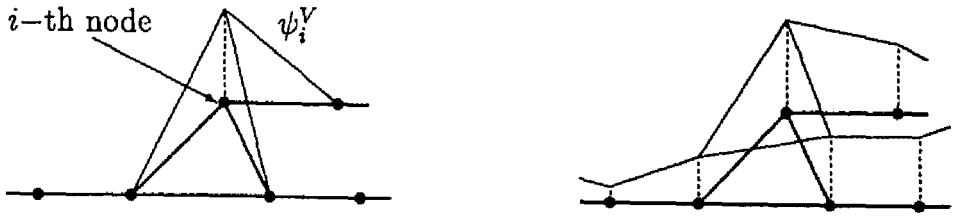

Figure 2.3: Basis ψ_i^V and typical V_h-function

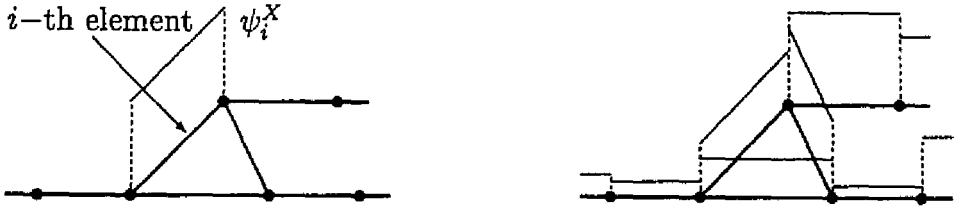

Figure 2.4: Basis ψ_i^X and typical X_h-function

The unknowns h and the bottom elevation z are assumed to be V_h-functions, whereas the unknown Q is approximated by an X_h-function. Being taken as primitive unknowns, h and Q are discretized as N_N-dimensional vector $\mathbf{h}$ whose $i-$th component is h_i, the $i-$th nodal value of h, and N_E-dimensional vector $\mathbf{Q}$ whose $i-$th component is Q_i, the $i-$th elemental value of Q, respectively. The vector $\mathbf{Q}$ is extended as $(N_E + N_B)-$dimensional vector $\tilde{\mathbf{Q}}$ whose $(N_E + i)-$th component is the $i-$th boundary value of Q.

The weak form of the continuity equation Eqn.(2.7) is written as

$$\int_\Omega \left(\frac{\partial A}{\partial t} + \frac{\partial Q}{\partial x} \right) \psi \, dx = \frac{d}{dt} \int_{\text{supp}\,\psi} A\psi \, dx + [Q\psi]_\Gamma - \int_{\text{supp}\,\psi} Q \frac{d\psi}{dx} \, dx = \int_{\text{supp}\,\psi} q\psi \, dx \tag{2.28}$$

where ψ = any weighting function in H^1, the Sobolev space which consists of functions whose first derivatives are square Lebesgue integrable, and supp = support of the set. Substituting ψ_i^V $(i = 1 \sim N_N)$ results in the vector form

$$\frac{d\mathbf{A}}{dt} + B\tilde{\mathbf{Q}} = \mathbf{q} \tag{2.29}$$

where $\mathbf{A}$ = N_N−dimensional vector whose i−th component is equal to $\int_{\text{supp}\,\psi_i^V} A\psi_i^V \, dx$, and B = incidence matrix, which is of $N_N \times (N_E + N_B)$ in size, $\mathbf{q}$ = N_N−dimensional vector whose i−th component is equal to the intensity of q concentrated at the i−th node. Altman and Boulos [5] prove that the matrix B so obtained is full rank.

The finite volume method is applied to the momentum equation Eqn.(2.22), which is integrated over a generic i−th element Ω_i^e as

$$\int_{\Omega_i^e} \left(\frac{\partial Q}{\partial t} + \frac{\partial F_M}{\partial x} + S_M \right) dx = \frac{d}{dt} \int_{\Omega_i^e} Q dx + \left[F_M \right]_{x_i^l}^{x_i^r} + \int_{\Omega_i^e} S_M \, dx = \int_{\Omega_i^e} \varphi \, dx \tag{2.30}$$

where x_i^l = inferior of Ω_i^e, and x_i^r = superior of Ω_i^e. Using estimations given by

$$\int_{\Omega_i^e} Q dx = \Delta x_i Q_i \tag{2.31}$$

$$\left[F_M \right]_{x_i^l}^{x_i^r} = -F_M(h_i^l, Q_i) + F_M(h_i^r, Q_i) \tag{2.32}$$

and

$$\int_{\Omega_i^e} S_M \, dx = \frac{\Delta x_i}{2} \sum_{k=1}^{4} w_k S_M \left(\frac{1 - c_k}{2} h_i^l + \frac{1 + c_k}{2} h_i^r, Q_i \right) \tag{2.33}$$

where Δx_i = measure of $\Omega_i^e = x_i^r - x_i^l$, h_i^l and h_i^r = nodal values of h at x_i^l and x_i^r, respectively, and w_k and c_k $(k = 1 \sim 4)$= constants in the 4-point Gauss quadrature rule as shown in Table 2.1, Eqn.(2.30) is reduced to the vector form

$$\frac{d}{dt} \left(\text{diag} \left[\Delta x_i \right] \mathbf{Q} \right) + \mathbf{M} = \int_{\Omega_i^e} \varphi \, dx \tag{2.34}$$

where diag represents a diagonal matrix whose ii−component is given as the value between the brackets, $\mathbf{M}$ = N_E−dimensional vector whose i−th component is equal to the sum

of the respective right hand sides of Eqns.(2.32) and (2.33). Then, from Eqns.(2.29) and

Table 2.1: Constants w_k and c_k in the 4-point Gauss quadrature rule

k	c_k	w_k
1	0.3478548451	-0.8611363116
2	0.6521451549	-0.3399810436
3	0.6521451549	0.3399810436
4	0.3478548451	0.8611363116

(2.34), (N_N+N_E)−dimensional simultaneous ordinary differential equations are obtained as

$$\frac{d\Xi(\mathbf{h},\tilde{\mathbf{Q}})}{dt} = \Psi(\mathbf{h},\tilde{\mathbf{Q}}) \tag{2.35}$$

where $\Xi(\mathbf{h},\tilde{\mathbf{Q}})$ and $\Psi(\mathbf{h},\tilde{\mathbf{Q}})$ = vector functions of $\mathbf{h}$ and $\tilde{\mathbf{Q}}$ given by

$$\Xi(\mathbf{h},\tilde{\mathbf{Q}}) = \begin{bmatrix} \mathbf{A} \\ \\ \mathrm{diag}\left[\Delta x_i\right]\mathbf{Q} \end{bmatrix} \tag{2.36}$$

and

$$\Psi(\mathbf{h},\tilde{\mathbf{Q}}) = \begin{bmatrix} -B\tilde{\mathbf{Q}}+\mathbf{q} \\ \\ -\mathbf{M}+\int_{\Omega_i^e}\varphi\, dx \end{bmatrix} \tag{2.37}$$

respectively. Using the implicit scheme, Eqn.(2.35) is discretized in the temporal domain as

$$\Xi(\mathbf{h}_+,\tilde{\mathbf{Q}}_+) - \Xi(\mathbf{h},\tilde{\mathbf{Q}}) - \Delta t\left(\Psi\left(\Theta\mathbf{h}_+,\Theta\tilde{\mathbf{Q}}_+\right) + \Psi\left((1-\Theta)\,\mathbf{h},(1-\Theta)\,\tilde{\mathbf{Q}}\right)\right) = \mathbf{0} \tag{2.38}$$

where Δt = temporal integration interval, Θ = implicit parameter, and subscript + refers to the time after Δt.

The boundary condition Eqn.(2.25) is incorporated into the model as N_B algebraic equations.

The total number of the equations obtained so far is equal to $(N_N + N_E + N_B)$, which is the same as that of components of the unknown vectors $\mathbf{h}$ and $\tilde{\mathbf{Q}}$. Therefore, the

Newton-Raphson iterative procedure is applied for the simultaneous solution to these equations.

2.3.1 Steady flow analysis

Flow analysis in steady state is rather important for the determination of the physical dimensions of channels and the layout of hydraulic structures. Beffa [9] executes backwater computations for transcritical flows. Kawachi *et al.* [48] and Kawachi *et al.* [44] exhibit excellent solution performance in open channel networks using the Newton-Raphson method.

The unknown vectors $\mathbf{h}$ and $\tilde{\mathbf{Q}}$ in steady flows may be obtained as the solution to

$$\Psi\left(\mathbf{h}, \tilde{\mathbf{Q}}\right) = 0 \tag{2.39}$$

which represents the fixed point of Eqn.(2.35).

2.4 Incorporation of hydraulic structures

The governing differential equations are applicable to gradual transitions without any modification.

The numerical scheme can be applied to sudden horizontal transitions where $x_i^l = x_i^r$, because any zero division does not appear. Contrary to sudden horizontal transitions, sudden vertical transitions, as shown in Figure 2.5, require proper alteration of the dynamic equation because the assumption of hydrostatic pressure may be significantly violated.

If h_d, water depth at the downstream node, is so large that reverse flow occurs, Eqn.(2.30) holds without any change. When h_d is small enough, h_u, water depth at the upstream node, becomes critical depth, and the algebraic equation

$$\frac{\partial F_M\left(h_u, Q_i\right)}{\partial h} = 0 \tag{2.40}$$

governs the flow. Assuming that the distance between the upstream and the downstream nodes is infinitesimal, these two extreme equations are appropriately linked by

$$(1-\theta_d)\frac{\partial F_M\left(h_u, Q_i\right)}{\partial h} + \theta_d f_i = 0 \tag{2.41}$$

where $f_i = (N_N + i)$−th component of the left hand side of Eqn.(2.38) (for unsteady flow

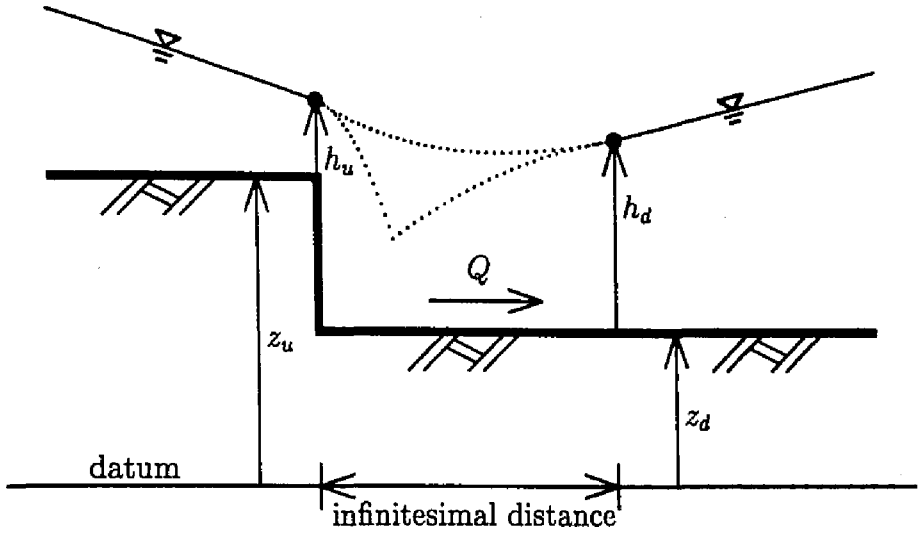

Figure 2.5: Definition sketch of sudden vertical transition

analysis) or Eqn.(2.39) (for steady flow analysis), and θ_d = linkage parameter given by

$$\theta_d = \frac{1 - \cos(\pi\theta_s\theta_w)}{2} \tag{2.42}$$

where submergency θ_s and down-windiness θ_w are respectively defined as

$$\theta_s = \begin{cases} 1 & (\eta_u \le \eta_d) \\ \frac{\eta_d - z_u}{h_u} & (z_u < \eta_d < \eta_u) \\ 0 & (\eta_d \le z_u) \end{cases} \tag{2.43}$$

$$\theta_w = \begin{cases} 1 & (Fr_u \le 0) \\ 1 - Fr_u^2 & (0 < Fr_u < 1) \\ 0 & (1 \le Fr_u) \end{cases} \tag{2.44}$$

where $\eta_u = z_u + h_u$ = elevation of upstream water surface, and $\eta_d = z_d + h_d$ = elevation of downstream water surface. The left hand side of Eqn.(2.41), which has regularity up to the second derivatives with respect to h_u, h_d, and Q, satisfies the necessary condition of solution convergency in the Newton-Raphson iteration process.

Other hydraulic structures may be modeled by compatible dynamic equations as well.

For gates, submerged flows is modeled as the algebraic equation

$$Q|Q| - 2gC_d^2a^2\Delta\eta = 0 \tag{2.45}$$

where C_d = discharge coefficient, a = opening area of the gate, and $\Delta\eta$ = difference between the water levels that bounds the gate. The corresponding momentum equation in Eqn.(2.38) or Eqn.(2.39), which is used when the gate is fully open so that it does not affect the flow, is replaced by Eqn.(2.45) when the flow through the gate submerges. When the flow through the gate is neither of the two cases, the two respective equations are linked by a regular parameter which is similar to the one used in Kawachi *et al.* [49].

2.5 Coupling of solute transport equation

The importance of water quality analysis is increasing nowadays in both socioeconomical and environmental aspects (Lee *et al.* [55]). Kawachi *et al.* [43] applied an upwind finite element model of locally one-dimensional flow to unsteady analysis of saline water in a simply connected estuarine reservoir. Szymkiewicz [86] develops a six-point implicit finite element scheme for a transport equation and analyzes its accuracy and stability. The finite difference method is examined by Komatsu *et al.* [51]. The technique presented here compatibly uses the finite element method and the finite volume method to be applicable to a parabolic PDE with dominating convection (Unami *et al.* [91]).

In order to analyze water quality in open channel networks, a parabolic PDE which describes the conservation law of mass of the solutant is solved. The solute transport equation, which governs the concentration, is stated as

$$A\frac{\partial C}{\partial t} - \frac{\partial}{\partial x}\left(AD_x\frac{\partial C}{\partial x}\right) + Q\frac{\partial C}{\partial x} = (C_q - C)q \tag{2.46}$$

where C = solute concentration, D_x = dispersion coefficient, and C_q = solute concentration which q has. For the sake of simplicity, the following assumptions are made.

1. The solute concentration C does not affect the flow field.

2. A, D_x, Q are constants in the temporal domain.

2.5.1 Upwind discretization scheme

Being a second order equation with a convection term, the solute transport equation requires a more sophisticated scheme than standard Galerkin scheme or simple finite

volume scheme. Thus, an upwind scheme is now introduced. A bilinear form $\beta(C,\psi)$ is defined as

$$\beta(C,\psi) = \int_\Omega \left(AD_x \frac{\partial C}{\partial x}\frac{\partial \psi}{\partial x} + Q\frac{\partial C}{\partial x}\psi \right) dx \tag{2.47}$$

for arbitrary C and ψ in H^1. A weak form of Eqn.(2.46) is written as

$$\frac{d}{dt}\int_\Omega AC\psi\, dx + \left[-AD_x \frac{\partial C}{\partial x}\psi \right]_\Gamma + \beta(C,\psi) = \int_\Omega (C_q - C)q\psi\, dx \tag{2.48}$$

where the path of integral is along the whole channel network. Using the local Peclet number Pe_i given by

$$Pe_i = \frac{Q_i \Delta x_i}{AD_x} \tag{2.49}$$

a weighting function ψ_i^C is defined with a constant dissipation parameter c, as shown in Table 2.2, and substituted into ψ in Eqn.(2.48). Note that this scheme approaches a standard Galerkin scheme if the Peclet number equals zero, and does a finite volume scheme if it diverges to infinity.

Table 2.2: Definition of weighting function ψ_i^C

	x directs the node	$-x$ directs the node
$Pe_i \geq 0$	$\left(\frac{x}{\Delta x_i}\right)^{\frac{1}{1+\lvert cPe_i\rvert}}$	$\left(\frac{\Delta x_i - x}{\Delta x_i}\right)^{1+\lvert cPe_i\rvert}$
$Pe_i < 0$	$\left(\frac{x}{\Delta x_i}\right)^{1+\lvert cPe_i\rvert}$	$\left(\frac{\Delta x_i - x}{\Delta x_i}\right)^{\frac{1}{1+\lvert cPe_i\rvert}}$

Specification of a boundary condition at a boundary node is achieved by proper replacement of the corresponding nodal equation, whichever the type of the boundary condition is.

2.5.2 Consistency and dissipation parameter

In order to verify the validity of the upwind scheme, consistency of the numerical solution with a weak solution is examined for the solute transport equation without the source

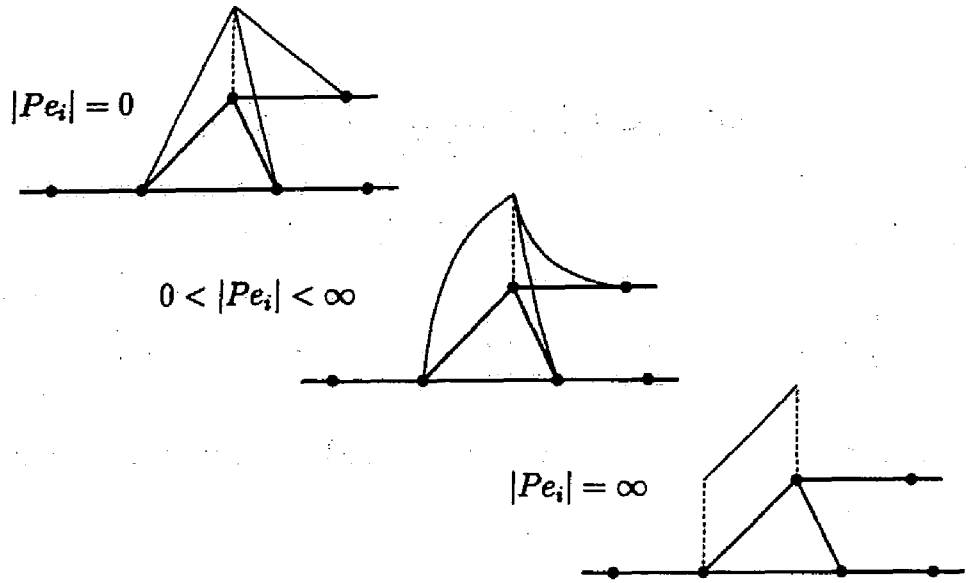

Figure 2.6: Weighting function ψ_i^C

term in steady state. The bilinear form $\beta(C, \psi)$ is assumed to be bounded and coercive so that there exists a weak solution (See Appendix B).

Suppose that $C \in H^1$ and the numerical solution $C_h \in V_h$ satisfy

$$\beta(C, \psi_i^C) = \beta(C_h, \psi_i^C) = 0 \tag{2.50}$$

for $i = 1 \sim N_N$. Then, error is estimated in terms of the equation

$$\beta(C_I - C_h, \psi_i^C) = \beta(C_I - C, \psi_i^C) \tag{2.51}$$

where C_I = the V_h–function whose nodal values are equal to respective those of C, as shown in Figure 2.7.

Since $C_I - C_h \in V_h$, the left hand side of Eqn.(2.51) is rewritten as

$$\beta(C_I - C_h, \psi_i^C) = \beta\left(\sum_{j=1}^{N_N} \epsilon_j \psi_j^V, \psi_i^C\right) = \sum_{j=1}^{N_N} \beta(\psi_j^V, \psi_i^C)\epsilon_j \tag{2.52}$$

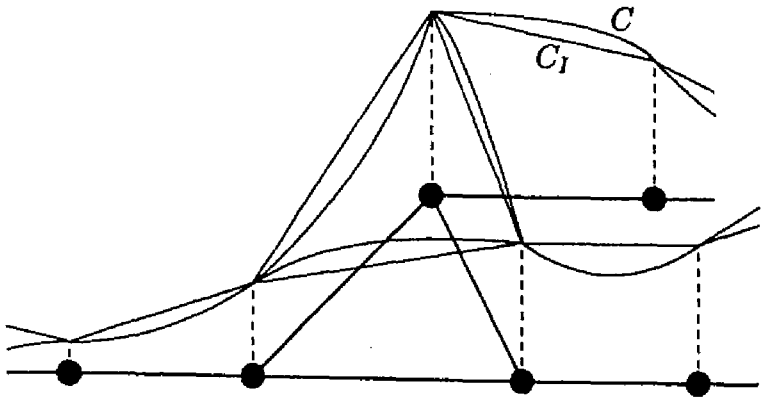

Figure 2.7: Interpolation of C

where $\epsilon_j = C - C_h$ at $j-$th node, and $\beta(\psi_j^V, \psi_i^C)$ is calculated as

$$\beta(\psi_j^V, \psi_i^C) = \begin{cases} \sum_{k=1}^{\nu_i} \beta_{ik}^e & (i = j) \\ -\beta_{ik}^e & \left(\Omega_{\kappa_{ik}}^e \text{ is bounded by the } i-\text{th and } j-\text{th nodes}\right) \\ 0 & (\text{otherwise}) \end{cases} \tag{2.53}$$

where ν_i = the number of elements connected to the $i-$th node, κ_{ij} = element number of $j-$th element connected to the $i-$th node, and β_{ik}^e = contribution from $\Omega_{\kappa_{ik}}$ to $i-$th node as given in Table 2.3. Consistency of the numerical solution C_h with C is established if the

Table 2.3: Representation of β_{ik}^e

	x in $\Omega_{\kappa_{ik}}^e$ directs the $i-$th node	$-x$ in $\Omega_{\kappa_{ik}}^e$ directs the $i-$th node
$Pe_{\kappa_{ik}} \geq 0$	$AD_x + \dfrac{(1+\lvert cPe_{\kappa_{ik}}\rvert)\, Q\Delta x_{\kappa_{ik}}}{2+\lvert cPe_{\kappa_{ik}}\rvert}$	$AD_x - \dfrac{Q\Delta x_{\kappa_{ik}}}{2+\lvert cPe_{\kappa_{ik}}\rvert}$
$Pe_{\kappa_{ik}} < 0$	$AD_x + \dfrac{Q\Delta x_{\kappa_{ik}}}{2+\lvert cPe_{\kappa_{ik}}\rvert}$	$AD_x - \dfrac{(1+\lvert cPe_{\kappa_{ik}}\rvert)\, Q\Delta x_{\kappa_{ik}}}{2+\lvert cPe_{\kappa_{ik}}\rvert}$

left hand side of Eqn.(2.51) approaches to zero when $C_I - C$ uniformly converges to zero, and it is guaranteed if all β_{ik}^e are positive because the rightest hand side of Eqn.(2.52) is rewritten for i such that ϵ_i is the maximum as

$$\sum_{j=1}^{N_N} \beta(\psi_j^V, \psi_i^C)\epsilon_j = \sum_{j \neq i} \beta(\psi_j^V, \psi_i^C)(\epsilon_j - \epsilon_i) = \sum_k \beta_{ik}^e(\epsilon_i - \epsilon_j) \tag{2.54}$$

where indices j and k are appropriately taken, using the equality

$$\beta(\psi_i^V, \psi_i^C) = -\sum_{j \neq i} \beta(\psi_j^V, \psi_i^C) \tag{2.55}$$

which is deduced from Eqn.(2.53). Thus, from the representation in Table 2.3, the inequality

$$\frac{|Q|\Delta x_i}{2 + |cPe_i|} < AD_x \tag{2.56}$$

is deduced for $i = 1 \sim N_E$, and the constraint of the dissipation parameter c

$$|c| \geq 1 \tag{2.57}$$

is obtained.

The effectiveness of the scheme is tested in a simple problem where $AD_x = 1$, $Q = 5$ and $\Delta x_i = 1$ in the domain $(0, 10)$. The solutions under the boundary condition $C(0) = 0$ and $C(10) = 1$ are shown in Table 2.4. No stable solution is obtained when $c = 0$, whereas stability is established when $c = 1$ and $c = 10$. The solution when $c = 1$ is better than that when $c = 10$ in terms of closeness to the exact solution.

Table 2.4: Solutions to $-\frac{d^2C}{dx^2} + 5\frac{dC}{dx} = 0$

x	$c = 0$	$c = 1$	$c = 10$	exact
0.000	0.00000000	0.00000000	0.00000000	0.00000000
1.000	-0.00069695	0.00000000	0.00000004	0.00000000
2.000	0.00092927	0.00000000	0.00000029	0.00000000
3.000	-0.00286524	0.00000000	0.00000196	0.00000000
4.000	0.00598861	0.00000002	0.00001287	0.00000000
5.000	-0.01467037	0.00000046	0.00008409	0.00000000
6.000	0.03353391	0.00000854	0.00054933	0.00000000
7.000	-0.07894274	0.00015794	0.00358821	0.00000031
8.000	0.18350279	0.00292184	0.02343791	0.00004540
9.000	-0.42887012	0.05405405	0.15309446	0.00673795
10.000	1.00000000	1.00000000	1.00000000	1.00000000

2.6 Demonstrative examples

2.6.1 Hypothetical channel of Wheatstone bridge type

To demonstrate the applicability of the numerical model described above, a hypothetical open channel network model is prepared as shown in Figure 2.8, which displays finite element spacing as well. The channel reaches R-1 through 7, arranged in a Wheatstone bridge like fashion, have rectangular cross sections. Henceforth, this model shall be referred to as the WB model. The bed elevation and the section width of each reach are shown in Figure 2.9. Gradual contraction of section is found in Reach R-2. The reaches R-2 and R-3 have sudden horizontal transitions, whereas the reaches R-5 and R-6 have sudden vertical transitions. Velocity-distribution coefficient $\alpha = 1.1$ and Manning's roughness coefficient $\mathbf{n} = 0.015$ are assumed constant along all the channel reaches in the network. A gate is installed across the reach R-4. Turnouts T-1 through T-8 are located at 8 nodes to withdraw water from the network and modeled as the source points of the lateral discharge q.

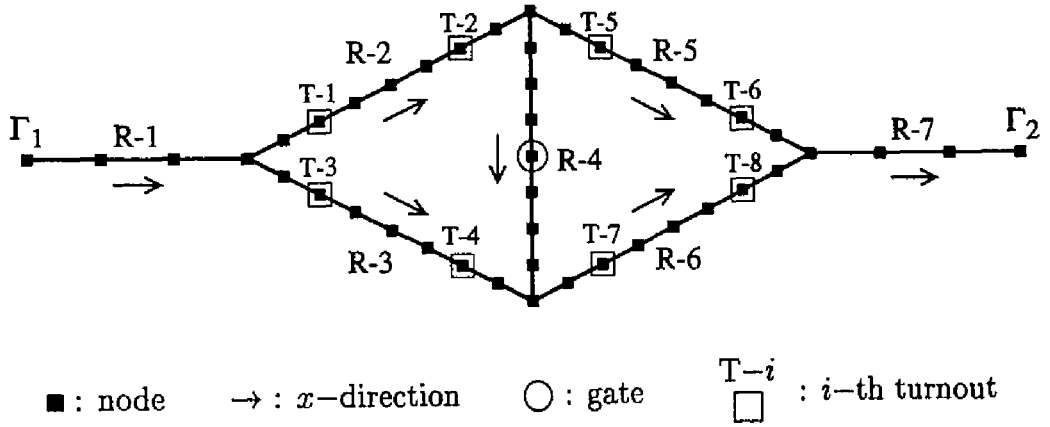

Figure 2.8: Open channel network of Wheatstone bridge type

First, the steady flow where $Q = 30.0[\mathrm{m}^3/\mathrm{s}]$ at Γ_1, $h = 2.0[\mathrm{m}]$ at Γ_2, the gate opening is equal to 2.0[m], and $2.5[\mathrm{m}^3/\mathrm{s}]$ of water is withdrawn from every turnout, is calculated. A trivial solution $Q = 0.0[\mathrm{m}^3/\mathrm{s}]$ and $h + z = 5.0[\mathrm{m}]$ is set up as a primitive initial estimate, and then the Newton-Raphson iteration process is performed. Solution convergency is not obtained when h at Γ_2 is directly specified as 2.0[m], but the process is successful when 5.0[m] is specified instead. 7 iterative cycles are needed to make the maximum absolute value of the left hand side of Eqn.(2.39) less than 10^{-11}. Prescribing the solution where h = 5.0[m] at Γ_2 for the initial estimate, solution for $h = 2.0[\mathrm{m}]$ at Γ_2 is successively obtained

after 10 iterative cycles. The flow at the gate is submerged, whereas the upstream depth of the sudden vertical transition in R-5 is critical. The calculated flow depth and discharge are shown in Figure 2.10.

Next, unsteady flow analysis for 24[hour] is executed with $\Delta t = 5$[min]. The lateral discharge from each turnout is doubled as 5.0[m^3/s] from $t = 6$[hour] to $t = 18$[hour]. The gate opening 2.0[m] and the boundary depth $h = 2.0$[m] at Γ_2 are fixed. The boundary discharge Q at Γ_1 is increased to 37.5[m^3/s] from $t = 0$[hour] to $t = 24$[hour]. The calculated flow depths and discharges at $t = 1$[hour], 7[hour], 13[hour], 19[hour], and 24[hour] are shown in Figures 2.11, 2.12, 2.13, 2.14, and 2.15, respectively. The results represent the surge propagating with appropriate celerity and the water depths at turnouts being hollowed when water is withdrawn. The number of iterative cycles is not greater than 5 in any of the temporal steps.

2.6.2 Environmental hydraulics

The scheme for the solute transport equation is tested in another channel network model with 77 nodes which connect 116 elements. Such a braided channel network is found in an estuary.

A steady state solution of flow is used for A and Q along the channel, whereas the mixing-length theory by Fujihara and Kawachi [26] is employed to determine the value of dispersion coefficient D_x from two other steady state solutions of flow under respective perturbed boundary conditions.

Steady states are calculated using the dissipation parameter $c = 0$ and 1 under the same Dirichlet boundary condition as shown in Figures 2.16 and 2.17, respectively. The solution takes physically meaningless negative values for $c = 0$, whereas sharp fronts of solute concentration are satisfactory represented for $c = 1$.

Setting the steady solution as the initial condition, unsteady simulation is executed for 40 days under a different boundary condition. Figures 2.18 and 2.19 show the calculated solute concentration 1 day and 40 days after, respectively. The solute asymptotically infiltrates into the inside of the channel network.

2.7 Conclusions

The governing equations of open channel unsteady flows are deduced. The numerical model using the finite element and the finite volume method is developed to solve the governing equations in a multiply connected open channel network with hydraulic structures. The dynamic equation is appropriately modified for sudden vertical transitions by a linkage parameter determined by submergence and down-windiness so as to ensure

functional continuity that the Newton-Raphson method requires. The upwind scheme for solute transport equations is added to the flow model to analyze water quality. Stability and versatility of the model are demonstrated in the example calculations from which highly satisfactory results are obtained. Thus, the model developed in this chapter is commonly used in Chapters 3, 4, and 6, where simulations of open channel flows are necessary.

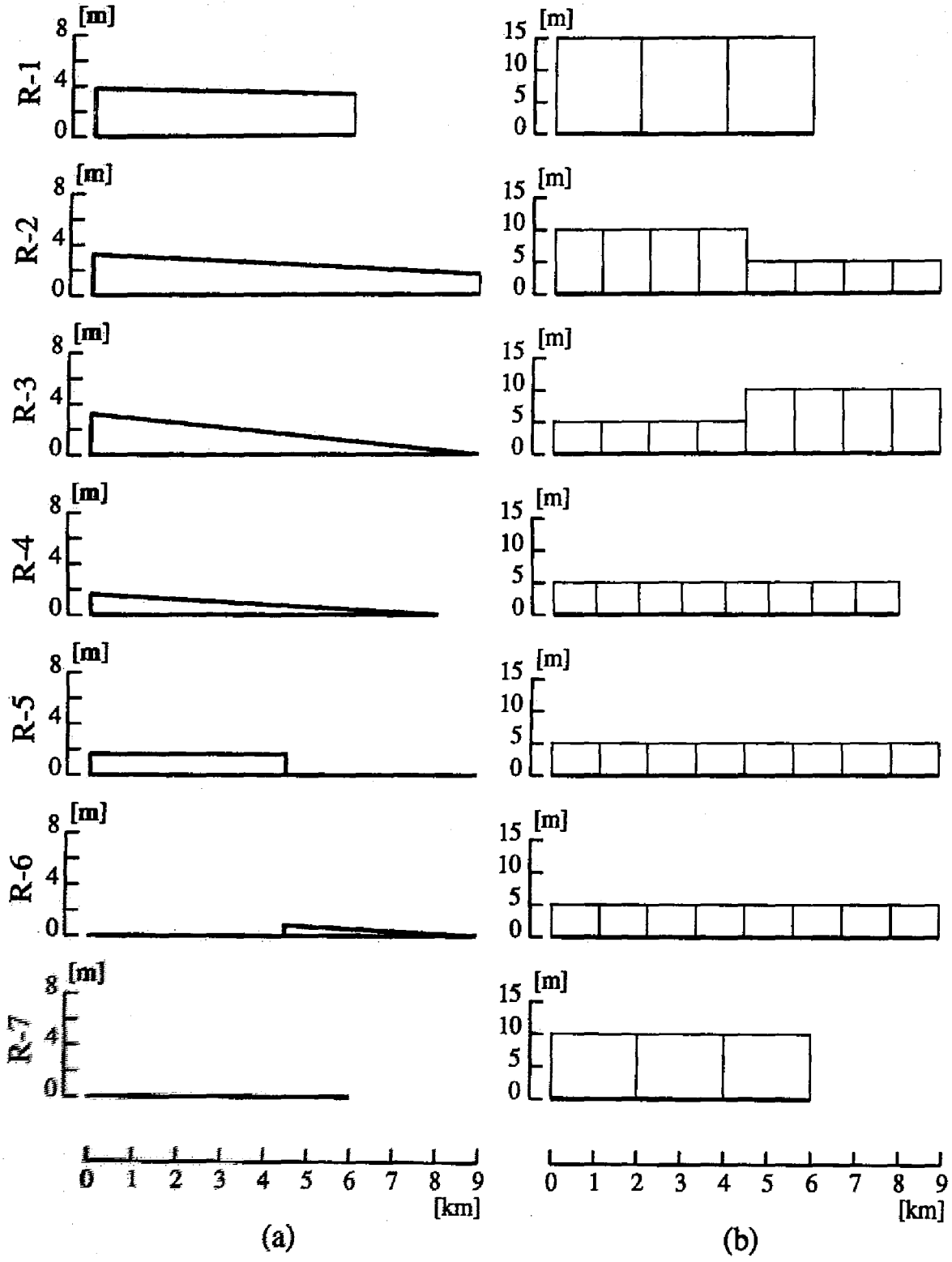

Figure 2.9: Channel geometry: (a) Bed elevation; (b) Section width

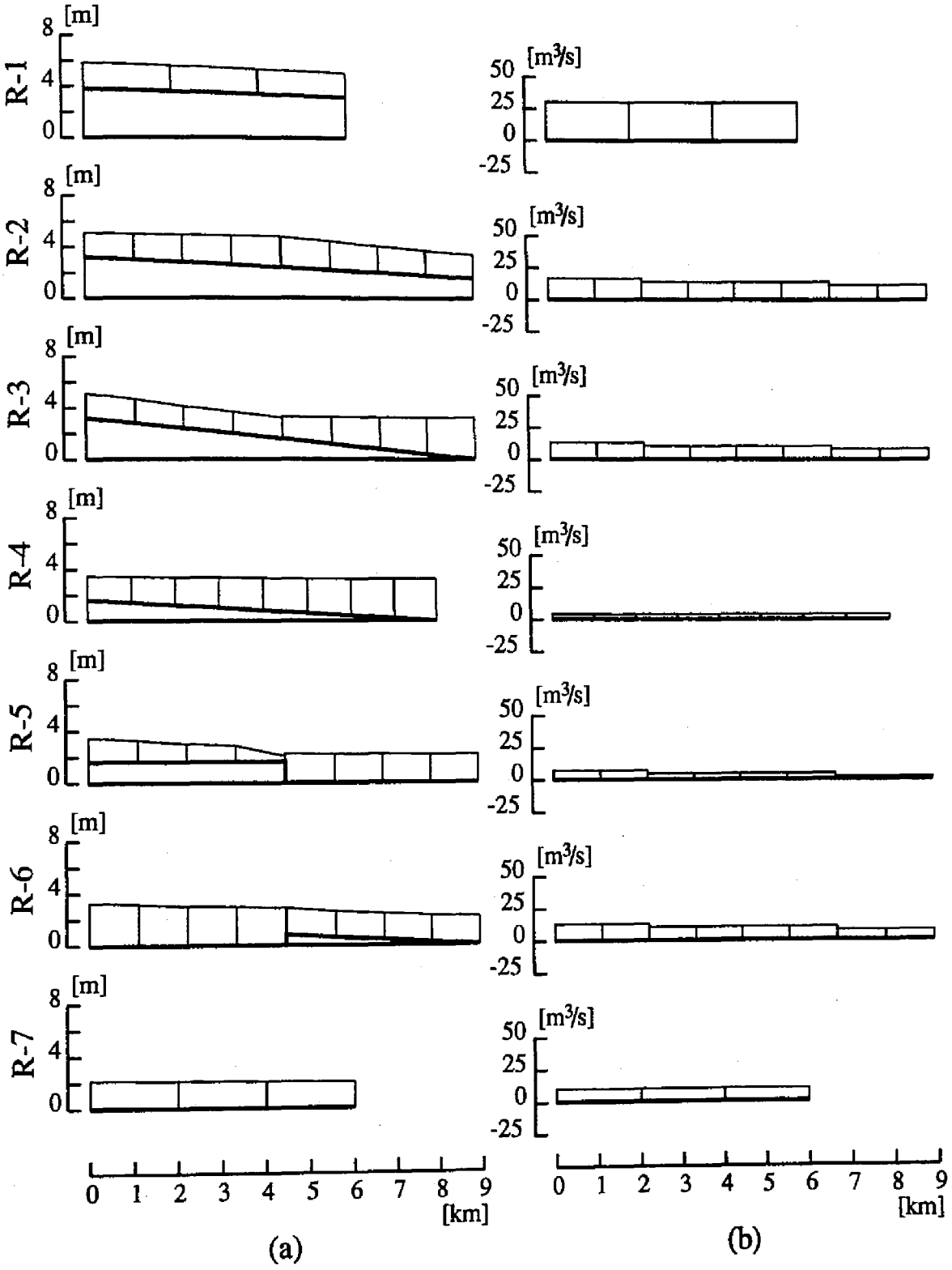

Figure 2.10: Calculated steady flow: (a) Bed and water elevations; (b) Discharge

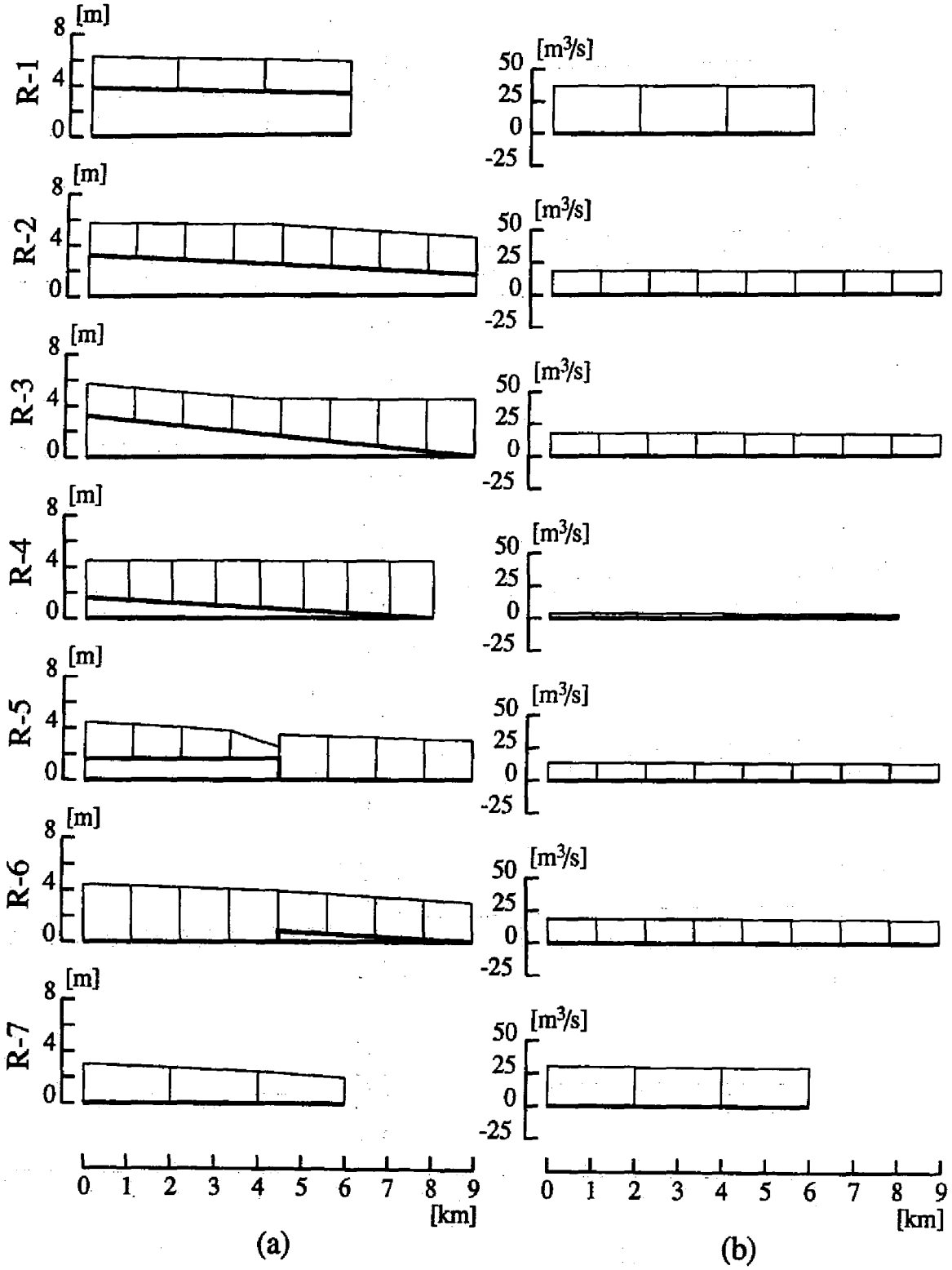

Figure 2.11: Calculated flow at $t = 1$[hour]: (a) Bed and water elevations; (b) Discharge

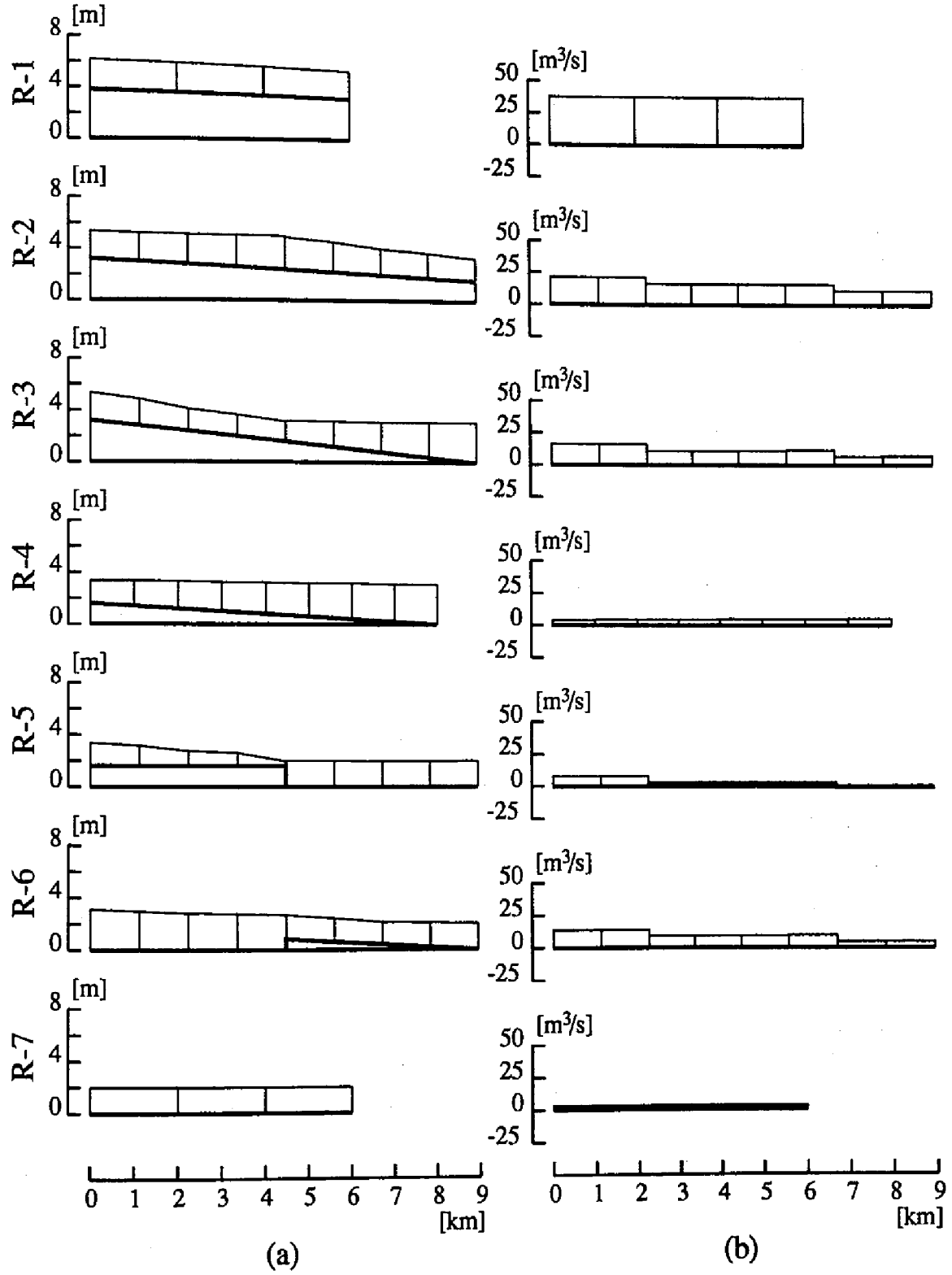

Figure 2.12: Calculated flow at $t = 7$[hour]: (a) Bed and water elevations; (b) Discharge

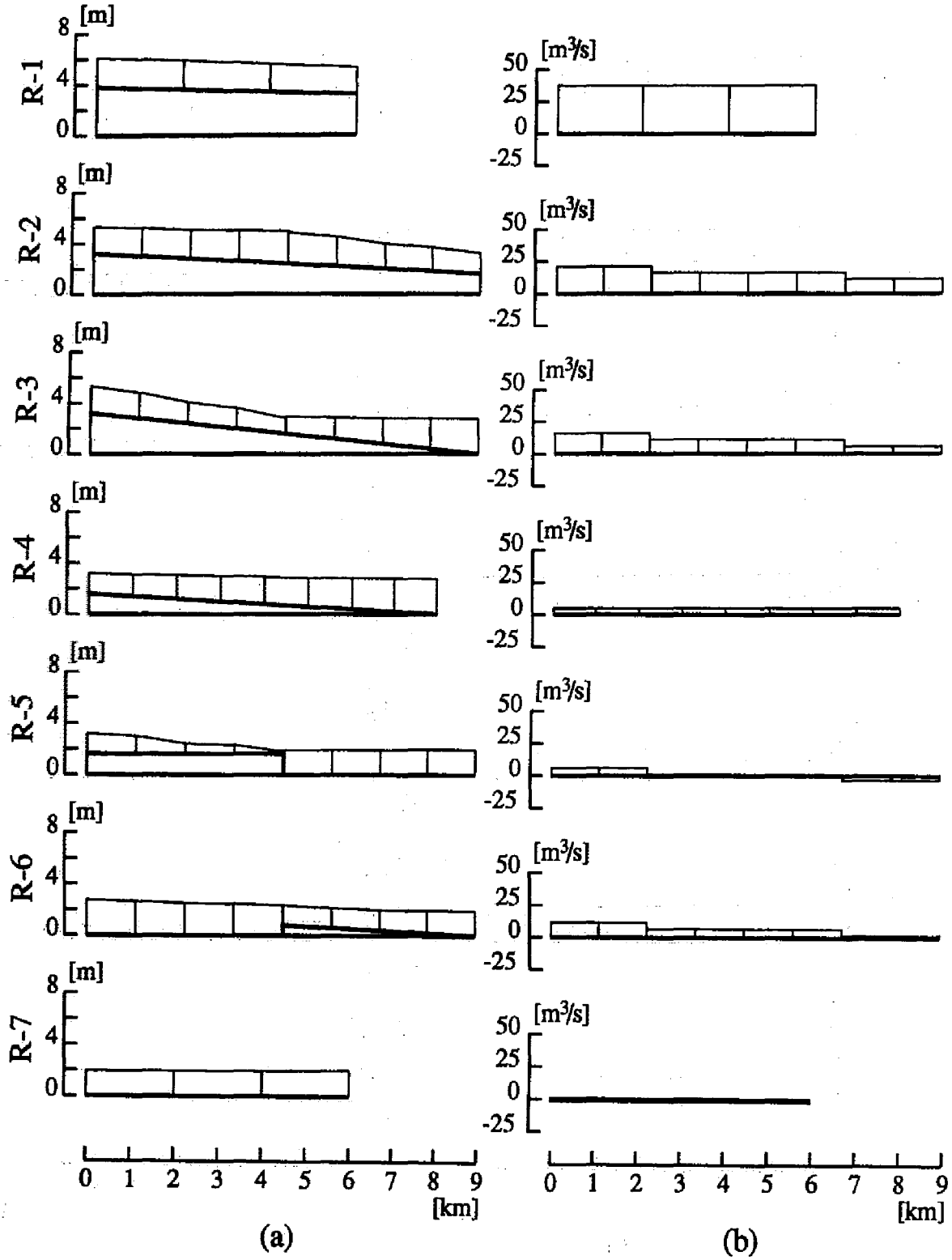

Figure 2.13: Calculated flow at $t = 13$[hour]: (a) Bed and water elevations; (b) Discharge

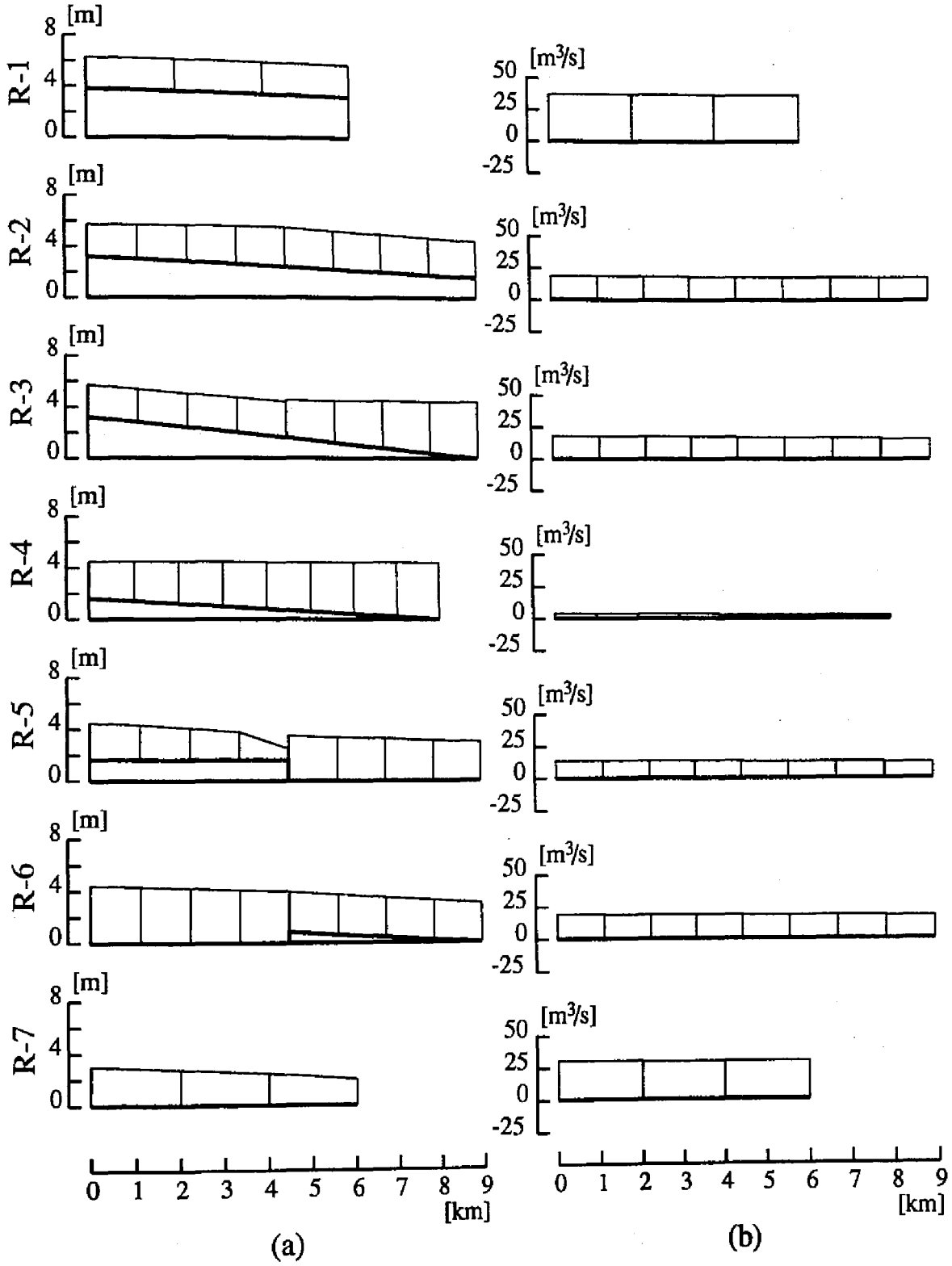

Figure 2.14: Calculated flow at $t = 19$[hour]: (a) Bed and water elevations; (b) Discharge

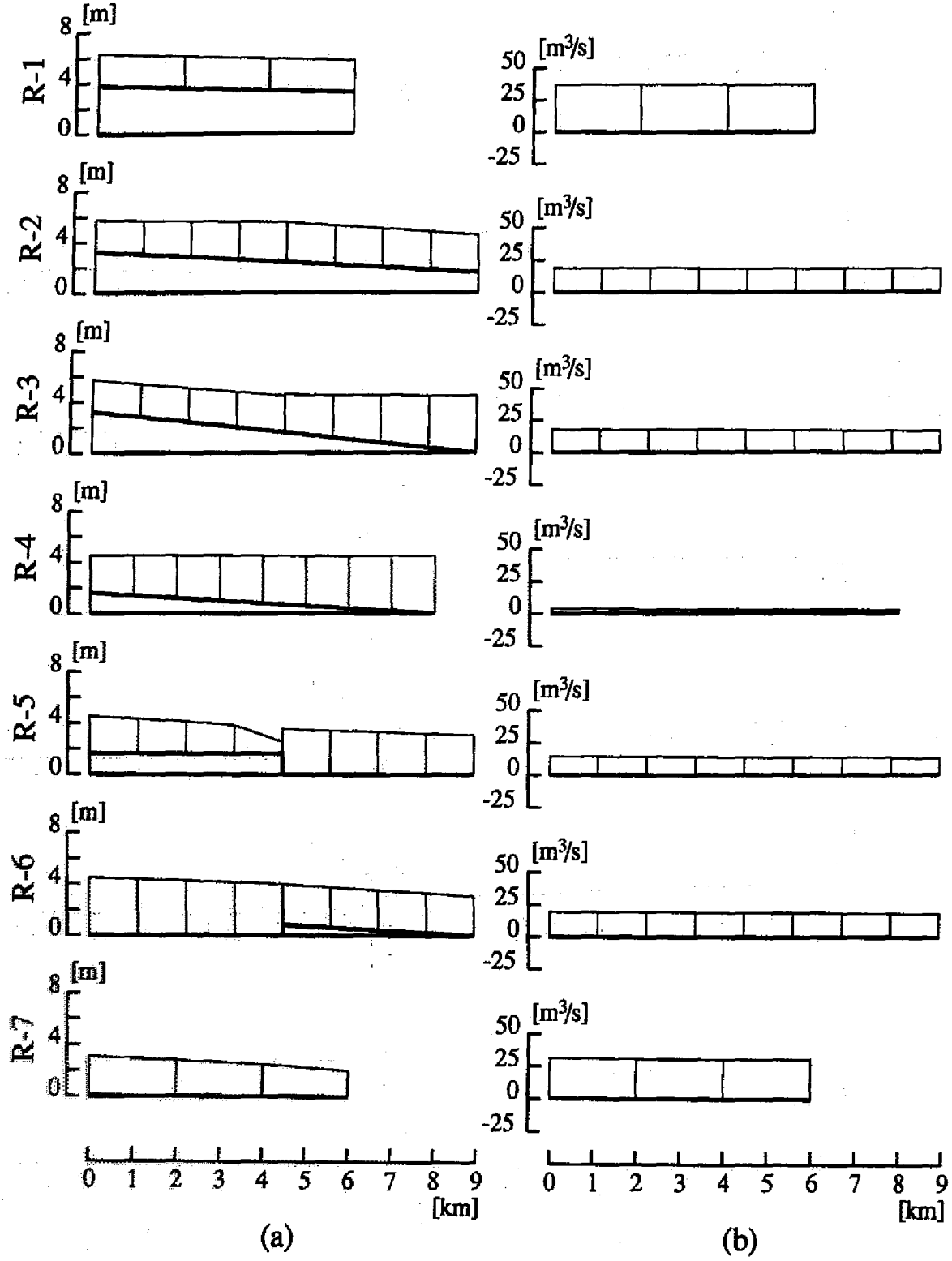

Figure 2.15: Calculated flow at $t = 24$[hour]: (a) Bed and water elevations; (b) Discharge

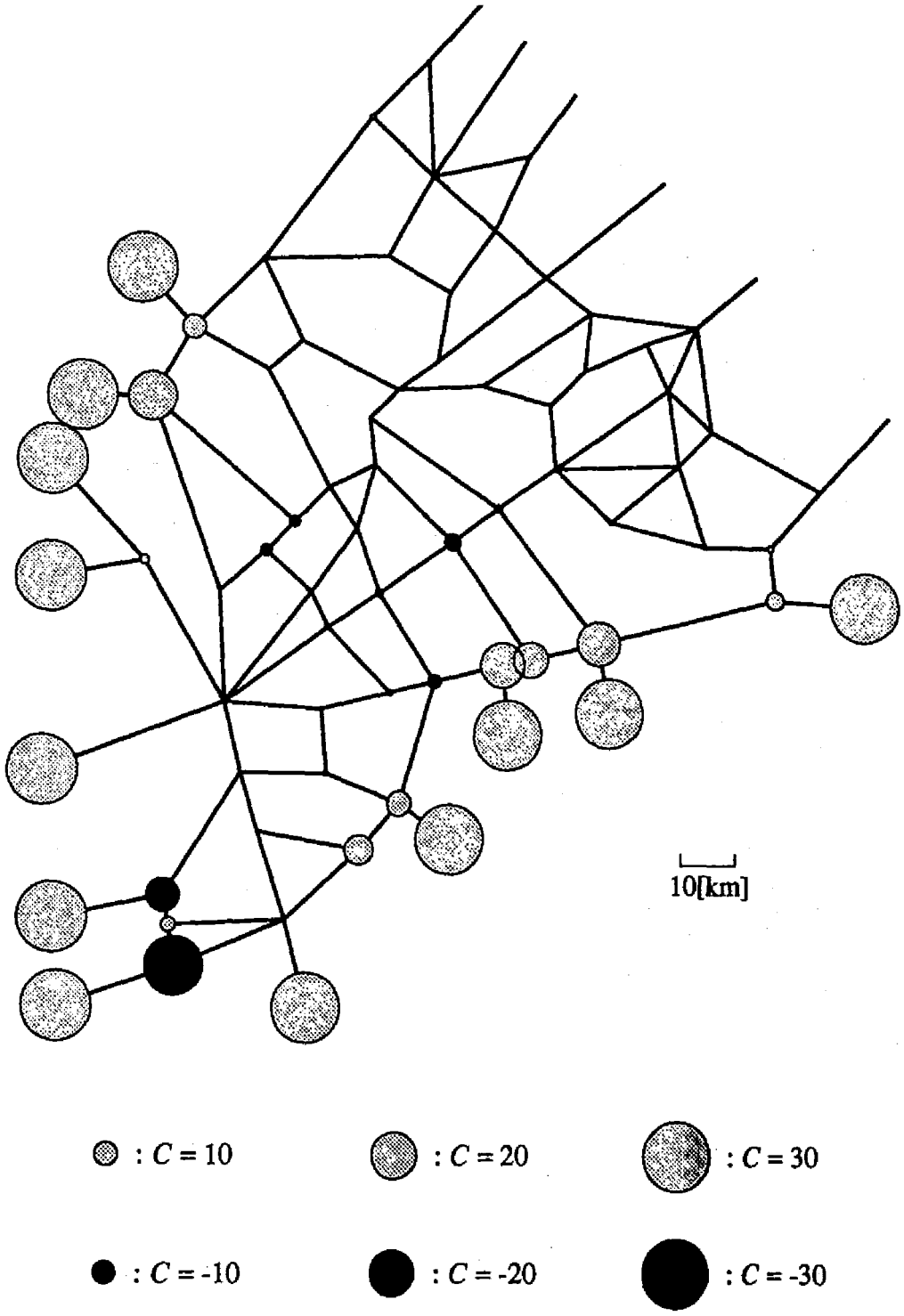

Figure 2.16: Solute concentration in steady state for $c = 0$

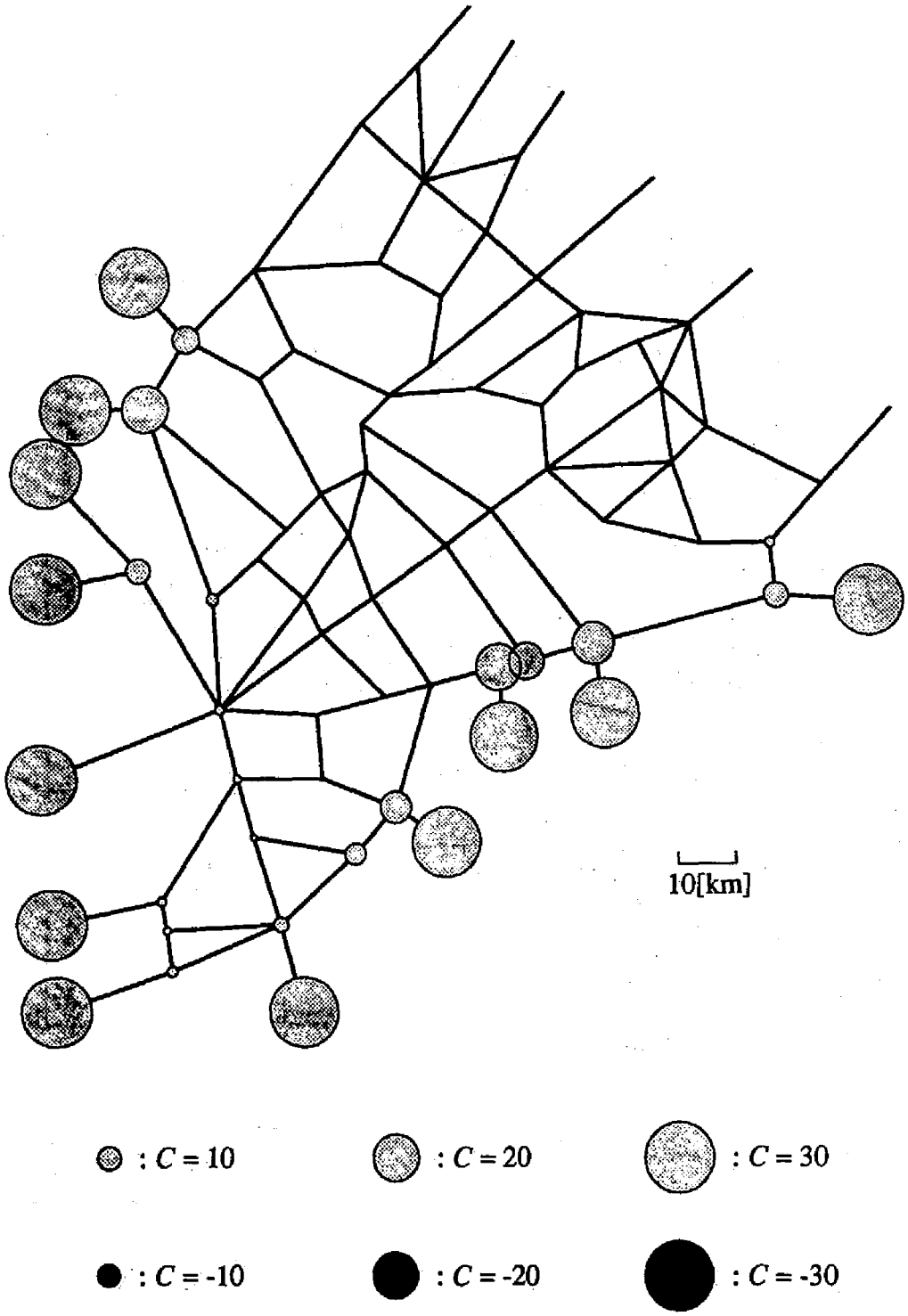

Figure 2.17: Solute concentration in steady state for $c = 1$

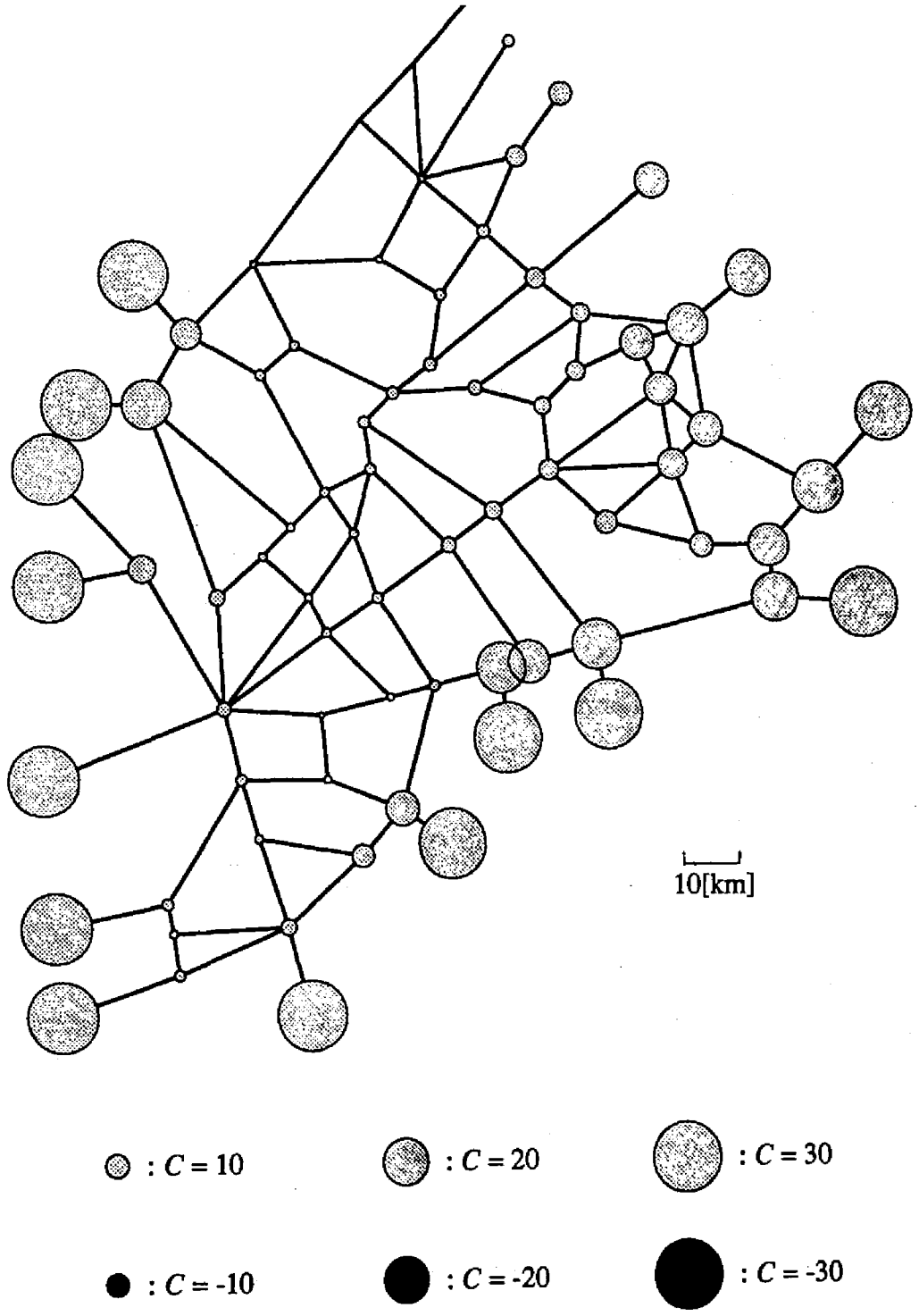

Figure 2.18: Solute concentration after 1 day

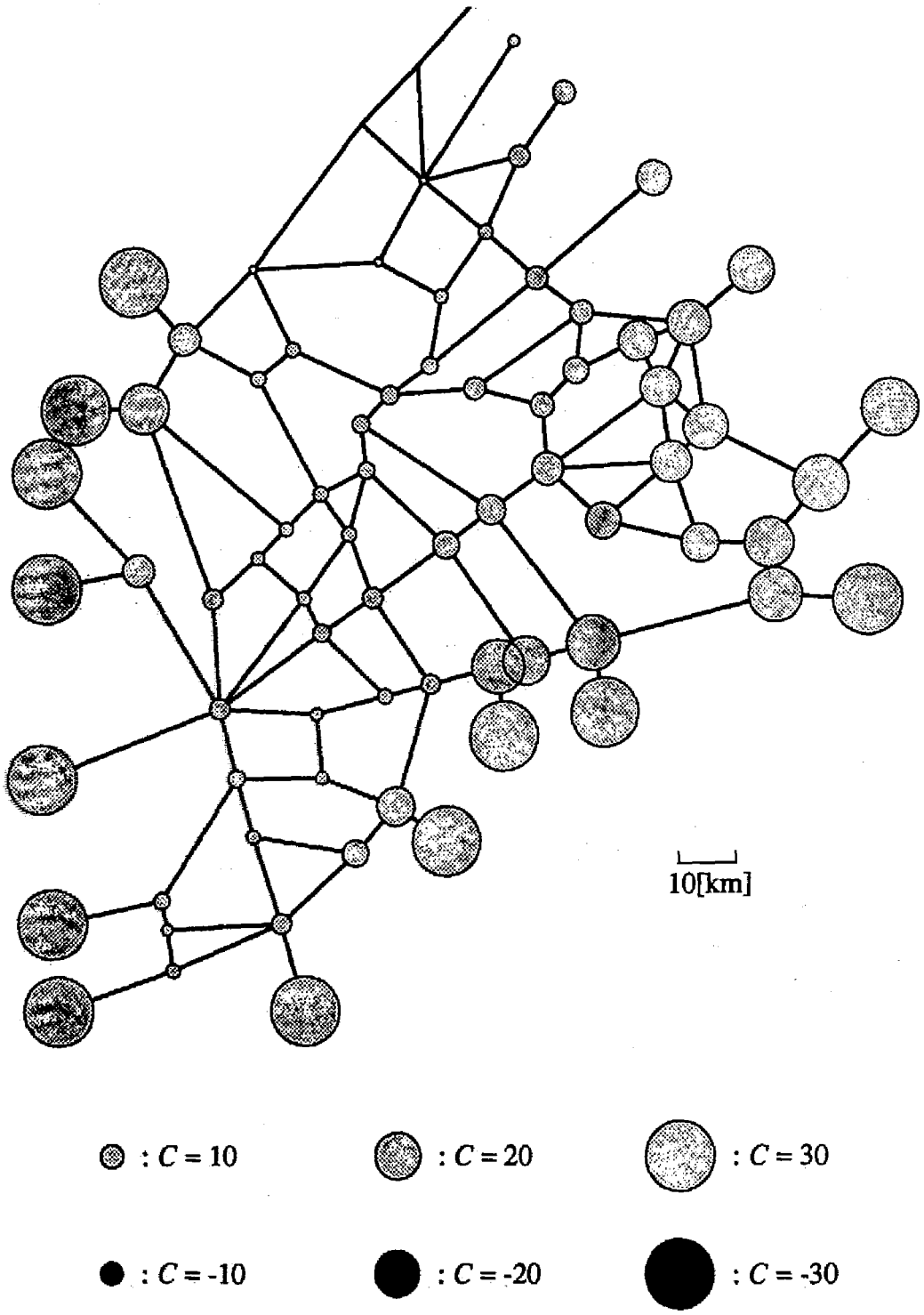

Figure 2.19: Solute concentration after 40 days

Chapter 3

Optimal Control of Open Channel Flows

3.1 Introduction

The ultimate purpose of hydraulic engineering is to provide information which is required in practical problems that arise in process of assessment, planning, design, and operation. Concerning water conveyance systems, researches ought to be focussed on not only simulating flows but also optimizing operational strategies, identifying channel parameters, and so on. Indeed Burt and Gartrell [12] summed up the usage of irrigation canal simulation models and pointed out that hundreds of trials in such models could develop control algorithms and operational strategies. Nevertheless, the establishment of rational approaches to these problems is a matter of urgency.

The gate stroking technique presented by Wylie [96] is to predetermine an operational strategy at the upstream discharge boundary in a single reach canal from prescribed initial and final conditions and downstream discharge boundary condition using the method of characteristics. Its practical application is reported by Falvey and Luning [25]. A finite difference scheme which is applicable to channel networks with branch junction is developed by Liu *et al.* [60]. This scheme is used for downstream control of canal systems (Liu *et al.* [61]; Liu *et al.* [62]). Other numerical procedures are compared by Bautista *et al.* [8]. The technique is interpreted mathematically as an exchange of time for space, where the original downstream boundary condition serves the initial condition in the Cauchy problem. Although the procedure does not prevent the well-posedness of the PDE in the sense of Petrovsky [75] because the PDE is hyperbolic, the operational strategy obtained may be of no practical use.

Defects of the gate stroking technique should dissolve in optimal control theory. Kawachi *et al.* [46] develop an optimal control model for determining release discharges of irrigation canals using the Pontryagin principle of maximum for ordinary differential equations.

However, the control theory for linear PDE deduced by Lions [59] can be extended to comprehensive control theory for nonlinear PDE so that more straightforward approach to optimization is available. In this context, each of the problems under discussion should be formulated as an optimal control problem which intends to minimize a functional determined by the solution to PDE system that depends on a control variable in a set of admissible control. Such a problem is characterized by the minimum principle which includes the adjoint problem of the PDE system. From this point of view, the minimization of residual from the targeted value in the solution of primitive Cauchy problem may take the place of the gate stroking techniques. Moreover, an identification problem is represented as an optimal control problem and efficiently solved with the use of adjoint problem, which Ligget and Chen [56] have already examined in the case of pipelines.

3.2 Formulation of optimal control problem

The governing equations of open channel network flows is rewritten in vector form as

$$\frac{\partial \mathbf{U}}{\partial t} + \frac{\partial \mathbf{F}}{\partial x} + \mathbf{S} = \mathbf{\Phi} \tag{3.1}$$

where $\mathbf{U}$ = conserved vector, $\mathbf{F}$ = flux vector, $\mathbf{S}$ = source vector, and $\mathbf{\Phi}$ = load vector, which are given by

$$\mathbf{U} = \begin{pmatrix} A \\ Q \end{pmatrix} \tag{3.2}$$

$$\mathbf{F} = \begin{pmatrix} Q \\ F_M \end{pmatrix} = \begin{pmatrix} Q \\ \dfrac{\alpha Q^2}{A} + g\displaystyle\int_0^h A(z)\,dz \end{pmatrix} \tag{3.3}$$

$$\mathbf{S} = \begin{pmatrix} 0 \\ S_M \end{pmatrix} = \begin{pmatrix} 0 \\ -g\displaystyle\int_0^h \frac{\partial A(z)}{\partial x}dz + gA\frac{\partial z_b}{\partial x} + gAS_f \end{pmatrix} \tag{3.4}$$

and

$$\mathbf{\Phi} = \begin{pmatrix} q \\ \varphi \end{pmatrix} \tag{3.5}$$

respectively. A well-posed problem requires that Eqn.(3.1) is equipped with an initial condition

$$\mathbf{y} = \mathbf{y}_0 \tag{3.6}$$

at $t = 0$ and a boundary condition

$$\mathbf{e} \cdot \mathbf{y}|_\Gamma = \tilde{b} \tag{3.7}$$

at $t > 0$, where $\mathbf{y}$ = state variable which is taken as $\begin{pmatrix} h \\ Q \end{pmatrix}$, $\mathbf{y}_0$ = specified initial value of $\mathbf{y}$, and $\mathbf{e} = \begin{pmatrix} \frac{\partial b}{\partial h} \\ \frac{\partial b}{\partial Q} \end{pmatrix}$. Without loss of generality, $\mathbf{e}$ is assumed unitary. Henceforth, the system defined by Eqns.(3.1) through (3.7) shall be referred to as the state system.

In the state system, the load vector $\mathbf{\Phi}$, the boundary condition, and the initial condition are externally specified though subject to certain constraints. Therefore, the whole of these is considered as the control variable $\mathbf{u}$ which is constrained in a set of admissible control U_{ad}, and controls the state system. Conversely, the control variable $\mathbf{u}$ is decomposed into contributions from the load vector $\mathbf{\Phi}$ in the domain, the boundary condition on the boundary, and the initial condition at the initial time.

An optimal control problem is formulated as the minimization problem of an appropriate functional, which depends on $\mathbf{u}$ and thus denoted by $J(\mathbf{u})$. A general form of the functional, which considers contribution of observation at the terminal time T, on the boundary, and in the domain, is given by

$$J(\mathbf{u}) = \frac{1}{2}\int_\Omega W(T)(\mathbf{y}(T) - \bar{\mathbf{y}}(T)) \cdot (\mathbf{y}(T) - \bar{\mathbf{y}}(T))\, dx + \frac{1}{2}\int_0^T \left[W(\mathbf{e}^\perp \cdot \mathbf{y} - \bar{y})^2\right]_\Gamma \, dt$$

$$+\frac{1}{2}\int_0^T \int_\Omega W(\mathbf{y} - \bar{\mathbf{y}}) \cdot (\mathbf{y} - \bar{\mathbf{y}})\, dx\, dt \tag{3.8}$$

where W = contribution factor which may depend on time and space, $\bar{\mathbf{y}}$ = targeted value of $\mathbf{y}$, $\bar{y}$ = targeted value of $\mathbf{e}^\perp \cdot \mathbf{y}$, and $\mathbf{e}^\perp$ = a unitary vector perpendicular to $\mathbf{e}$. A control variable $\mathbf{u}$ that satisfies

$$J(\mathbf{u}) = \inf_{\mathbf{u}_{ad} \in U_{ad}} J(\mathbf{u}_{ad}) \tag{3.9}$$

is referred to as an optimal control.

3.3 Minimum principle and adjoint system

The minimum principle which characterizes an optimal control is deduced in the framework of the variational calculus. The set of admissible control U_{ad} is assumed to be convex. A new variable, which is called the adjoint variable and denoted by $\boldsymbol{\lambda}$, is used for describing the minimum principle.

Suppose that $\mathbf{u}$ is an optimal control. If $\mathbf{u}$ is replaced by another one $\mathbf{u}^\varepsilon$ which is written as

$$\mathbf{u}^\varepsilon = \mathbf{u} + \varepsilon(\mathbf{u}_{ad} - \mathbf{u}),\ \mathbf{u}_{ad} \in U_{ad} \tag{3.10}$$

where ε = positive real number, then the functional to be minimized changes from $J(\mathbf{u})$ to $J(\mathbf{u}^\varepsilon)$. Defining $\delta J(\mathbf{u})$, the right hand derivative of $J(\mathbf{u})$ with respect to ε, as

$$\delta J(\mathbf{u}) = \lim_{\varepsilon \to +0} \frac{J(\mathbf{u}^\varepsilon) - J(\mathbf{u})}{\varepsilon} \tag{3.11}$$

the inequality

$$\delta J(\mathbf{u}) \geq 0 \tag{3.12}$$

holds for any $\mathbf{u}_{ad} \in U_{ad}$ because $J(\mathbf{u}^\varepsilon)$ is not less than $J(\mathbf{u})$.

Let $\mathbf{y}$ be the solution of the state system under the optimal control $\mathbf{u}$. If $\mathbf{u}$ is replaced by $\mathbf{u}^\varepsilon$, the state system should be also rewritten as

$$\frac{\partial \mathbf{U}^\varepsilon}{\partial t} + \frac{\partial \mathbf{F}^\varepsilon}{\partial x} + \mathbf{S}^\varepsilon = \mathbf{\Phi}^\varepsilon \tag{3.13}$$

with the initial condition

$$\mathbf{y}^\varepsilon = \mathbf{y}_0^\varepsilon \tag{3.14}$$

and the boundary condition

$$\mathbf{e} \cdot \mathbf{y}^\varepsilon|_\Gamma = \tilde{b}^\varepsilon \tag{3.15}$$

where superscript ε refers to the value when $\mathbf{u}^\varepsilon$ is chosen as the control variable. Subtracting Eqns.(3.1), (3.6), and (3.7) from Eqns.(3.13), (3.14), and (3.15), respectively, dividing

them by ϵ, and passing the limit ϵ to zero bring the partial differential equation

$$\frac{\partial \delta \mathbf{U}}{\partial t} + \frac{\partial \delta \mathbf{F}}{\partial x} + \delta \mathbf{S} = \delta \mathbf{\Phi} \tag{3.16}$$

with the initial condition

$$\delta \mathbf{y} = \delta \mathbf{y}_0 \tag{3.17}$$

and boundary condition

$$\mathbf{e} \cdot \delta \mathbf{y}|_\Gamma = \delta \tilde{b} \tag{3.18}$$

where the notation δ represents the right hand derivative with respect to ϵ as similarly defined as Eqn.(3.11).

The left hand side of Eqn.(3.16) multiplied by $\boldsymbol{\lambda}$ is integrated by parts as

$$\int_0^T \int_\Omega \boldsymbol{\lambda} \cdot \left(\frac{\partial \delta \mathbf{U}}{\partial t} + \frac{\partial \delta \mathbf{F}}{\partial x} + \delta \mathbf{S} \right) dx\, dt = \int_\Omega \left([\boldsymbol{\lambda} \cdot \delta \mathbf{U}]_0^T - \int_0^T \frac{\partial \boldsymbol{\lambda}}{\partial t} \cdot \delta \mathbf{U}\, dt \right) dx$$

$$+ \int_0^T \left([\boldsymbol{\lambda} \cdot \delta \mathbf{F}]_\Gamma - \int_\Omega \frac{\partial \boldsymbol{\lambda}}{\partial x} \cdot \delta \mathbf{F}\, dx \right) dt + \int_0^T \int_\Omega \boldsymbol{\lambda} \cdot \delta \mathbf{S}\, dx\, dt$$

$$= \int_\Omega \left[\left(\frac{\partial \mathbf{U}}{\partial \mathbf{y}} \right)^T \boldsymbol{\lambda} \cdot \delta \mathbf{y} \right]_0^T dx + \int_0^T \left[\left(\frac{\partial \mathbf{F}}{\partial \mathbf{y}} \right)^T \boldsymbol{\lambda} \cdot \delta \mathbf{y} \right]_\Gamma dt$$

$$- \int_0^T \int_\Omega \left(\left(\frac{\partial \mathbf{U}}{\partial \mathbf{y}} \right)^T \frac{\partial \boldsymbol{\lambda}}{\partial t} + \left(\frac{\partial \mathbf{F}}{\partial \mathbf{y}} \right)^T \frac{\partial \boldsymbol{\lambda}}{\partial x} - \left(\frac{\partial \mathbf{S}}{\partial \mathbf{y}} \right)^T \boldsymbol{\lambda} \right) \cdot \delta \mathbf{y}\, dx\, dt \tag{3.19}$$

on $\Omega \times [0, T]$. The rightest hand side of Eqn.(3.19) is equalized to the integral of the right hand side of Eqn.(3.16) multiplied by $\boldsymbol{\lambda}$ as

$$\delta J_T - \delta J_I + \delta J_B + \delta J_\Gamma - \delta J_\Omega = \delta J_D \tag{3.20}$$

where

$$\delta J_I = \int_\Omega \left(\frac{\partial \mathbf{U}}{\partial \mathbf{y}} \right)^T \boldsymbol{\lambda}(0) \cdot \delta \mathbf{y}_0\, dx \tag{3.21}$$

$$\delta J_T = \int_\Omega \left(\frac{\partial \mathbf{U}}{\partial \mathbf{y}}\right)^T \boldsymbol{\lambda}(T) \cdot \delta \mathbf{y}(T)\, dx \tag{3.22}$$

$$\delta J_B = \int_0^T \left[\left(\mathbf{e} \cdot \left(\frac{\partial \mathbf{F}}{\partial \mathbf{y}}\right)^T \boldsymbol{\lambda}\right) \delta \tilde{b}\right]_\Gamma dt \tag{3.23}$$

$$\delta J_\Gamma = \int_0^T \left[\left(\mathbf{e}^\perp \cdot \left(\frac{\partial \mathbf{F}}{\partial \mathbf{y}}\right)^T \boldsymbol{\lambda}\right) \left(\mathbf{e}^\perp \cdot \delta \mathbf{y}\right)\right]_\Gamma dt \tag{3.24}$$

$$\delta J_\Omega = \int_0^T \int_\Omega \left(\left(\frac{\partial \mathbf{U}}{\partial \mathbf{y}}\right)^T \frac{\partial \boldsymbol{\lambda}}{\partial t} + \left(\frac{\partial \mathbf{F}}{\partial \mathbf{y}}\right)^T \frac{\partial \boldsymbol{\lambda}}{\partial x} - \left(\frac{\partial \mathbf{S}}{\partial \mathbf{y}}\right)^T \boldsymbol{\lambda}\right) \cdot \delta \mathbf{y}\, dx\, dt \tag{3.25}$$

and

$$\delta J_D = \int_0^T \int_\Omega \boldsymbol{\lambda} \cdot \delta \Phi\, dx\, dt \tag{3.26}$$

using Eqns.(3.17) and (3.18).

Let the adjoint variable $\boldsymbol{\lambda}$ be governed by the adjoint PDE

$$\left(\frac{\partial \mathbf{U}}{\partial \mathbf{y}}\right)^T \frac{\partial \boldsymbol{\lambda}}{\partial t} + \left(\frac{\partial \mathbf{F}}{\partial \mathbf{y}}\right)^T \frac{\partial \boldsymbol{\lambda}}{\partial x} - \left(\frac{\partial \mathbf{S}}{\partial \mathbf{y}}\right)^T \boldsymbol{\lambda} = -W(\mathbf{y} - \bar{\mathbf{y}}) \tag{3.27}$$

with the terminal condition

$$\left(\frac{\partial \mathbf{U}}{\partial \mathbf{y}}\right)^T \boldsymbol{\lambda} = W\left(\mathbf{y}(T) - \bar{\mathbf{y}}(T)\right) \tag{3.28}$$

and the boundary condition

$$\mathbf{e}^\perp \cdot \left(\frac{\partial \mathbf{F}}{\partial \mathbf{y}}\right)^T \boldsymbol{\lambda}|_\Gamma = W\left(\mathbf{e}^\perp \cdot \mathbf{y}|_\Gamma - \bar{y}\right). \tag{3.29}$$

This system is referred to as the adjoint system. Substituting Eqns.(3.27), (3.28), and

(3.29) into Eqns.(3.25), (3.22), and (3.24), Eqn.(3.12) is reduced to the minimum principle

$$\delta J(\mathbf{u}) = \delta J_D + \delta J_I - \delta J_B \geq 0 \tag{3.30}$$

because $\delta J(\mathbf{u})$ is derived from the right hand side of Eqn.(3.8) as

$$\delta J(\mathbf{u}) = \int_\Omega W(T)(\mathbf{y}(T) - \bar{\mathbf{y}}(T)) \cdot \delta\mathbf{y}\, dx + \int_0^T \left[W(\mathbf{e}^\perp \cdot \mathbf{y} - \bar{y})(\mathbf{e}^\perp \cdot \delta\mathbf{y})\right]_\Gamma dt$$

$$+ \int_0^T \int_\Omega W(\mathbf{y} - \bar{\mathbf{y}}) \cdot \delta\mathbf{y}\, dx\, dt \tag{3.31}$$

which is equal to $\delta J_T + \delta J_\Gamma - \delta J_\Omega$.

It should be remarked that the adjoint variable $\boldsymbol{\lambda}$ contains the whole information to judge whether the control variable $\mathbf{u}$ is an optimal one or not. Therefore, the adjoint problem to solve the adjoint system, as well as the simulation problem to solve the state system, holds significance for approaching the optimal control problem.

3.4 Numerical scheme for adjoint system

Eqn.(3.27) consists of two equations

$$\frac{\partial A}{\partial h}\frac{\partial \lambda_1}{\partial t} + \left(-\frac{\alpha Q^2}{A^2}\frac{\partial A}{\partial h} + gA\right)\frac{\partial \lambda_2}{\partial x}$$

$$-\left(-g\frac{\partial A(h)}{\partial x} + g\frac{\partial A}{\partial h}\frac{\partial z_b}{\partial x} + g\frac{\partial (AS_f)}{\partial h}\right)\lambda_2 = -W_1(\mathbf{y} - \bar{\mathbf{y}}) \tag{3.32}$$

and

$$\frac{\partial \lambda_2}{\partial t} + \frac{\partial \lambda_1}{\partial x} + \frac{2\alpha Q}{A}\frac{\partial \lambda_2}{\partial x} - gA\frac{\partial S_f}{\partial Q}\lambda_2 = -W_2(\mathbf{y} - \bar{\mathbf{y}}) \tag{3.33}$$

where λ_1 and λ_2 = the first and the second components of $\boldsymbol{\lambda}$, and W_1 and W_2 = the first and the second rows of W. The finite element and the finite volume methods are used for the resolution of Eqns.(3.32) and (3.33), respectively. The weak form of Eqn.(3.32) is written as

$$\frac{d}{dt}\int_{\text{supp}\,\psi} \frac{\partial A}{\partial h}\lambda_1 \psi\, dx + \left[\left(-\frac{\alpha Q^2}{A^2}\frac{\partial A}{\partial h} + gA\right)\lambda_2 \psi\right]_\Gamma$$

$$-\int_{\text{supp}\,\psi}\left(\left(-\frac{\alpha Q^2}{A^2}\frac{\partial A}{\partial h}+gA\right)\frac{\partial \psi}{\partial x}+\left(\frac{2\alpha Q^2}{A^3}\left(\frac{\partial A}{\partial h}\right)^2-\frac{\alpha Q^2}{A^2}\frac{\partial^2 A}{\partial h^2}+g\frac{\partial A}{\partial h}\right)\frac{\partial h}{\partial x}\psi\right)\lambda_2\,dx$$

$$-\int_{\text{supp}\,\psi}\left(-g\frac{\partial A(h)}{\partial x}+g\frac{\partial A}{\partial h}\frac{\partial z_b}{\partial x}+g\frac{\partial (AS_f)}{\partial h}\right)\lambda_2\psi\,dx=\int_{\text{supp}\,\psi}-W_1\left(\mathbf{y}-\bar{\mathbf{y}}\right)\psi\,dx \tag{3.34}$$

whereas Eqn.(3.33) is integrated as

$$\frac{d}{dt}\int_{\Omega_i^e}\lambda_2\,dx+[\lambda_1]_{\Gamma_i^e}+\int_{\Omega_i^e}\left(\frac{2\alpha Q}{A}\frac{\partial \lambda_2}{\partial x}-gA\frac{\partial S_f}{\partial Q}\lambda_2\right)dx=\int_{\Omega_i^e}-W_2\left(\mathbf{y}-\bar{\mathbf{y}}\right)\,dx \tag{3.35}$$

over a generic i-th element Ω_i^e. A numerical model is obtained in the same manner as in the state system but $\dfrac{\partial \lambda_2}{\partial x}$ in Eqn.(3.35) has to be estimated in a special way. In order to do so, the values of λ_2 at the two boundaries of the $i-$th element is first estimated by

$$\lambda_{2i}^l=\frac{1}{2}\lambda_{2i}+\frac{1}{2}\sum_{j=1,\kappa_{ij}^l\neq i}^{\nu_i^l}\lambda_{2\kappa_{ij}^l}\cos\theta_{ij}^l \tag{3.36}$$

and

$$\lambda_{2i}^r=\frac{1}{2}\lambda_{2i}+\frac{1}{2}\sum_{j=1,\kappa_{ij}^r\neq i}^{\nu_i^r}\lambda_{2\kappa_{ij}^r}\cos\theta_{ij}^r \tag{3.37}$$

where $\lambda_{2i}=\lambda_2$ value in Ω_i^e, $\lambda_{2i}^l=$ estimated value of λ_2 at x_i^l, $\lambda_{2i}^r=$ estimated value of λ_2 at x_i^r, $\nu_i^l=$ the number of elements connected to x_i^l, $\nu_i^r=$ the number of elements connected to x_i^r, $\kappa_{ij}^l=$ element number of the $j-$th element connected to x_i^l, $\kappa_{ij}^r=$ element number of the $j-$th element connected to x_i^r, $\theta_{ij}^r=$ angle between Ω_i^e and $\Omega_{\kappa_{ij}^r}^e$, and $\theta_{ij}^l=$ angle between Ω_i^e and $\Omega_{\kappa_{ij}^l}^e$, but specified boundary values are used for boundary nodes. Then, the integration is performed as

$$\int_{\Omega_i^e}\frac{2\alpha Q}{A}\frac{\partial \lambda_2}{\partial x}\,dx=\alpha Q_i\left(\lambda_{2i}^r-\lambda_{2i}^l\right)\sum_{k=1}^{4}\frac{w_k}{A\left(\dfrac{1-c_k}{2}h_i^l+\dfrac{1+c_k}{2}h_i^r\right)} \tag{3.38}$$

using the 4-point Gauss quadrature rule.

3.5 Applications to hypothetical open channels

The numerical model is applied to the WB model shown in Figure 2.8. Setting the terminal time T as 24[hour], a boundary observation problem (Unami *et al.* [94]) and then a mixed observation problem are approached. A terminal time observation problem (Unami *et al.* [93]) in a different situation where the terminal time T is equal to 3[hour] is solved using an iterative procedure.

3.5.1 Boundary observation boundary control problem

An optimization problem that improves the operational strategy of release discharge Q at the discharge boundary Γ_1 is formulated. Thus the control variable $\mathbf{u}$ is defined as $Q|_{\Gamma_1}$ and assumed to be constrained in the set of admissible control $U_{ad} = [0, 50]$. The functional $J(\mathbf{u})$ is set as

$$J(\mathbf{u}) = \frac{1}{2}\int_0^T (Q - 10)^2|_{\Gamma_2}\, dt \tag{3.39}$$

to make the discharge Q at the water depth boundary Γ_2 close to 10.0[m^3/s]. The initial condition is the steady flow state with $\tilde{Q} = 30.0$[m^3/s], $\tilde{h} = 2.0$[m], and the lateral discharge is equal to -2.5[m^3/s] at every turnout. The gate is fully open so as not to affect the flow. The operational strategy is chosen as the same one as in the unsteady flow analysis in Chapter 2, where the control variable $\mathbf{u}$ is kept at 37.5[m^3/s] throughout the temporal domain $(0, T)$. This primitive strategy is referred to as the strategy <S-1> and results in excessive $Q|_{\Gamma_2}$ as plotted in Figure 3.2. Since Eqn.(3.30) defines the contribution of $\mathbf{u} = Q|_{\Gamma_1}$ to $\delta J(\mathbf{u})$, the value of $J(\mathbf{u})$ is expected to decrease when $\mathbf{u}$ decreases on a temporal subdomain where $\mathbf{e} \cdot \left(\frac{\partial \mathbf{F}}{\partial \mathbf{y}}\right)^T \boldsymbol{\lambda}$ at Γ_1, which is referred to as sensitivity, is positive and when $\mathbf{u}$ increases on a temporal subdomain where the sensitivity is negative. Referring to the sensitivity plotted in Figure 3.3, an improved strategy <S-2> can be given by changing $\mathbf{u}$ as shown in Figure 3.4, so that $Q|_{\Gamma_2}$ changes as shown in Figure 3.5. That change of strategy actually decreases the value of $J(\mathbf{u})$ from 19650 to 6640.0, though the strategy <S-2> is not an optimal control because the sensitivity for <S-2> depicted in Figure 3.6 does not satisfy the inequality Eqn.(3.30). Accordingly, the control variable $\mathbf{u}$ is changed again as the strategy <S-3> shown in Figure 3.7 and yields $Q|_{\Gamma_2}$ as plotted in Figure 3.8. The value of $J(\mathbf{u})$ becomes as small as 4085.6, and the sensitivity is damped down as shown in Figure 3.9. Thus, the strategy <S-3> is considered close to an optimal control.

3.5.2 Mixed observation domain control problem

Next, the control variable $\mathbf{u}$ is changed to φ, which is dominated by the gate opening, and sensitivity becomes λ_2. The functional $J(\mathbf{u})$ is also reset as

$$J(\mathbf{u}) = \frac{1}{2}\int_\Omega \begin{pmatrix} 1 & 0 \\ 0 & 1 \end{pmatrix} (\mathbf{y}(T) - \mathbf{y}_0) \cdot (\mathbf{y}(T) - \mathbf{y}_0)\, dx + \frac{1}{2}\int_0^T (Q-10)^2|_{\Gamma_2}\, dt$$

$$+\frac{1}{2}\int_{6[\text{hour}]}^{18[\text{hour}]} \int_\Omega \begin{pmatrix} 100\delta(x-x_q) & 0 \\ 0 & 0 \end{pmatrix} \left(\mathbf{y} - \begin{pmatrix} 2 \\ 0 \end{pmatrix}\right) \cdot \left(\mathbf{y} - \begin{pmatrix} 2 \\ 0 \end{pmatrix}\right) dx\, dt \qquad (3.40)$$

where $\hat{\delta}$ = Dirac's delta function, and x_q = the spatial point on which the turnout T-5 is located, to formulate a mixed observation domain control problem. In this functional, two terms are added to the one in the previous problem in order to sustain the terminal value of $\mathbf{y}$ and the water depth at the turnout T-5 between 6[hour] and 18[hour] close to the initial value $\mathbf{y}_0$ and 2.0[m], respectively. Sensitivity under the strategy <S-3> is shown in Figure 3.10 and suggests that φ should be smaller approximately between 5[hour] and 18[hour]. However, the sensitivity fluctuates after t = 22[hour] and does not clearly indicate the contribution of φ to the terminal value. Therefore, a revised strategy <S-4> is determined as shown in Figure 3.11. The strategy <S-4> anticipates the domain observation from t = 6[hour] at t = 5[hour]. The terms of the functional, which are equal to 661.61, 4085.6, and 2545.5, respectively, in the strategy <S-3>, change to 658.12, 3869.0, and 635.06, respectively, in the strategy <S-4>. In total, the value of $J(\mathbf{u})$ decreases from 7292.7 to 5162.2. The calculated flow depths and discharges under the strategy <S-4> at t = 1[hour], 7[hour], 13[hour], 19[hour], and 24[hour] are shown in Figures 3.13, 3.14, 3.15, 3.16, and 3.17, respectively. In comparison with the results given in Chapter 2, which is under the strategy <S-1>, these results exhibit much unsteadiness in flow.

3.5.3 Terminal time observation domain control problem

A transient flow from the initial steady state to another is controlled using the functional

$$J(\mathbf{u}) = \frac{1}{2}\int_\Omega \begin{pmatrix} 1 & 0 \\ 0 & 1 \end{pmatrix} (\mathbf{y}(T) - \mathbf{y}_T) \cdot (\mathbf{y}(T) - \mathbf{y}_T)\, dx \qquad (3.41)$$

where $\mathbf{y}_T$ = targeted value of $\mathbf{y}$ in a steady state, where no water is withdrawn from the 8 turnouts. The terminal time T is reset as 3[hour]. The lateral discharges at the 8 turnouts are iteratively revised to minimize the functional $J(\mathbf{u})$. The iteration procedure is to adding the value of λ_1, the sensitivity in this case, multiplied by a relaxation parameter α_q to the earlier value of q at each turnout. From the initial guess where q = 0 at all

turnouts, 20 iterations are executed with $\alpha_q = 0.3$. The hysteresis of the functional value is summarized in Table 3.1. In $\mathbf{y}$ obtained after 20 iterations, the errors from $\mathbf{y}_T$ in water depth h and discharge Q are less than 0.133[m] and 1.590[m^3/s], respectively. The strategy of q at each turnout, as shown in Figure 3.18, is skilled but practically realizable. Therefore, this iteration procedure is considered to give an efficient and effective approach to an optimal control.

Table 3.1: Hysteresis of Functional Value

Iteration number	Value of $J(\mathbf{u})$
0	318.8
1	78.04
2	56.46
3	43.28
4	35.02
5	28.66
6	23.92
7	20.22
8	17.35
9	15.08
10	13.29
11	11.86
12	10.71
13	9.777
14	9.019
15	8.397
16	7.882
17	7.452
18	7.090
19	6.782
20	6.517

3.6 Conclusions

Comprehensive synthesis of optimal control problems in open channel flows is presented in the framework of the variational calculus. The minimum principle which characterizes an optimal control is described using the adjoint system. The numerical scheme is developed to solve the adjoint system introducing the special interpolation procedure for the discretized adjoint variable. The boundary observation boundary control problem, the mixed observation domain control problem, and the terminal time observation domain

control problem are demonstratively solved to point out the assignment of the adjoint system in optimization procedure.

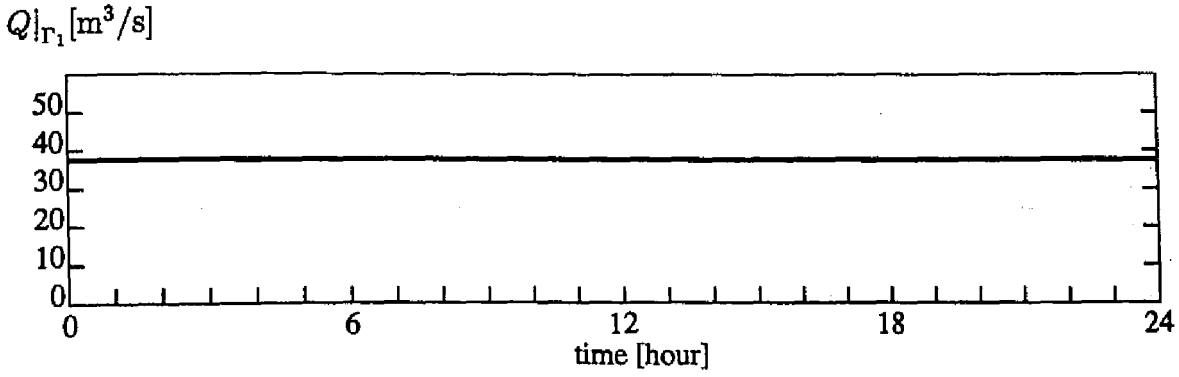

Figure 3.1: Specified discharge at Γ_1 in <S-1>

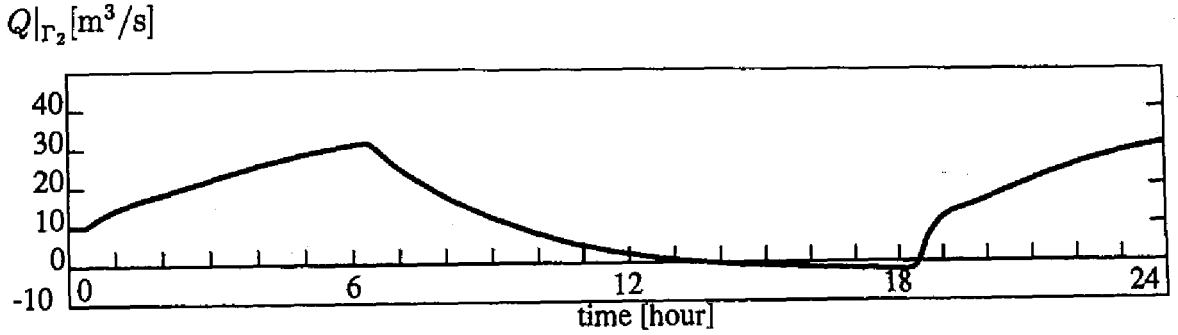

Figure 3.2: Resulting discharge at Γ_2 in <S-1>

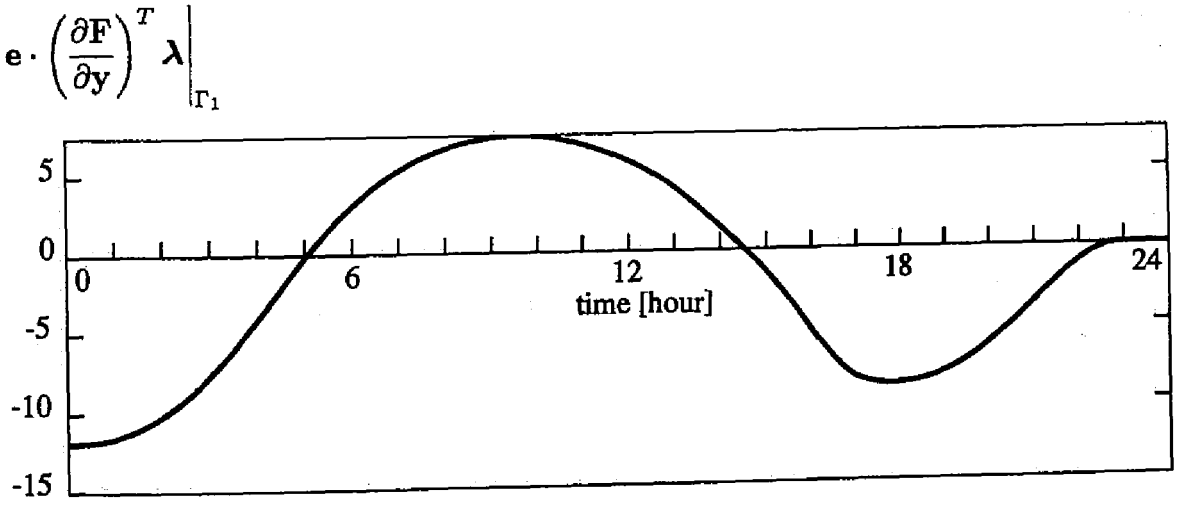

Figure 3.3: Sensitivity at Γ_1 in <S-1>

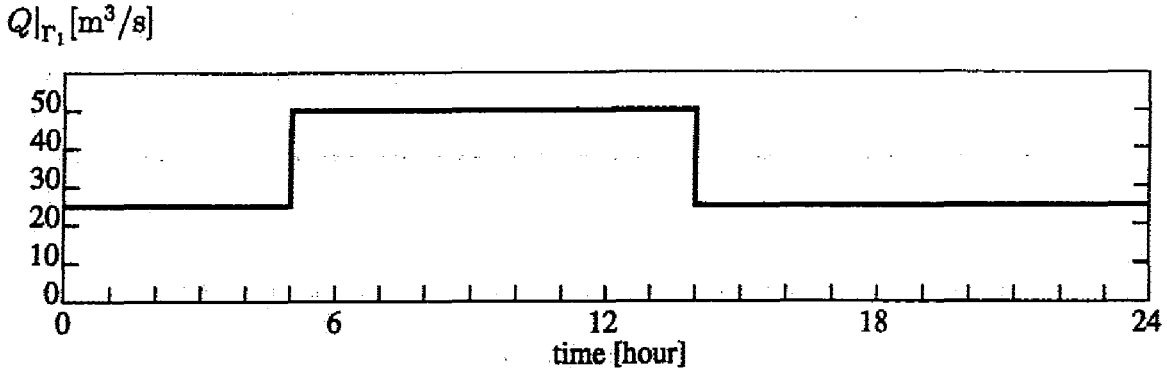

Figure 3.4: Specified discharge at Γ_1 in <S-2>

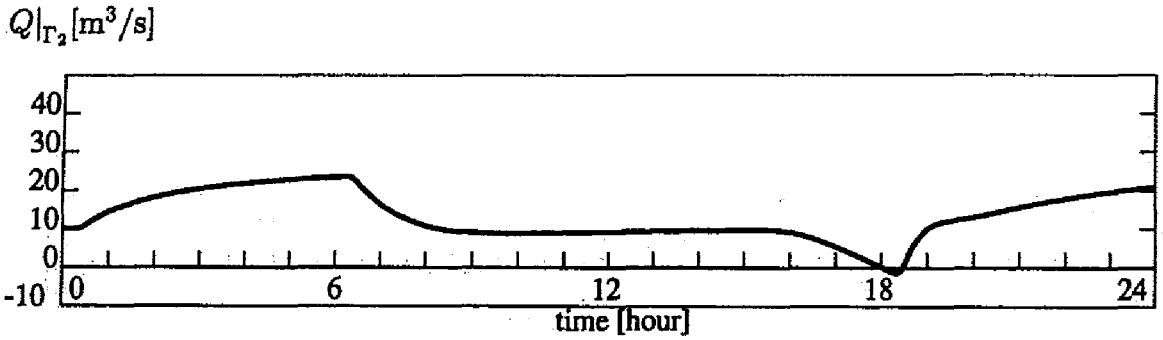

Figure 3.5: Resulting discharge at Γ_2 in <S-2>

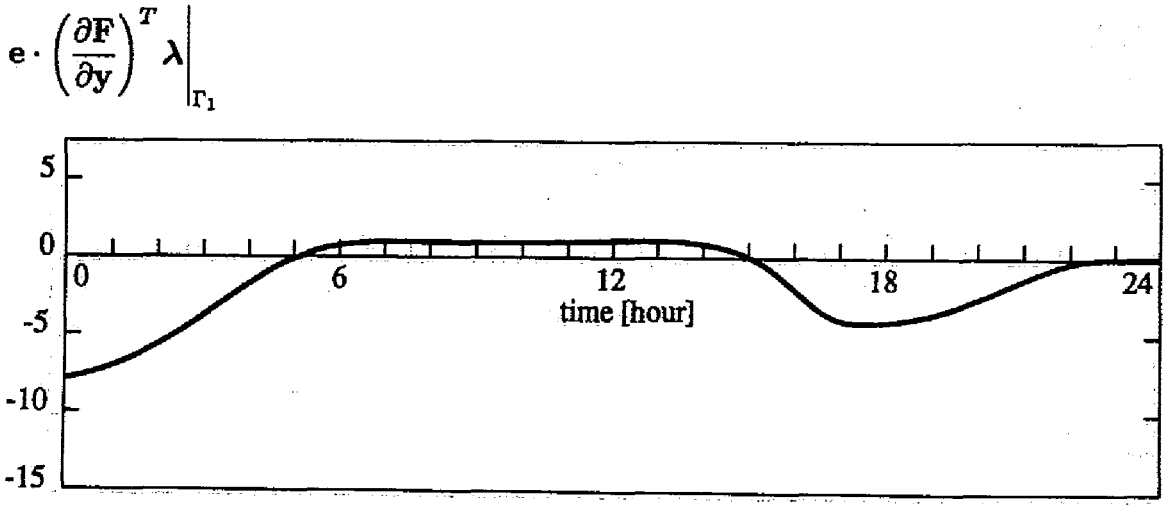

Figure 3.6: Sensitivity at Γ_1 in <S-2>

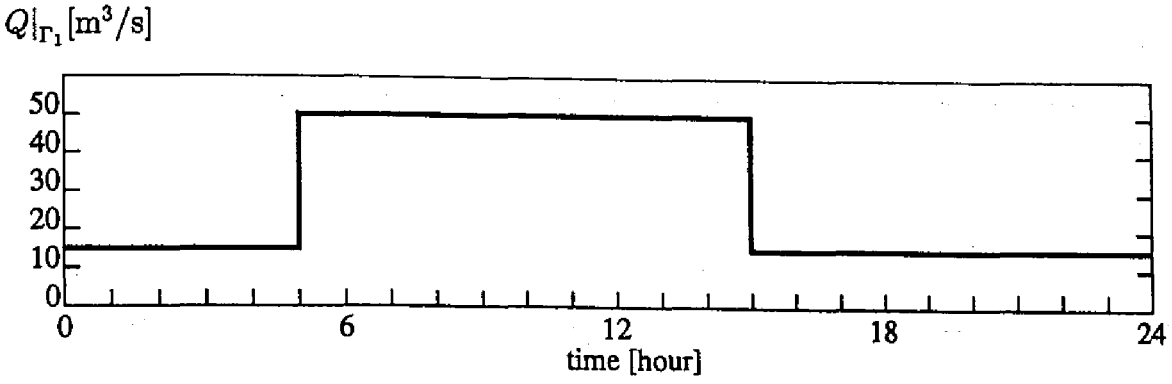

Figure 3.7: Specified discharge at Γ_1 in <S-3>

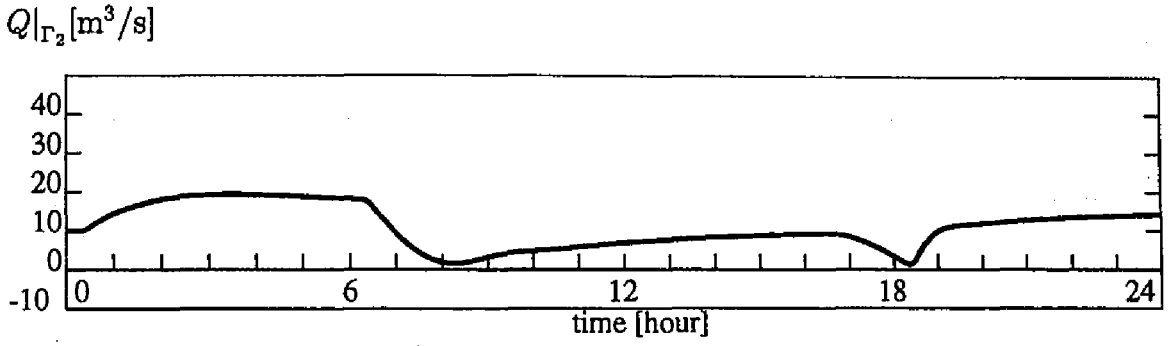

Figure 3.8: Resulting discharge at Γ_2 in <S-3>

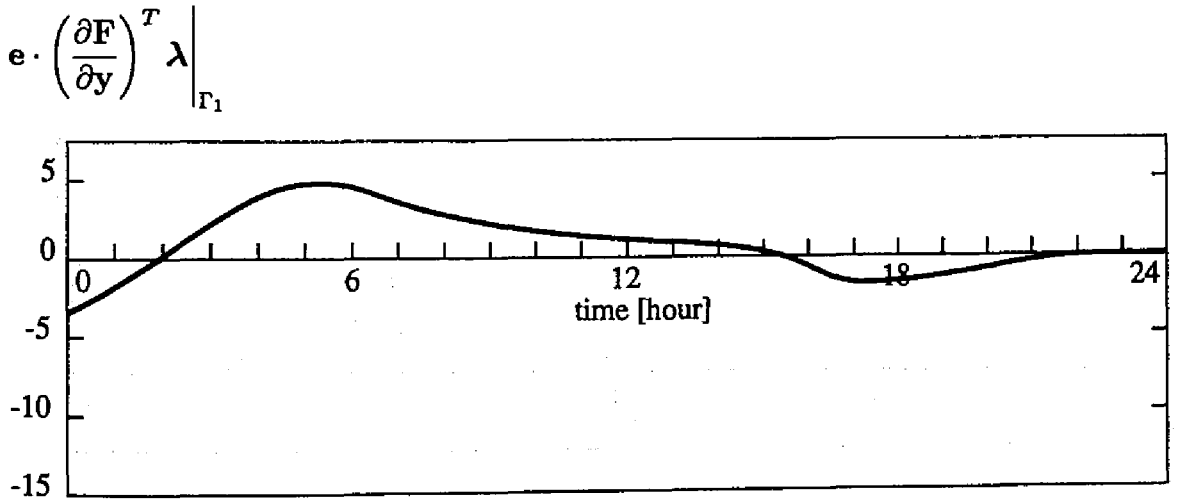

Figure 3.9: Sensitivity at Γ_1 in <S-3>

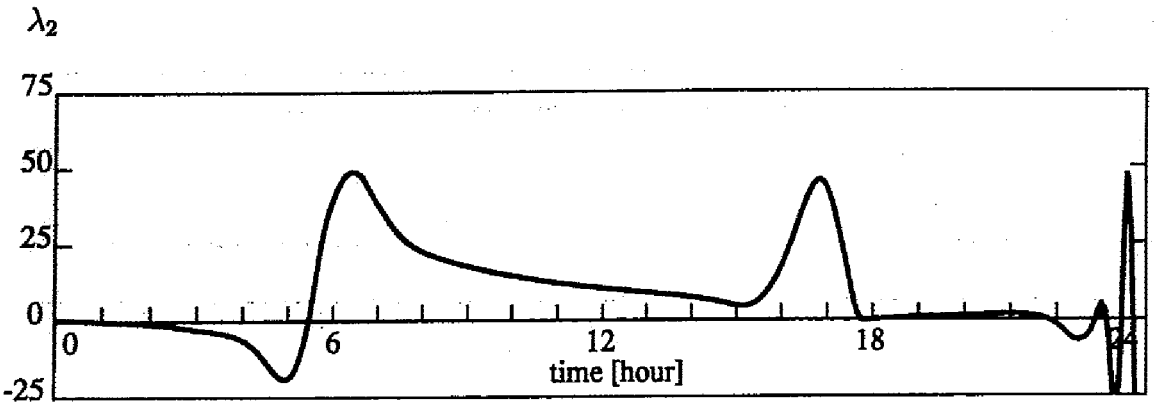

Figure 3.10: Sensitivity at the gate in <S-3>

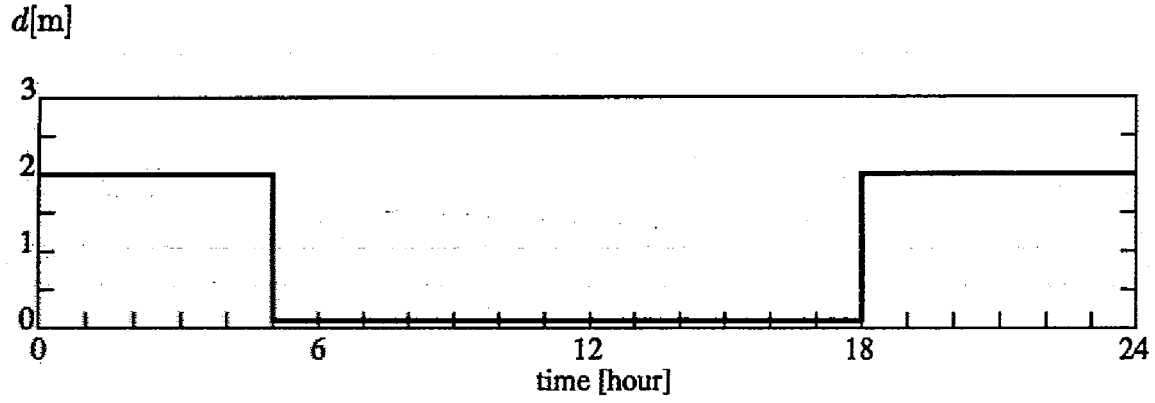

Figure 3.11: Specified gate opening in <S-4>

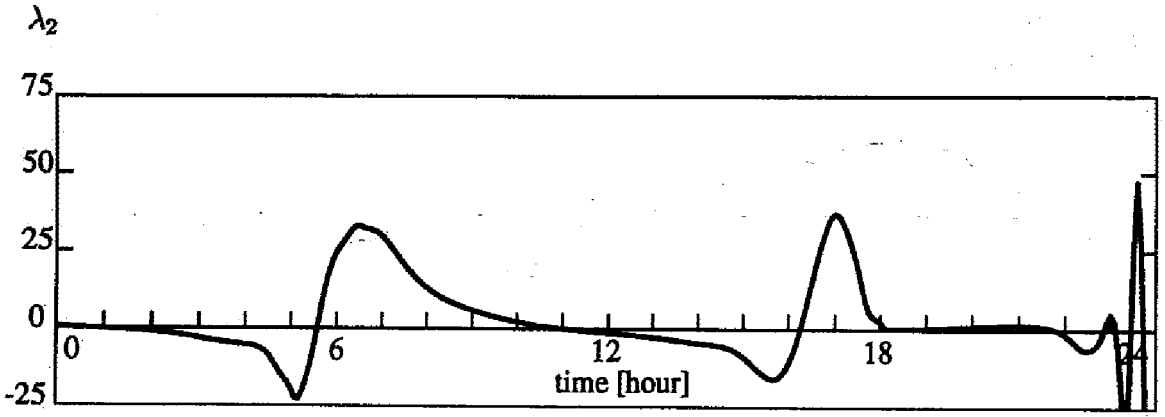

Figure 3.12: Sensitivity at the gate in <S-4>

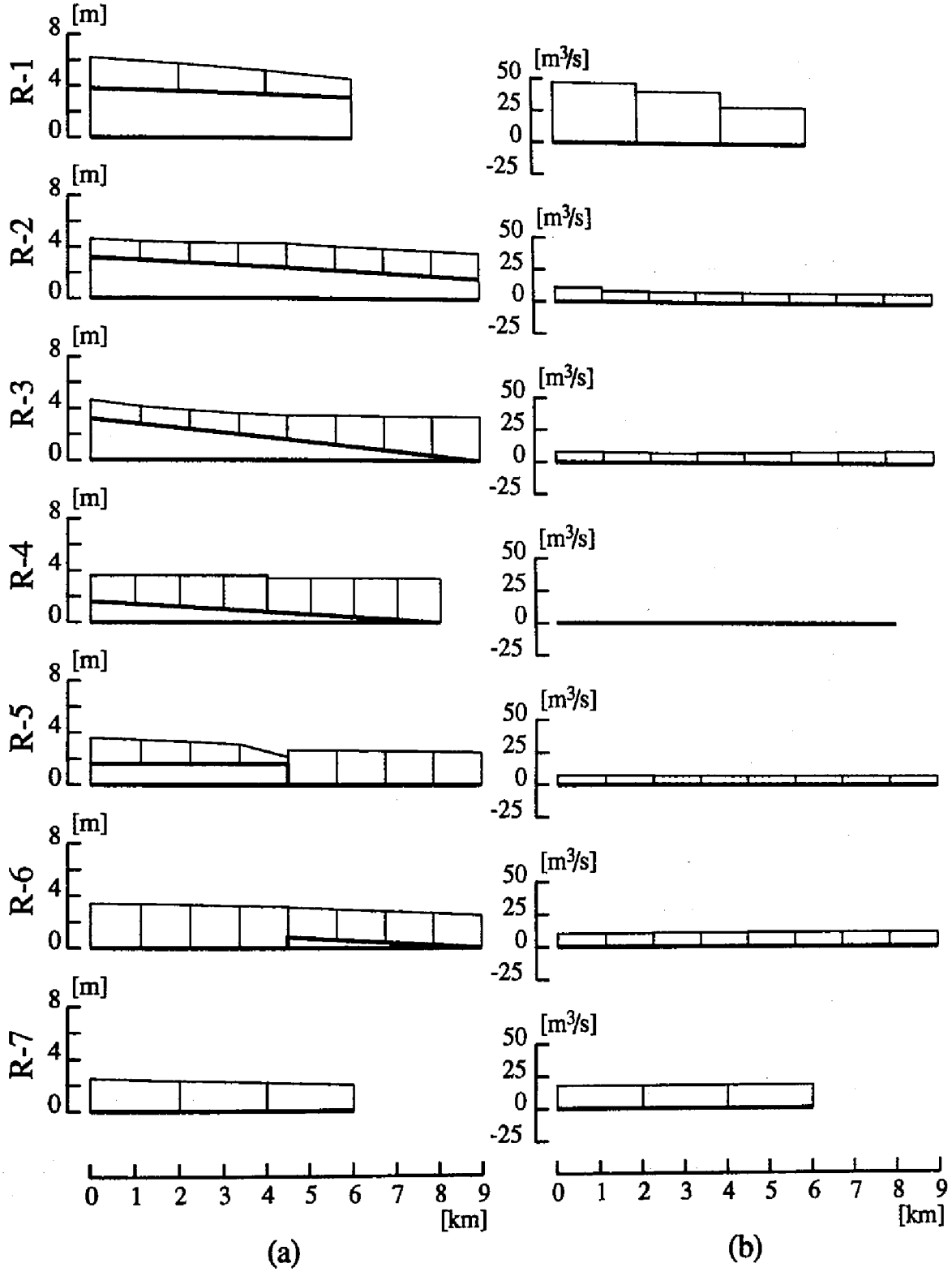

Figure 3.13: Calculated flow at $t = 1$[hour]: (a) Bed and water elevations; (b) Discharge

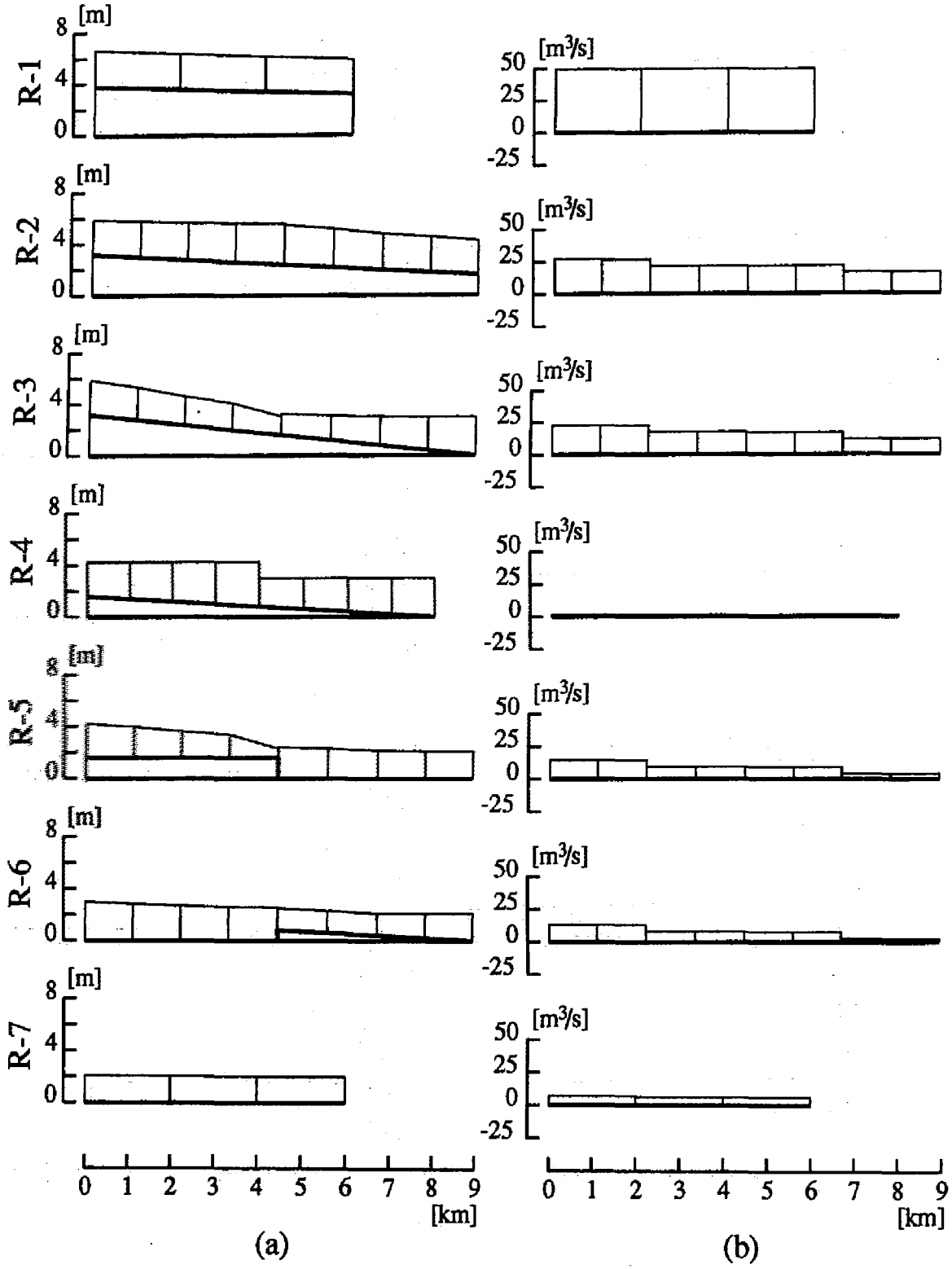

Figure 3.14: Calculated flow at $t = 7$[hour]: (a) Bed and water elevations; (b) Discharge

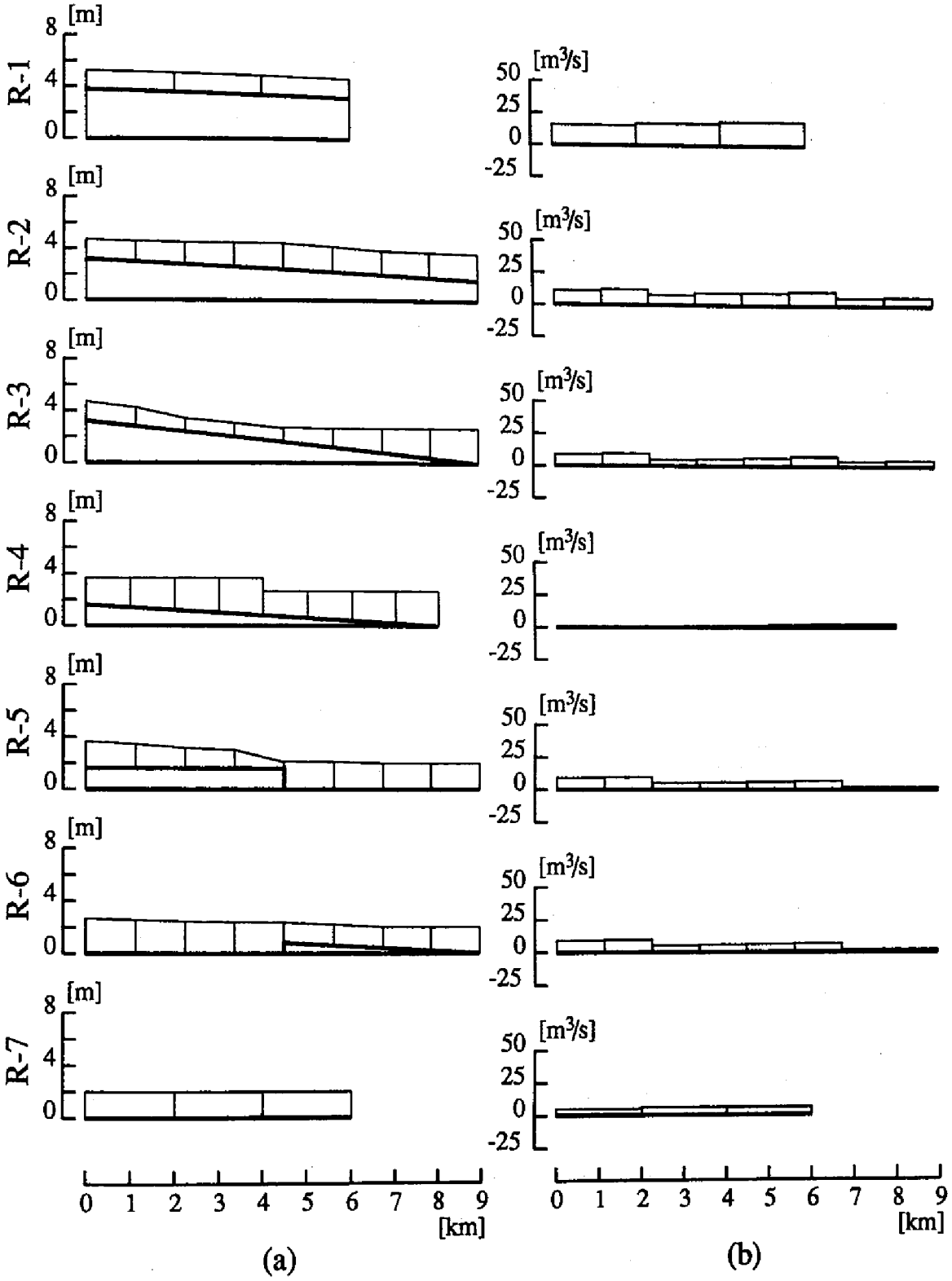

Figure 3.15: Calculated flow at $t = 13$[hour]: (a) Bed and water elevations; (b) Discharge

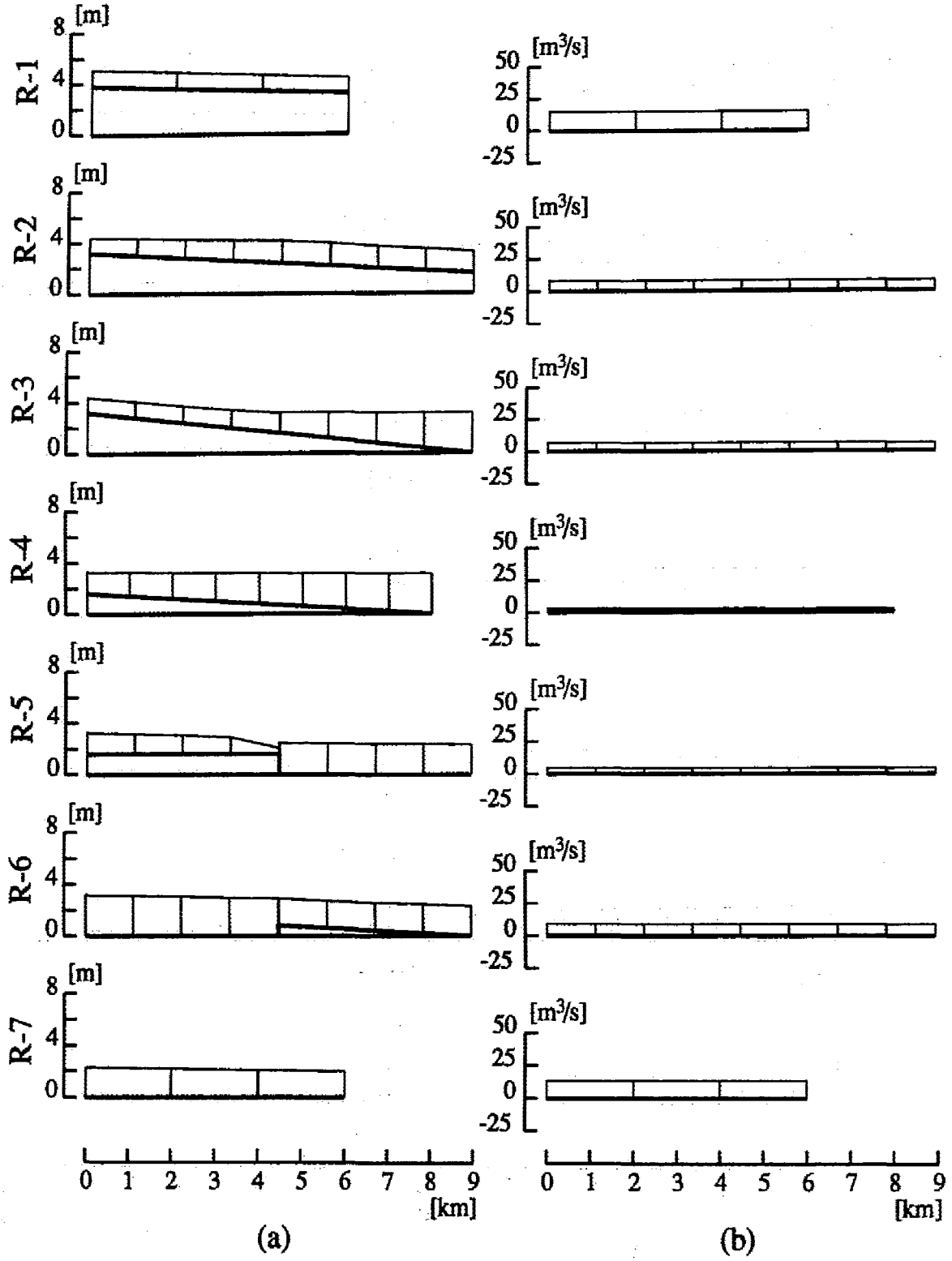

Figure 3.16: Calculated flow at $t = 19$[hour]: (a) Bed and water elevations; (b) Discharge

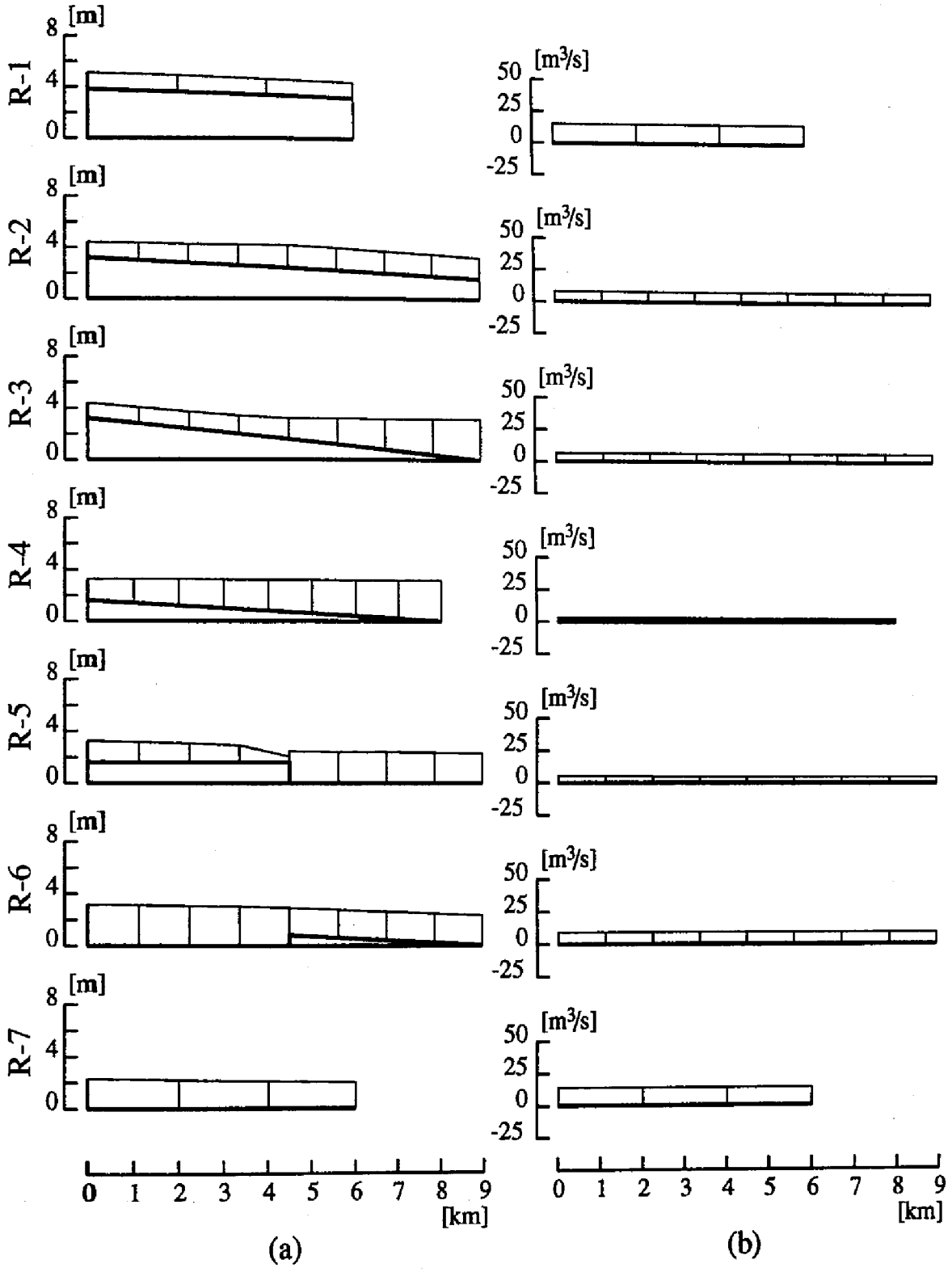

Figure 3.17: Calculated flow at $t = 24$[hour]: (a) Bed and water elevations; (b) Discharge

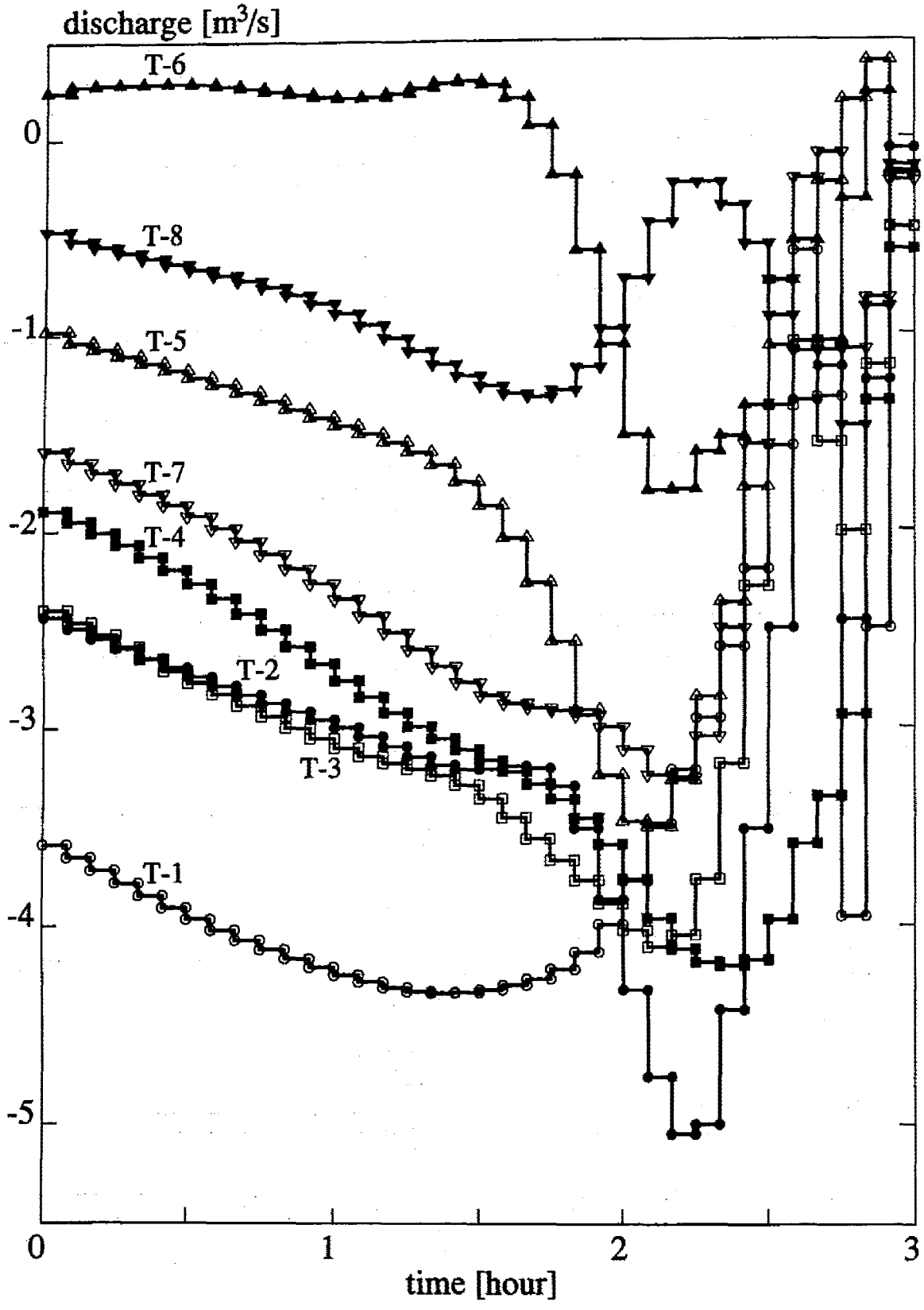

Figure 3.18: Strategy of q at each turnout obtained after 20 iterations

Chapter 4

Reliability Analysis in Markov Process Model

4.1 Introduction

In a water conveyance system where the disturbance of water demand is not predictable and satisfactory operational strategy cannot be established, the steady flow analysis based on the discharge data obtained from the averaged water demand is the principal tool for the hydraulic design of the system. Then, the statistical characteristics of water demand in such a system raise an inverse problem, that is the question whether the steady flow surface profile for the mean value is sufficiently reliable if the water demanded stochastically is actually withdrawn from the turnout.

Statistical approach that predicts the reliability of a system is just developing in the realm of irrigation engineering despite being the orthodox one in the drainage engineering (Easa [23]; Easa [24]; Gates and Al-Zahrani [28]; Gates and Al-Zahrani [29]; Zoppou and Li [99]). Gates *et al.* [30] propose an optimal design criterion of structural parameters in an irrigation delivery system under various environmental uncertainties such as precipitation, cross-section geometry, or management practices, where the optimizations are performed by the Monte Carlo simulations. This method is extended by Alshaikh and Taher [4]. Gupta *et al.* [32] assess the reliability of pipeline water distribution systems that depends on the pipe break and pump failure. This concept of reliability can be transplanted to the open channels, because these accidents are considered equivalents for disturbances, which are due to stochastic characteristics of lateral discharges, in the steady flow.

The reliability of water conveyance system under uncertain water demand might be evaluated by the Monte Carlo simulations. However, demand patterns will be significantly many in a system with numerous turnouts. In this chapter, assuming that an averaged demand pattern determines an averaged steady flow surface profile, propriety of the steady state is discussed in the framework of theoretical statistics coupled with the unsteady flow

dynamics (Unami *et al.* [95]). The reliability is defined by the probability that surface profile disturbed from the steady state by the fluctuation of water demand remains in a prescribed allowable domain through a specified examination period. The knowledge of the interdependence of the reliability, the allowable domain, and the examination period is demonstratively applied to a hypothetical irrigation system so as to determine allowable surface domains warranted by a lower bound of the reliability.

4.2 Markov process model

The disturbance of the lateral discharge q causes deviation of the surface profile which is represented by $\mathbf{h}$ in the flow model. Therefore, the N_N-dimensional vector $\mathbf{h}$ is assigned to the stochastic variable in the Markov process model.

It is natural to assume that $\mathbf{h}$ as a function of t is a Markov process, i.e., that $P(t, \mathbf{h}, t^+, \mathcal{G})$, the transition probability that $\mathbf{h}^+$ is found inside of $\mathcal{G}$, any subset of N_N-dimensional real Euclidean space $\mathbb{R}^{N_N}$, at time t^+ provided $\mathbf{h} = \mathbf{h}$ is observed at time $t < t^+$, does not depends on $\mathbf{h}$ at any time before t. Under this assumption, the probability density function $p = p(t, \mathbf{h}, t^+, \mathbf{h}^+)$ defined by

$$P(t, \mathbf{h}, t^+, \mathcal{G}) = \int_{\mathcal{G}} p(t, \mathbf{h}, t^+, \mathbf{h}^+) d\mathbf{h}^+ \tag{4.1}$$

satisfies the Chapman-Kolmogorov's equation

$$p(t, \mathbf{h}, t^+, \mathbf{h}^+) = \int_{\mathbb{R}^{N_N}} p(t, \mathbf{h}, t^*, \mathbf{h}^*) p(t^*, \mathbf{h}^*, t^+, \mathbf{h}^+) d\mathbf{h}^* \tag{4.2}$$

for $\mathbf{h}^*$ at time $t < t^* < t^+$. Considering Eqn.(4.2) and the stochastic continuity equation

$$P\left(t, \mathbf{h}, t^*, \mathbb{R}^{N_N}\right) = 1 \tag{4.3}$$

the temporal difference quotient of p can be expanded as

$$\begin{aligned}
&\frac{p(t, \mathbf{h}, t^+, \mathbf{h}^+) - p(t^*, \mathbf{h}, t^+, \mathbf{h}^+)}{t^* - t} \\
&= \frac{1}{t^* - t} \left(\int_{\mathbb{R}^{N_N}} p(t, \mathbf{h}, t^*, \mathbf{h})^* p(t^*, \mathbf{h}^*, t^+, \mathbf{h}^+) d\mathbf{h}^* - p(t^*, \mathbf{h}, t^+, \mathbf{h}^+) \int_{\mathbb{R}^{N_N}} p(t, \mathbf{h}, t^*, \mathbf{h}^*) d\mathbf{h}^* \right) \\
&= \frac{1}{t^* - t} \int_{\mathbb{R}^{N_N}} \left(p(t^*, \mathbf{h}^*, t^+, \mathbf{h}^+) - p(t^*, \mathbf{h}, t^+, \mathbf{h}^+) \right) p(t, \mathbf{h}, t^*, \mathbf{h}^*) d\mathbf{h}^* \\
&= \frac{1}{t^* - t} \int_{\|\mathbf{h}^* - \mathbf{h}\| \geq \varepsilon} \left(p(t^*, \mathbf{h}^*, t^+, \mathbf{h}^+) - p(t^*, \mathbf{h}, t^+, \mathbf{h}^+) \right) p(t, \mathbf{h}, t^*, \mathbf{h}^*) d\mathbf{h}^*
\end{aligned}$$

$$+\frac{1}{t^*-t}\sum_{i=1}^{N_N}\frac{\partial p(t^*,\mathbf{h},t^+,\mathbf{h}^+)}{\partial h_i}\int_{\|\mathbf{h}^*-\mathbf{h}\|<\varepsilon}(h_i^*-h_i)p(t,\mathbf{h},t^*,\mathbf{h}^*)d\mathbf{h}^*$$

$$+\frac{1}{t^*-t}\sum_{i,j=1}^{N_N}\frac{1}{2}\frac{\partial^2 p(t^*,\mathbf{h},t^+,\mathbf{h}^+)}{\partial h_i h_j}\int_{\|\mathbf{h}^*-\mathbf{h}\|<\varepsilon}(h_i^*-h_i)(h_j^*-h_j)p(t,\mathbf{h},t^*,\mathbf{h}^*)d\mathbf{h}^*$$

$$+\frac{1}{t^*-t}\sum_{i,j=1}^{N_N}\frac{1}{2}\frac{\partial^2 p(t^*,\mathbf{h},t^+,\mathbf{h}^+)}{\partial h_i h_j}\int_{\|\mathbf{h}^*-\mathbf{h}\|<\varepsilon}o\left(\|\mathbf{h}^*-\mathbf{h}\|^2\right)p(t,\mathbf{h},t^*,\mathbf{h}^*)d\mathbf{h}^* \tag{4.4}$$

where o denotes infinitesimal and ε is taken small enough. Thus, p is governed by the FPPDE

$$\frac{\partial p}{\partial t}+\sum_{i,j=1}^{N_N}d_{ij}\frac{\partial^2 p}{\partial h_i\partial h_j}+\sum_{i=1}^{N_N}d_i\frac{\partial p}{\partial h_i}=0 \tag{4.5}$$

where $d_{ij}=ij-$component of the diffusion tensor, which is denoted by D, and $d_i=i-$th component of the drift vector, which is denoted by $\mathbf{d}$, given by

$$d_{ij}=d_{ij}(t,\mathbf{h})=\frac{1}{2}\lim_{t^*\to t}\frac{1}{t^*-t}\int_{\|\mathbf{h}^*-\mathbf{h}\|<\varepsilon}(h_i^*-h_i)(h_j^*-h_j)p(t,\mathbf{h},t^*,\mathbf{h}^*)d\mathbf{h}^* \tag{4.6}$$

and

$$d_i=d_i(t,\mathbf{h})=\lim_{t^*\to t}\frac{1}{t^*-t}\int_{\|\mathbf{h}^*-\mathbf{h}\|<\varepsilon}(h_i^*-h_i)p(t,\mathbf{h},t^*,\mathbf{h}^*)d\mathbf{h}^* \tag{4.7}$$

respectively.

4.3 Reliability

The surface profile is designed in terms of the reliability J_S in the steady state which is realized under the averaged lateral discharge q. For $\mathbf{h}_0$ in the steady state, the drift vector $\mathbf{d}$ can be discarded, and the diffusion tensor D is assumed independent of time.

Now, the reliability J_S is defined using the probability density function p as

$$J_S=\int_{G_0}p(-T_e,\mathbf{h},0,\mathbf{h}_0)d\mathbf{h} \tag{4.8}$$

where T_e = examination period where small disturbance around the steady state is ex-

pected, and G_s allowable surface profile domain given by

$$G_s = \left\{ \mathbf{h} \in \mathbb{R}^{N_N} \left| \max_i \left| \frac{h_i - h_{0i}}{\Delta h_i^a} \right| < 1 \right. \right\} \tag{4.9}$$

where $\Delta h_i^a = i-$th component of an allowable deviation vector $\Delta \mathbf{h}^a$ which is in $\mathbb{R}^{N_N}$.

Indeed it is difficult to evaluate J_S directly, but a lower bound of J_S can be found in the following manner.

First, being a positive-semidefinite symmetric matrix, D is transformed into a diagonal matrix $\mathrm{diag}[\lambda_i^D]$ by an orthogonal matrix W_D as

$$\mathrm{diag}\left[\lambda_i^D\right] = W_D^T D W_D \tag{4.10}$$

where $\lambda_i^D = i-$th eigenvalue of D. Second, the $\mathbf{h}$-coordinate system is transformed into the $\mathbf{H}-$coordinate system by

$$\mathbf{h} = W_D \mathrm{diag}\left[\sqrt{\lambda_i^D}\right] \mathbf{H} + \mathbf{h}_0 \tag{4.11}$$

and $ij-$component of $W_D \mathrm{diag}\left[\sqrt{\lambda_i^D}\right]$ is denoted by t_{ij}. Then, since $\mathbf{d} = 0$, Eqn.(4.5) becomes equivalent to the heat equation

$$\frac{\partial \Phi}{\partial t} + \Delta^{\mathbf{H}} \Phi = 0 \tag{4.12}$$

where $\Phi = \Phi(t, \mathbf{H}) = p(t, \mathbf{h}, 0, \mathbf{h}_0)$ in the $\mathbf{H}-$coordinate system, and $\Delta^{\mathbf{H}} =$ Laplace operator in the $\mathbf{H}-$coordinate system. Since

$$P(0, 0, 0, \Omega_0) = \int_{\Omega_0} \Phi(0, \mathbf{H}) d\mathbf{H} = 1 \tag{4.13}$$

holds for any domain Ω_0 which contains the origin, it is deduced that Φ is the fundamental solution of the partial differential operator $\dfrac{\partial}{\partial t} + \Delta^{\mathbf{H}}$, which is known as

$$\Phi(t, \mathbf{H}) = \begin{cases} \dfrac{1}{\left(2\sqrt{-\pi t}\right)^{N_N}} \exp\left(\dfrac{\| \mathbf{H} \|^2}{4t}\right) & (t \leq 0) \\ 0 & (t > 0) \end{cases} \tag{4.14}$$

where N_N is assumed to be equal to or greater than 3. Third, an integral J_S^* to be a lower bound of J_S is related to the magnitude of G_s as

$$J_S^* = \int_{\|\mathbf{H}\|<\varrho} \Phi(-T_e, \mathbf{H}) d\mathbf{H} = \int_{\|\mathbf{H}\|<\varrho} \frac{1}{\left(2\sqrt{-\pi t}\right)^{N_N}} \exp\left(\frac{\| \mathbf{H} \|^2}{-4T_e}\right) d\mathbf{H}$$

$$= \frac{1}{\Gamma(N_N/2)} \int_0^{\varrho^2/4T_e} r^{N_N/2-1} \exp(-r) dr \tag{4.15}$$

where ϱ = positive real number which is chosen so that the linear transformation Eqn.(4.11) maps the open ball $B(\mathbf{0}, \varrho)$ in the $\mathbf{H}$–coordinate system to a set which is contained by G_s in the $\mathbf{h}$-coordinate system, Γ = gamma function, and r = radius in the polar coordinate system. Actually, ϱ is served by

$$\varrho = \min_i \left(\frac{|\Delta h_i^a|}{\sum_{j=1}^{N_N} |t_{ij}|} \right) \tag{4.16}$$

4.4 Surface profile design

The theory developed in the previous section is applied to a design problem of surface profile with reliability, that is to decide the allowable surface profile domain G_s warranted by the lower bound of reliability J_S^*.

Provided that J_S^* and the period T_e are specified, there exists a unique ϱ which satisfies Eqn.(4.15) because the integral at the right hand side of Eqn.(4.15) is monotone increasing with respect to ϱ. Thus, reversing Eqn.(4.16),

$$\Delta h_i^a = \varrho \sum_{j=1}^{N_N} |t_{ij}| \tag{4.17}$$

determines the allowable deviation vector $\Delta \mathbf{h}^a$ that prescribes G_s.

Numerical approximation of the constant diffusion tensor D at the neighborhood of $\mathbf{h}_0$ is performed by repetitive implementations of unsteady flow simulation during a finite time increment Δt_0. For that purpose, a simplified demand pattern model, that the deviation of lateral discharge at j–th turnout q_j cannot but equal either Δq_j or $-\Delta q_j$ and that the sign of q_j changes in Δt_0 on average, is adopted. Then, when there are M_q turnouts in total, 2_q^M stochastic events that prescribe q exist. Noting that both probabilities such that $q_j = \Delta q_j$ and $q_j = -\Delta q_j$ are equal to $\frac{1}{2}$, the ij-component of the diffusion tensor D

is approximated by

$$d_{ij} = \frac{1}{2^{M_q+1}\Delta t_0} \sum_{k=0}^{2_q^M-1} (h_{0i}^k - h_{0i})(h_{0j}^k - h_{0j}) \tag{4.18}$$

where h_{0i}^k = $i-$th component of h which is the simulation result at $t = \Delta t_0$ under the $k-$th stochastic event specifying the initial condition $h = h_0$.

Sequential implementations of the Householder tridiagonalization, the bisection method, and the inverse iteration method are effective in numerical computations of the decomposition Eqn.(4.10) (See Appendix C). Then, t_{ij} for $i, j = 1 \sim N_N$ are directly calculated from the eigenvalues and the eigenvectors. Thus, the allowable deviation vector $\Delta \mathbf{h}^a$ is decided by Eqn.(4.17) provided ϱ for specified J_S^* and T_e is known.

4.5 Application

A test problem in the WB model as shown in Figure 2.8 is solved. The steady state to be examined is the same as in the Chapter 2.

The 256 (= 2^8) water demand patterns that specify q are determined by $\Delta q_j = 0.5[\mathrm{m}^3/\mathrm{s}]$ for $j = 1 \sim 8$. After 256 runs of the unsteady flow model, the diffusion tensor D is obtained from Eqn.(4.18). Next, D is decomposed in accordance with Eqn.(4.10).

The steady surface profile $\mathbf{h}_0$ with the allowable domain G_s for (J_S^*, T_e) = (0.95, 180[min]) is illustrated in Figures 4.1 through 4.3. The runs differ in the time increment Δt_0 that is 5[min], 15[min], and 45[min] respectively.

Although this numerical error should be allowed for, yet the results are considered to demonstrate quantitative details of G_s, which enlarges with Δt_0, increases around the turnouts and is affected by the depth in the steady state.

4.6 Conclusions

The problem of reliability in the design of surface profile is reduced to solving the heat equation. The method developed here has an advantage that the reliability in a long period can be obtained through predetermined number (= 2_q^M) of unsteady flow simulations in a much smaller period that is identical with the time increment Δt_0 in the Markov process model. If a Monte Carlo model be utilized in the application problem, it would be needed to execute unsteady flow simulations throughout the period T_e under plenty of water demand patterns that pseudo random numbers arrange.

The proposed concept serves as a guide to the manager of irrigation systems where

the initiative of demand side should be esteemed. If the examination of steady state reveals that the reliability is too little, introducing water control systems that regulate unsteady flows or augmenting canal free boards should be discussed. Conversely, adequate reliability warrants the demand side that there is no restriction of withdrawal from the turnout.

If there are no field data which are available to the estimation of the parameters Δq_i and Δt_0 in the demand pattern model, the distribution function of the water demand should be determined by detailed analysis of farm management. That will be a pivotal point in applications to real world.

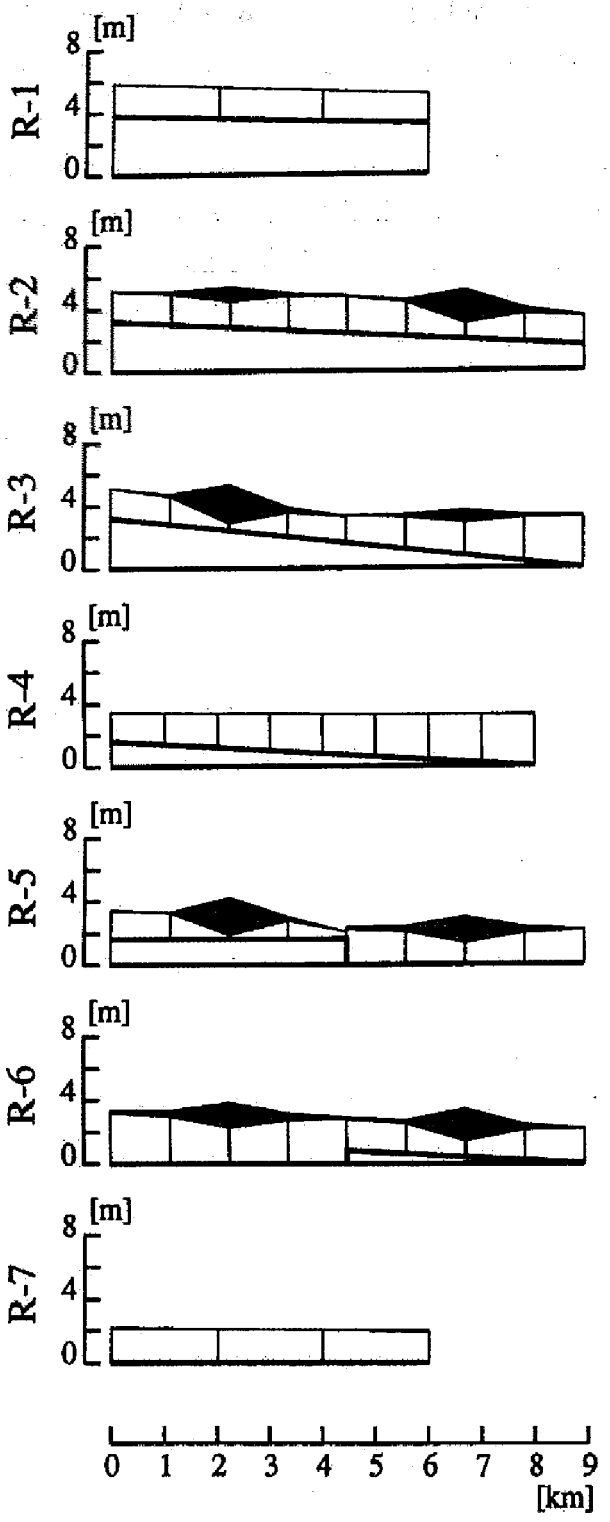

Figure 4.1: Admissible surface profile for $\Delta t_0 = 5$[min]

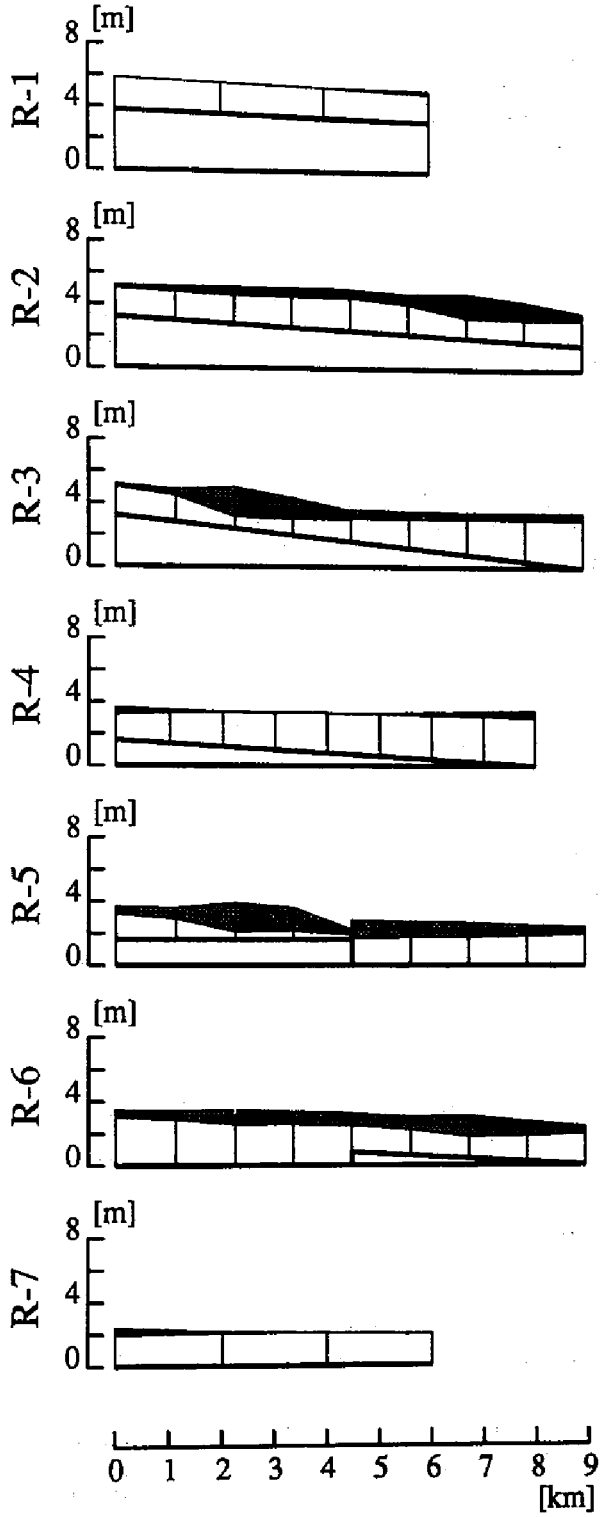

Figure 4.2: Admissible surface profile for $\Delta t_0 = 15$[min]

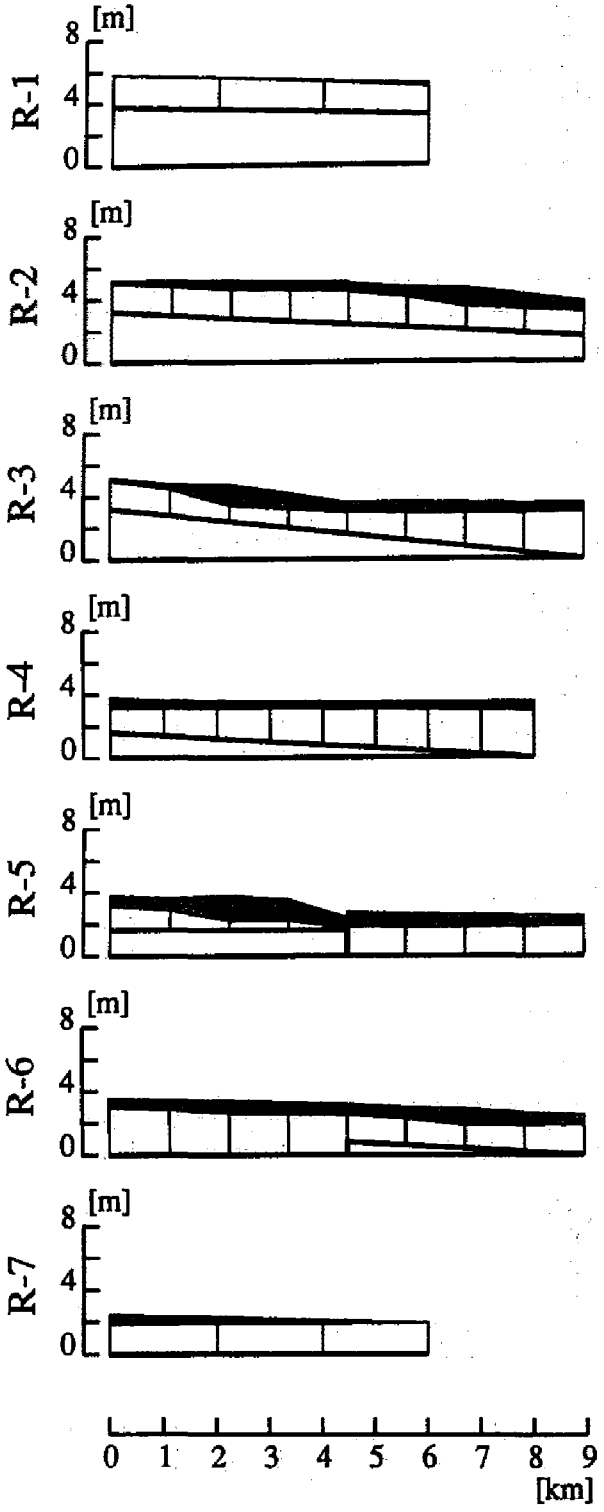

Figure 4.3: Admissible surface profile for $\Delta t_0 = 45$[min]

Chapter 5

Maximization of Reservoir Reliability

5.1 Introduction

The irreversibility of information dominates fundamental approach to decision making problems in reservoir management. Being governed by stochastic characteristics of the water balance, the future variation in the storage of a reservoir is predicted only by making use of the probability. Therefore, a decision support model for the water storage system that consists of a reservoir and its stochastic environment should be developed to maximize a reliability which is mathematically well defined.

Pegram [74] summarizes the fundamental concepts of the reservoir reliability and presents some methods to calculate the mean first passage time in terms of Markov chain. Yeh [97] reviews linear programming, dynamic programming, nonlinear programming, and simulation models developed for reservoir operations. These approaches are continuously expanding as in Nardini *et al.* [71], who integrates risk aversion and average-performance optimization, and Karamouz and Vasiliadis [42], who propose a Bayesian stochastic dynamic programming model. Buchberger *et al.* [11] applied the FPPDE that governs the probability density function of a continuous Markov process to the equilibrium storage analysis of a reservoir. For a management purpose, however, the reliability should be defined so as to deal with a non-equilibrium state to make an appropriate decision at any time no matter how the storage is. Mishchenko and Pontryagin [65] presented an optimal control problem of a Markov process with absorbing barriers, which is considered as a well defined reliability. Since the Markov process is governed by the FPPDE, which is a parabolic partial differential equation, the approach taken by Lions [58] gives the maximum principle which characterizes the necessary condition to optimize the reliability so defined. An optimization model of the reliability will serve as a decision support model.

A finite element model is developed to solve the FPPDE that governs the reliability of a

reservoir and is applied to an irrigation tank without forced spill (Kawachi *et al.* [47]) and an irrigation dam (Unami *et al.* [88]). The model is proved applicable to multi-purpose reservoirs as well (Kawakatsu [50]). In this chapter, in order to establish a comprehensive decision support model for reservoir management in a non-equilibrium state, a spillway at a boundary of the storage space is modeled as a reflecting barrier (Unami *et al.* [89]; Unami *et al.* [90]). Then, the adjoint problem of reliability is formulated so as to describe the maximum principle that provides the necessary condition to maximize a functional. Using an upwind finite element numerical scheme that stably calculates the reliability and the adjoint variable, the contribution of release strategy to the current reliability is quantitatively determined.

5.2 Markov process model of reservoir storage

The continuity of the water balance in a reservoir is written as the ordinary differential equation

$$\frac{dX}{dt} = u + d \tag{5.1}$$

where X = storage, u = deterministic component of virtual inflow discharge, which consists of the inflow discharge and the negative release discharge, and d = stochastic component of virtual inflow discharge. Being driven by the stochastic component of virtual inflow discharge d, the storage X is a random variable. Furthermore, the storage X is a Markov process because Eqn.(5.1) implies that X does not depend on its hysteresis. Thus, FPPDE for 1-dimensional stochastic variable is applicable to the storage X as

$$\frac{\partial p}{\partial t} + d_{11}\frac{\partial^2 p}{\partial X^2} + (d_1 + u)\frac{\partial p}{\partial X} = 0 \tag{5.2}$$

where the probability density function p is with respect to X. The practical condition that the storage X should satisfy is

$$X \in G_a = (X_{\min}, X_{\max}) \ , \quad t < t_f \tag{5.3}$$

where G_a = allowable storage domain, $X_{\min}$ = allowable minimum storage, $X_{\max}$ = allowable maximum storage, and t_f = specified final time. The reliability $y = y(t, x, t_f)$ for any storage X at time $t \leq t_f$ is defined as the probability such that X remains in G_a until the final time t_f provided that $X = X \in G_a$ is observed at the time t. Note that another

probability density function ϖ determined by

$$y(t, X, t_f) = \int_{X_{\min}}^{X_{\max}} \varpi(t, X, t_f, X^+) dX^+ \tag{5.4}$$

satisfies the FPPDE Eqn.(5.2) because it satisfies the Chapman-Kolmogorov's equation and the stochastic continuity equation in the domain G_a. Since the FPPDE is a linear equation, the reliability y which is an integral of ϖ, a solution to the FPPDE, is also a solution to the FPPDE. Thus, the governing equation of the reliability y is

$$\frac{\partial y}{\partial t} + d_{11}\frac{\partial^2 y}{\partial X^2} + (d_1 + u)\frac{\partial y}{\partial X} = 0 \tag{5.5}$$

whose final condition is given by

$$y(t_f) = 1 \tag{5.6}$$

because the probability such that X is found in G_a at the final time t_f provided that $X = X \in G_a$ is observed at the same final time t_f is clearly equal to 1. A Dirichlet boundary condition at $X = X_{\min}$

$$y|_{X=X_{\min}} = 0 \tag{5.7}$$

is posed because of the definition of the reliability, whereas a Neumann boundary condition at $X = X_{\max}$

$$\left.\frac{\partial y}{\partial X}\right|_{X=X_{\max}} = 0 \tag{5.8}$$

is prescribed to represent the forced spill.

5.3 Optimal control of reliability

The optimization problem that maximizes the reliability y at a specified initial time t_i is formulated as an optimal control problem. The current storage $X_c = X$ at t_i is assumed to be observed. Since the deterministic component of virtual discharge u is considered as the control variable, the functional $J_R(u)$ defined by

$$J_R(u) = y(t_i)|_{X=X_c} = \int_{X_{\min}}^{X_{\max}} y\hat{\delta}(X - X_c) dX \tag{5.9}$$

is to be maximized.

A small variation in the control variable u, which is denoted by δu, is supposed to induce δy, the small variation in the reliability y. These variations satisfy the partial differential equation

$$\frac{\partial \delta y}{\partial t} + d_{11}\frac{\partial^2 \delta y}{\partial X^2} + (d_1 + u)\frac{\partial \delta y}{\partial X} + \frac{\partial y}{\partial X}\delta u = 0 \tag{5.10}$$

with the final condition

$$\delta y(t_f) = 0 \tag{5.11}$$

and the boundary conditions

$$\delta y|_{X=X_{\min}} = 0 \tag{5.12}$$

and

$$\left.\frac{\partial \delta y}{\partial X}\right|_{X=X_{\max}} = 0 \tag{5.13}$$

for the fixed final and boundary values.

The maximum principle is obtained in a similar manner as in Chapter 3. The left hand side of Eqn.(5.10) multiplied by λ, the adjoint variable for the FPPDE, is integrated by parts over the domain $(t_i, t_f) \times G_a$ as

$$\begin{aligned}
&\int_{t_i}^{t_f}\int_{X_{\min}}^{X_{\max}} \lambda\left(\frac{\partial \delta y}{\partial t} + d_{11}\frac{\partial^2 \delta y}{\partial X^2} + (d_1+u)\frac{\partial \delta y}{\partial X} + \frac{\partial y}{\partial X}\delta u\right) dX dt \\
&= \int_{X_{\min}}^{X_{\max}} \left([\lambda \delta y]_{t_i}^{t_f} - \int_{t_i}^{t_f} \frac{\partial \lambda}{\partial t}\delta y dt\right) dX \\
&+ \int_{t_i}^{t_f} \left(\left[d_{11}\lambda\frac{\partial \delta y}{\partial X}\right]_{X_{\min}}^{X_{\max}} - \left[\frac{\partial (d_{11}\lambda)}{\partial X}\delta y\right]_{X_{\min}}^{X_{\max}} + \int_{X_{\min}}^{X_{\max}} \frac{\partial^2 (d_{11}\lambda)}{\partial X^2}\delta y dX\right. \\
&\left. + [(d_1+u)\,\lambda \delta y]_{X_{\min}}^{X_{\max}} - \int_{X_{\min}}^{X_{\max}} \frac{\partial (d_1+u)\lambda}{\partial X}\delta y dX\right) dt + \int_{t_i}^{t_f}\int_{X_{\min}}^{X_{\max}} \lambda\frac{\partial y}{\partial X}\delta u dX dt
\end{aligned} \tag{5.14}$$

and then reduced to the maximum principle

$$\delta y(t_i)|_{x=X} = \int_{t_i}^{t_f}\int_{X_{\min}}^{X_{\max}} \lambda\frac{\partial y}{\partial X}\delta u dX dt \tag{5.15}$$

if λ satisfies the adjoint FPPDE

$$\frac{\partial \lambda}{\partial t} + \frac{\partial^2 (d_{11}\lambda)}{\partial X^2} + \frac{\partial (d_1 + u)\lambda}{\partial X} = 0 \tag{5.16}$$

with the initial condition

$$\lambda(t_i) = \hat{\delta}(X) \tag{5.17}$$

and the boundary conditions

$$\lambda|_{x=x_{\min}} = 0 \tag{5.18}$$

and

$$\left(\frac{\partial (d_{11}\lambda)}{\partial X} - (d_1 + u)\lambda \right) \Bigg|_{X=X_{\max}} = 0 \tag{5.19}$$

that comprise the adjoint system. Conversely, the necessary condition to maximize the functional $J_R(u)$ is that the control variable u is maximized or minimized in the subdomain where $\lambda \dfrac{\partial y}{\partial X}$ is positive or negative, respectively. Thus, $\lambda \dfrac{\partial y}{\partial X}$ is considered as the the sensitivity which represents the contribution of u to $J_R(u)$.

5.4 Decision support model

5.4.1 Identification of coefficients in FPPDE

If time series data of the storage are available, the diffusion coefficient d_{11} and the drift coefficient d_1 are estimated in each of the spatiotemporal subdomains which are properly partitioned allowing for the prescription of the operational manual of the reservoir. The estimation is performed as

$$d_{11} = \frac{1}{2M_s} \sum_{\Lambda_s} \frac{(X_{i,j+1} - X_{i,j})^2}{t_{i,j+1} - t_{i,j}} \tag{5.20}$$

and

$$d_1 = \frac{1}{M_s} \sum_{\Lambda_s} \frac{X_{i,j+1} - X_{i,j}}{t_{i,j+1} - t_{i,j}} \tag{5.21}$$

where $t_{i,j}$ = time at the j−th stage of the i−th series of data, $X_{i,j} = X$ at $t_{i,j}$, Λ_s = set of indices i and j such that the spatiotemporal point $\left(\frac{X_{i,j+1}+X_{i,j}}{2}, \frac{t_{i,j+1}-t_{i,j}}{2}\right)$ falls on the spatiotemporal subdomain, and M_s = number of elements of Λ_s.

5.4.2 Numerical solvers for FPPDE and its adjoint equation

In common with the solute transport equation Eqn.(2.46), FPPDE Eqn.(5.5) and its adjoint equation Eqn.(5.16) are 1-dimensional parabolic partial differential equations, which the upwind scheme developed in Chapter 2 can be applied. Using the calculated solutions of y and λ by the upwind scheme, the sensitivity $\lambda\frac{\partial y}{\partial X}$ is obtained. Since an increment considering the sensitivity $\lambda\frac{\partial y}{\partial X}$ may revise the control variable u so as to maximize the functional $J_R(u)$, these numerical solvers serve as a decision support model to maximize the reservoir reliability.

5.5 Applications to existing reservoirs

Applicability of the decision support model is examined in two existing reservoirs of Y and K dams. The locations, the purposes, the irrigation areas, the operation periods, the maximum storages, and the periods of available water level data of these dams are summarized in Table 5.1. Using the water level-storage curves as shown in Figures 5.1 and 5.2, the water levels are converted to the storages which are depicted in Figures 5.3 and 5.4.

Tables 5.2 and 5.3 show the division of subdomains, allowing for the seasonal variation of hydrological characteristics, and identified coefficients.

Eqns.(5.5) through (5.8) where the control variable u is specified as 0 are numerically solved so that the reliability is obtained as shown in Figures 5.5 and 5.6 for Y and K dams, respectively. The storage of Y dam is almost full at the beginning of operation period in every year, but that of K dam is more indeterminate.

Table 5.1: Key parameters of dams

Dam	Y	K
Location	Shiga prefecture, Japan	Okayama prefecture, Japan
Purpose	irrigation only	irrigation, industry, electricity
Irrigation area	paddy fields of 2,760 ha	paddy fields of 12,500 ha
Operation period	16 April through 1 October	throughout the year
Maximum storage	7.691 [10^6 m^3]	15.897 [10^6 m^3]
Available data	15 years of 1980 through 1994	38 years of 1957 through 1994

In order to increase the reliability at an initial time, decisions to improve the control variable u is taken in the spatiotemporal domain according to the sensitivity $\lambda\frac{\partial y}{\partial X}$, which is numerically calculated when a certain current storage X_c is assumed to be observed at the initial time t_i. The current storage $X_c = 7.280$ [10^6m^3], which is the normal full water storage, at t_i = 16th of April is assumed in Y dam, whereas the current storage X_c = 7.450 [10^6 m^3] at t_i = 1st of January is assumed in K dam. The calculated sensitivities, as illustrated in Figures 5.7 and 5.8, considerably decreases in spatiotemporal points where the probability of realization is small, and allowed for in the decisions made as follows.

- For Y dam, $u = 1$ [m^3/s] is prescribed if:
  - 3.640 [10^6m^3] $< X <$ 7.280 [10^6m^3] from 1st of June to 30th of June.
- For K dam, $u = 1$ [m^3/s] is prescribed if:
  - 7.450 [10^6m^3] $< X <$ 12.869 [10^6m^3] from 1st of May to 15th of May,
  - 10.009 [10^6m^3] $< X <$ 12.869 [10^6m^3] from 15th of May to 31st of May,
  - 10.009 [10^6m^3] $< X <$ 13.897 [10^6m^3] from 1st of June to 14th of June,
  - 4.201 [10^6m^3] $< X <$ 7.450 [10^6m^3] from 4th of September to 30th of September, or
  - 0.000 [10^6m^3] $< X <$ 4.201 [10^6m^3] from 1st of October to 31st of October.

The revised reliability under these u is depicted in Figures 5.9 and 5.10. The values of the functional $J_R(u)$ increase from 0.8054 to 0.9524 and from 0.2524 to 0.6577 in Y and K dams, respectively.

Apart from the optimization procedure described above, the conceptual question of when to run the model is posed. If it is possible to anticipate occurrence of a certain storage at a future current time in advance, a decision assuming it can be made even in another earlier current time. However, it does not necessarily improve the reliability at the earlier current time. It is the reliability at a future imaginary current time that an anticipating release strategy improves.

5.6 Conclusions

The optimization problem of the reservoir reliability defined by the appropriate probability has been solved in terms of the sensitivity. Being parabolic partial differential equations, the governing equations are effectively solved using the upwind finite element scheme. The numerical model serves as a decision support model, and the demonstrative example of application proves its validity as well as poses the question what is the

meaning of anticipating less probable events. It is remarked that observation should be made objectively though it is related to subjective current time in the mathematical formulation.

The coefficients d_{11} and d_1 are estimated from time series data of the virtual inflow discharge. Otherwise, the coefficients are determined by the virtual inflow discharge data which are deduced from the runoff analysis and the demand prediction. The reliability of the model itself depends on the coefficients being estimated properly.

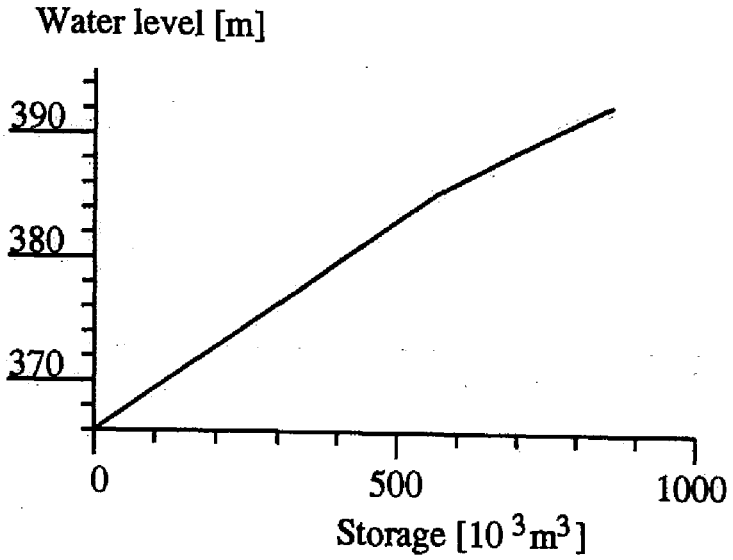

Figure 5.1: Storage-water level curve for Y dam

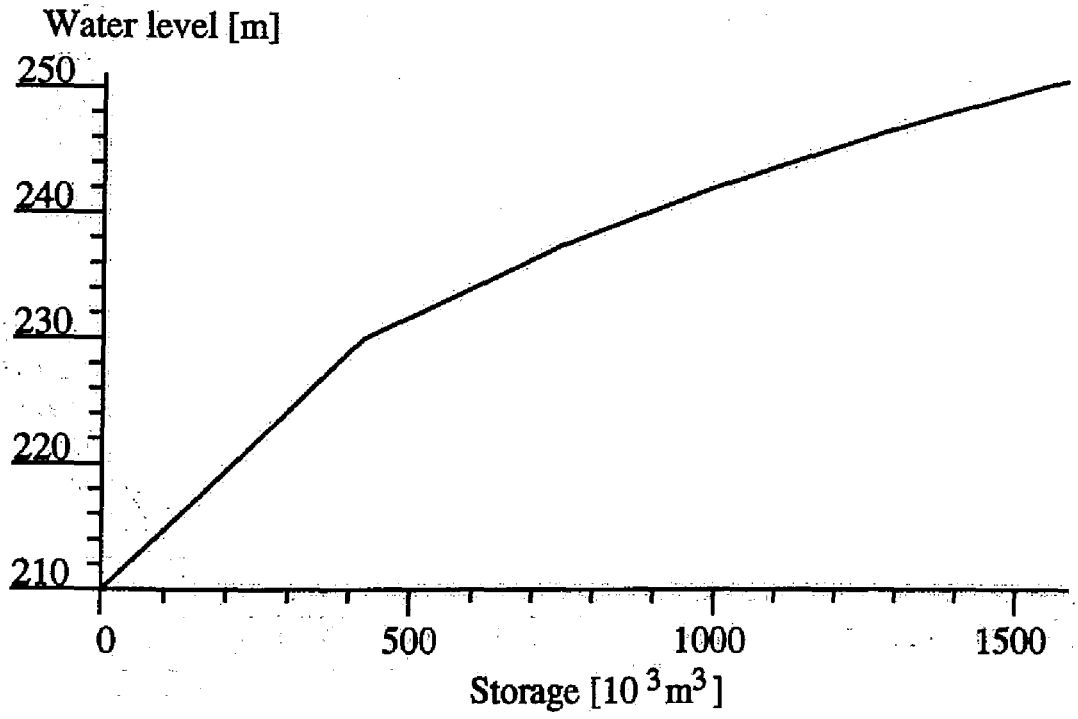

Figure 5.2: Storage-water level curve for K dam

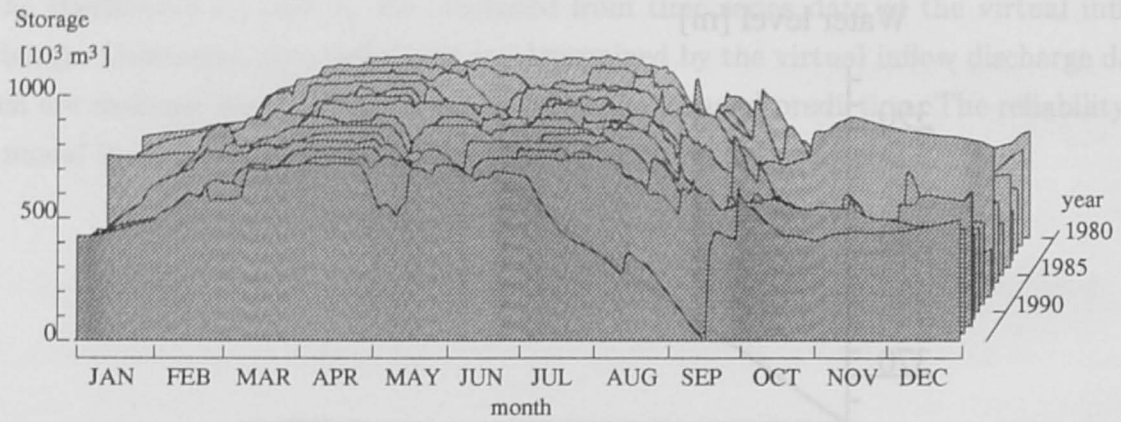

Figure 5.3: Storage variation in Y dam

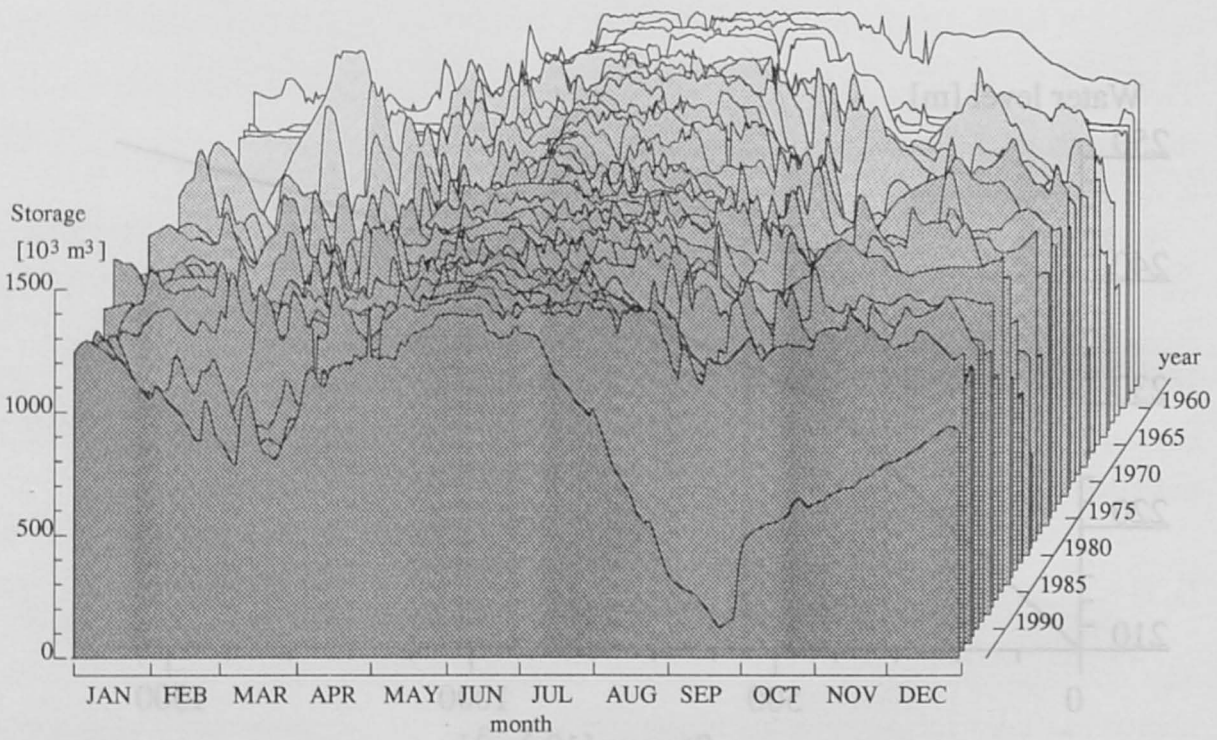

Figure 5.4: Storage variation in K dam

Table 5.2: Division of subdomains and identified coefficients for Y dam: M_s (above); d_{11} (middle); d_1 (below)

	Spatial subdomains $[10^6 m^3]$					
Temporal subdomains Date (Day)	0.000 ~ 1.820	1.820 ~ 3.640	3.640 ~ 5.710	5.710 ~ 7.280	7.280 ~ 7.403	7.403 ~ 7.691
4/16 (1)	71				26	23
~	9364				5366	10047
4/22 (7)	0.03540				0.00359	-0.04977
4/23 (8)	77				40	
~	101410				12911	
4/30 (15)	-0.97321				-0.01745	
5/ 1 (16)	16			72	13	
~	151850			170460	11147	
5/ 7 (22)	-1.40530			-0.59989	-0.07557	
5/ 8 (23)	21			68	16	
~	165870			68184	9266	
5/14 (29)	-0.39749			0.04270	-0.02215	
5/15 (30)	56			164	31	
~	76407			117640	23391	
5/31 (46)	-0.05696			-0.24651	0.08213	
6/ 1 (47)	62			128	18	
~	307890			108720	31306	
6/14 (60)	0.26789			0.13767	-0.16649	
6/15 (61)	41			178	21	
~	60969			149050	14210	
6/30 (76)	0.19146			0.41564	-0.12610	
7/ 1 (77)	33			156	19	
~	57238			39539	102100	
7/14 (90)	-0.16022			0.00690	0.10641	
7/15 (91)	24			222	9	
~	66243			49134	106460	
7/31 (107)	-0.07986			-0.09020	0.20829	
8/ 1 (108)	14		31	165		
~	20721		176320	161350		
8/14 (121)	-0.07020		-0.79650	-0.75476		
8/15 (122)	17		114	124		
~	66596		139700	488120		
8/31 (138)	-1.14830		-0.57112	-0.39091		
9/ 1 (139)	34		96	20		
~	123340		201090	10047		
9/10 (148)	-1.6407		-1.10090	-0.65367		
9/11 (149)	26	89	179	21		
~	1015400	422410	635420	2233400		
10/ 1 (169)	0.57485	-0.01904	0.03065	-0.38178		

Table 5.3: Division of subdomains and identified coefficients for K dam: M_s (above); d_{11} (middle); d_1 (below)

	Spatial subdomains [$10^6 m^3$]						
Temporal subdomains	0.000 ~	4.201 ~	7.450 ~	10.009 ~	12.869 ~	13.897 ~	15.136 ~
Date (Day)	4.201	7.450	10.009	12.869	13.897	15.136	15.898
1/ 1 (1)	28	148	263	599	98	11	182
~	22773	167230	203220	197150	156820	194050	26403
1/31 (31)	0.15542	0.17455	-0.24956	-0.14340	0.33208	-0.18992	-0.09028
2/ 1 (32)	188		353	411	86	35	
~	166600		401360	393590	563410	783000	
2/29 (60)	-0.10495		-0.22787	-0.07494	-0.21919	0.18437	
3/ 1 (61)	178		320	559	95	26	
~	443100		624140	734850	886850	1161200	
3/31 (91)	0.52578		0.78730	0.43828	-0.06893	0.01960	
4/ 1 (92)	15		89	337	88	41	
~	44747		514010	861110	1377700	730380	
4/15 (106)	0.33292		1.14230	0.83776	0.83489	-0.06941	
4/16 (107)	23			311	181	55	
~	1686200			513010	957350	788800	
4/30 (121)	1.89430			0.61781	0.35930	0.06101	
5/ 1 (122)	166				278	126	
~	368100				380650	535680	
5/15 (136)	0.87126				0.44848	0.26683	
5/16 (137)	95				189	324	
~	104140				224920	189060	
5/31 (152)	0.46150				0.53279	0.42558	
6/ 1 (153)	22				46	436	
~	132310				162580	108110	
6/14 (166)	0.63506				0.94407	0.34153	
6/15 (167)	8				46	187	
~	4102000				348660	207970	
6/21 (173)	-9.07000				-1.53940	-0.69227	
6/22 (174)	27				124	181	
~	3361900				560400	349160	
6/30 (182)	1.39240				0.11096	-0.00840	
7/ 1 (183)	13				177	354	
~	1139200				333800	316600	
7/15 (197)	1.28660				0.24177	-0.03110	
7/16 (198)	25				222	315	
~	94931				96294	168980	
7/31 (213)	-0.84913				-0.26004	-0.07449	
8/ 1 (214)	33				126	95	
~	160640				126210	156100	
8/ 7 (220)	-1.32040				-0.90610	-0.42770	
8/ 8 (221)	20			244	226	132	
~	15441000			1655200	1310700	463130	
8/24 (237)	-1.55010			-0.90681	-0.42588	-0.26207	
8/25 (238)	10		18	240	62	39	
~	356190		348320	556380	1707500	736650	
9/ 3 (247)	-2.69560		-2.18570	-1.36850	-1.28780	-0.92048	
9/ 4 (248)	27	24	246	563	110	56	
~	606380	216990	498590	739790	1335900	946740	
9/30 (274)	0.52117	-0.88691	-0.56437	-0.34695	0.05065	-0.68768	
10/ 1 (275)	20	91	238	710	68	51	
~	754250	455920	372020	235860	689780	101290	
10/31 (305)	-1.38700	-0.14552	-0.00984	0.13160	-0.19892	0.08531	
11/ 1 (306)	38	82	246	568	168	38	
~	534750	169530	50028	402080	154160	571270	
11/30 (335)	-0.16188	-0.27541	-0.06148	0.10534	-0.16848	0.12707	
12/ 1 (336)	42	81	234	729	82	8	
~	103270	179400	171280	107850	89559	301850	
12/31 (366)	0.66856	-0.20245	-0.26759	-0.18100	-0.11212	-0.07033	

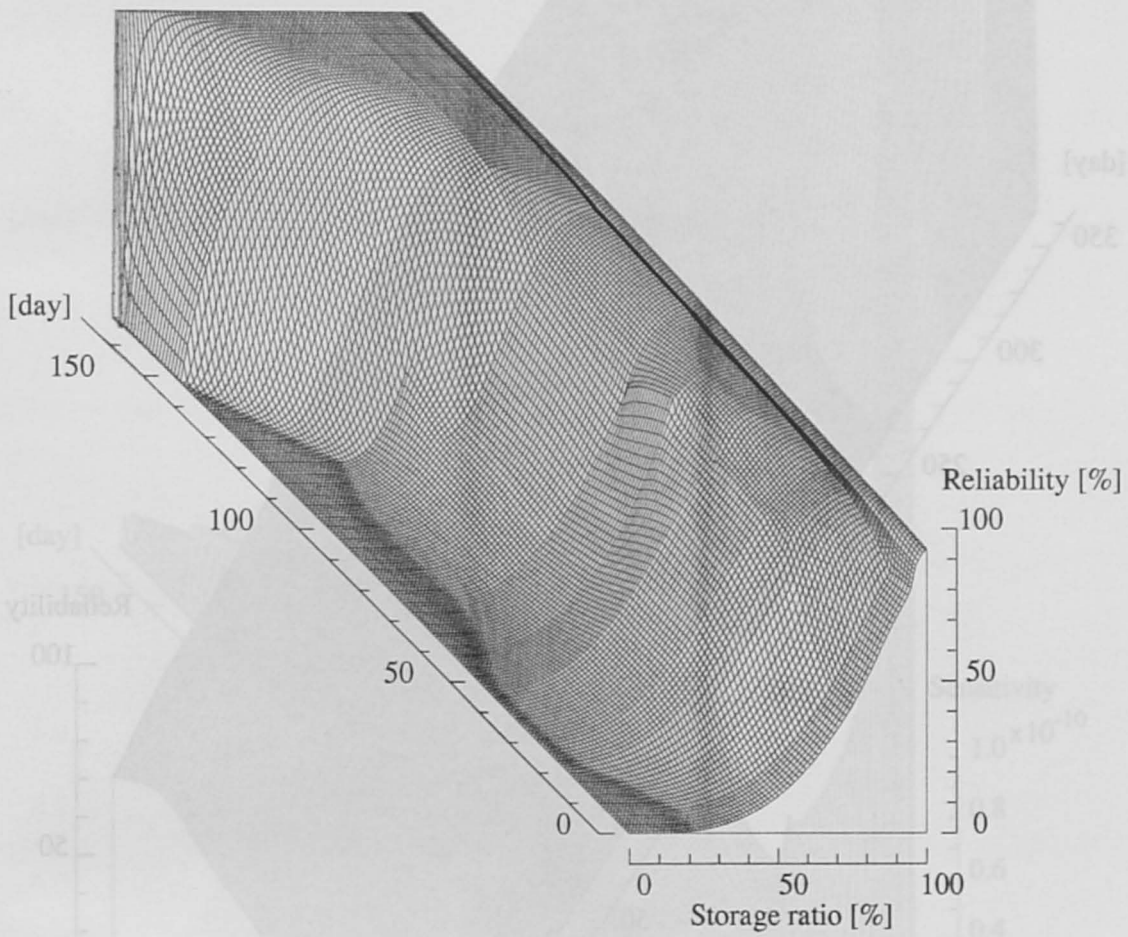

Figure 5.5: Reliability in Y dam when $u = 0$

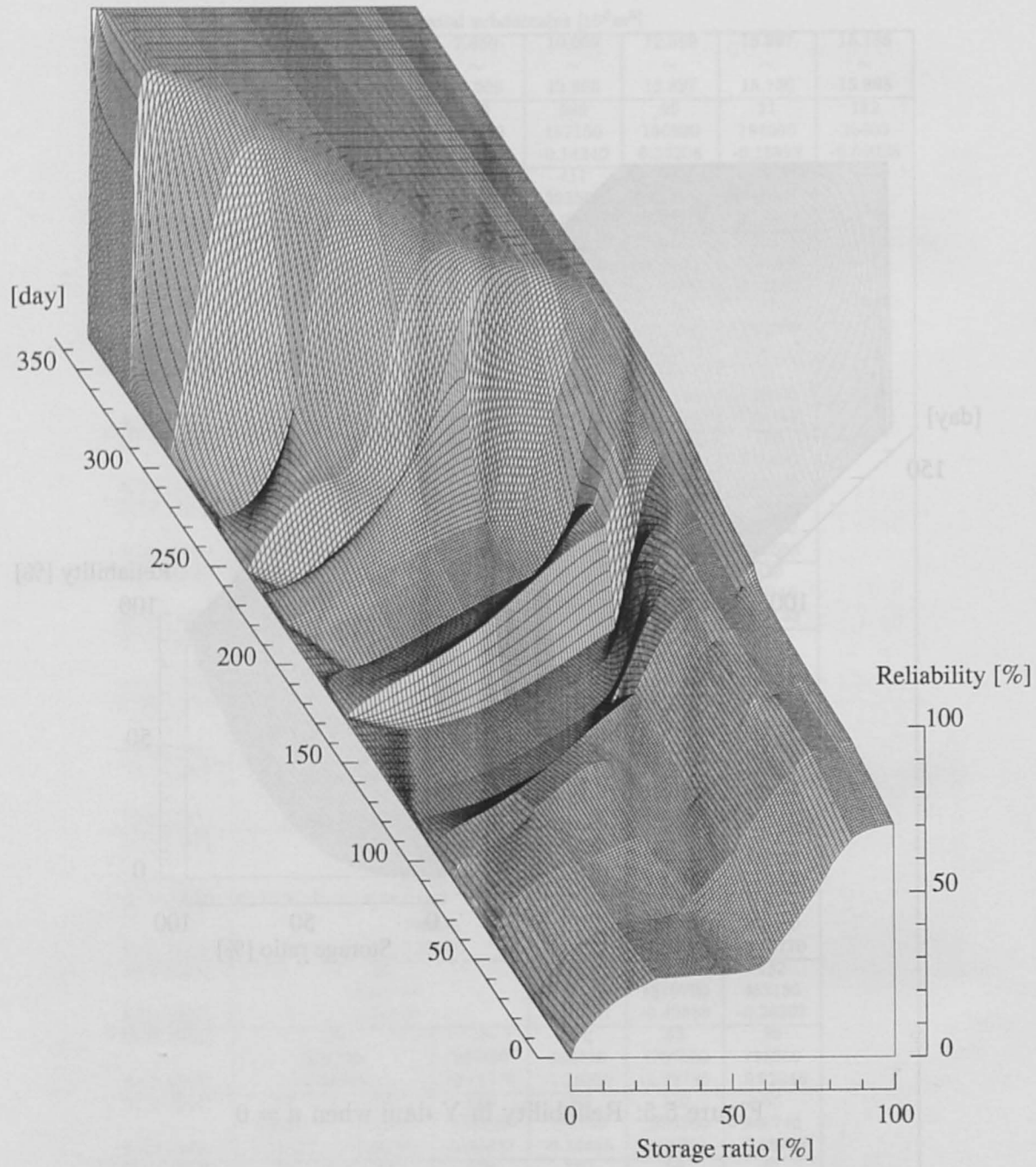

Figure 5.6: Reliability in K dam when $u = 0$

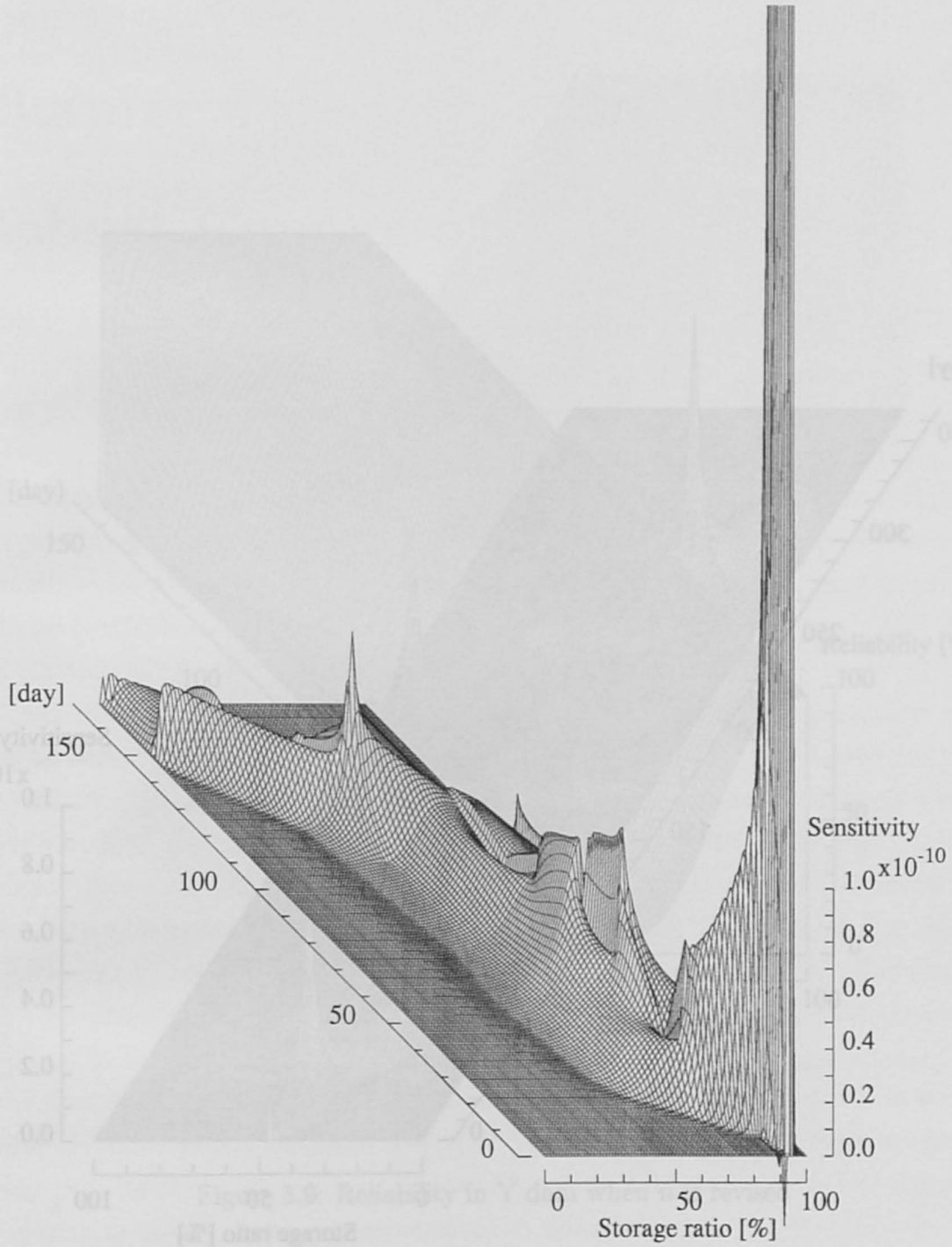

Figure 5.7: Sensitivity in Y dam

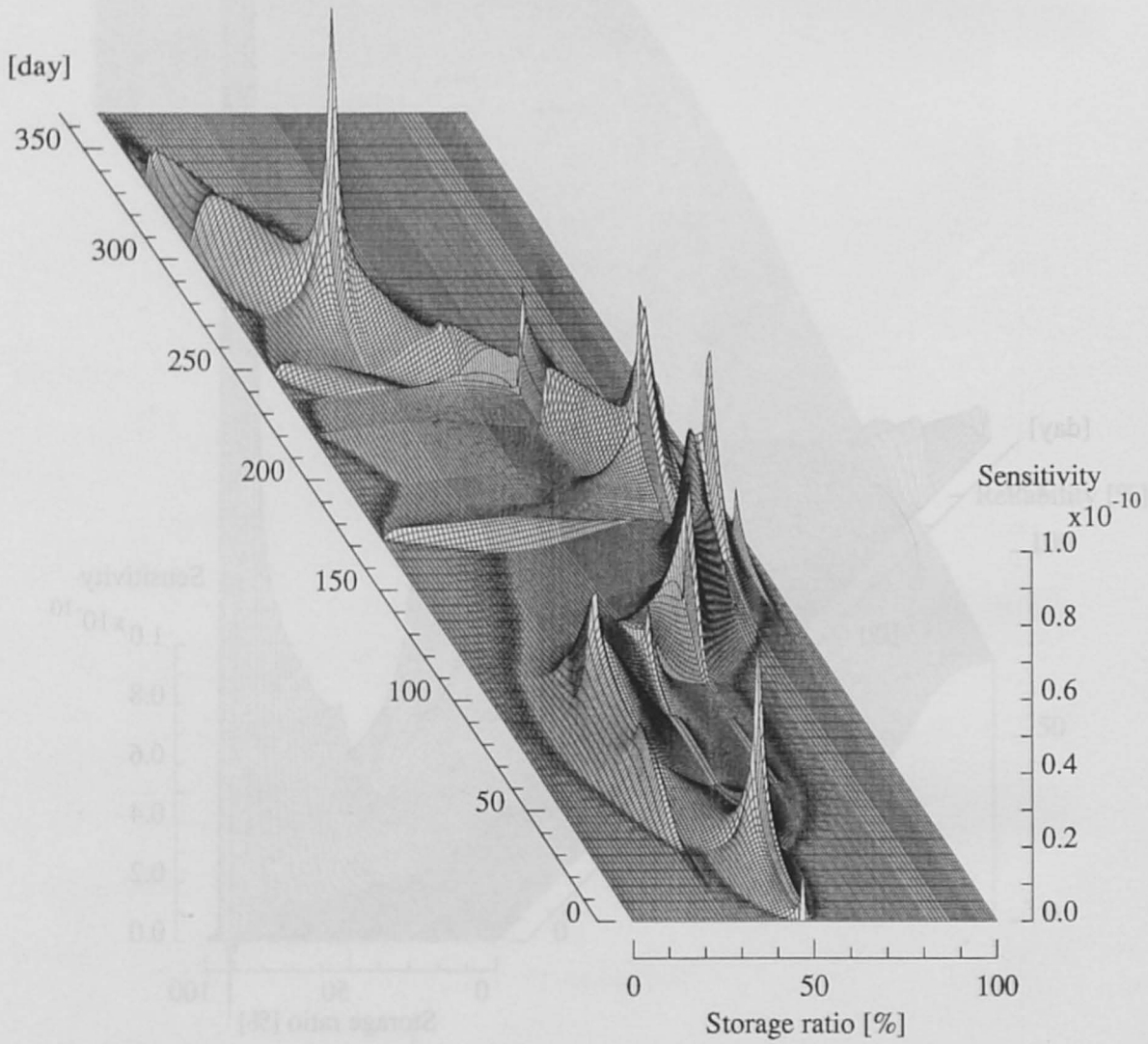

Figure 5.8: Sensitivity in K dam

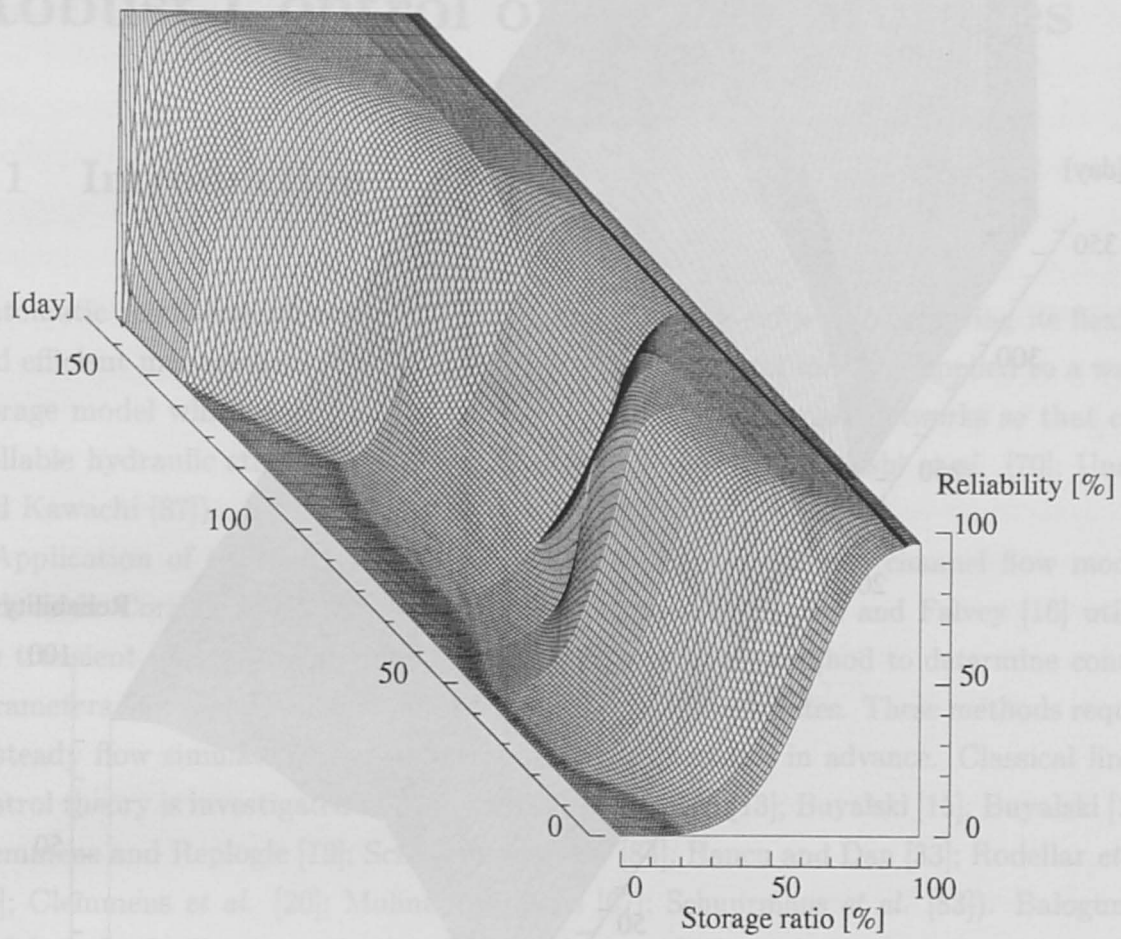

Figure 5.9: Reliability in Y dam when u is revised

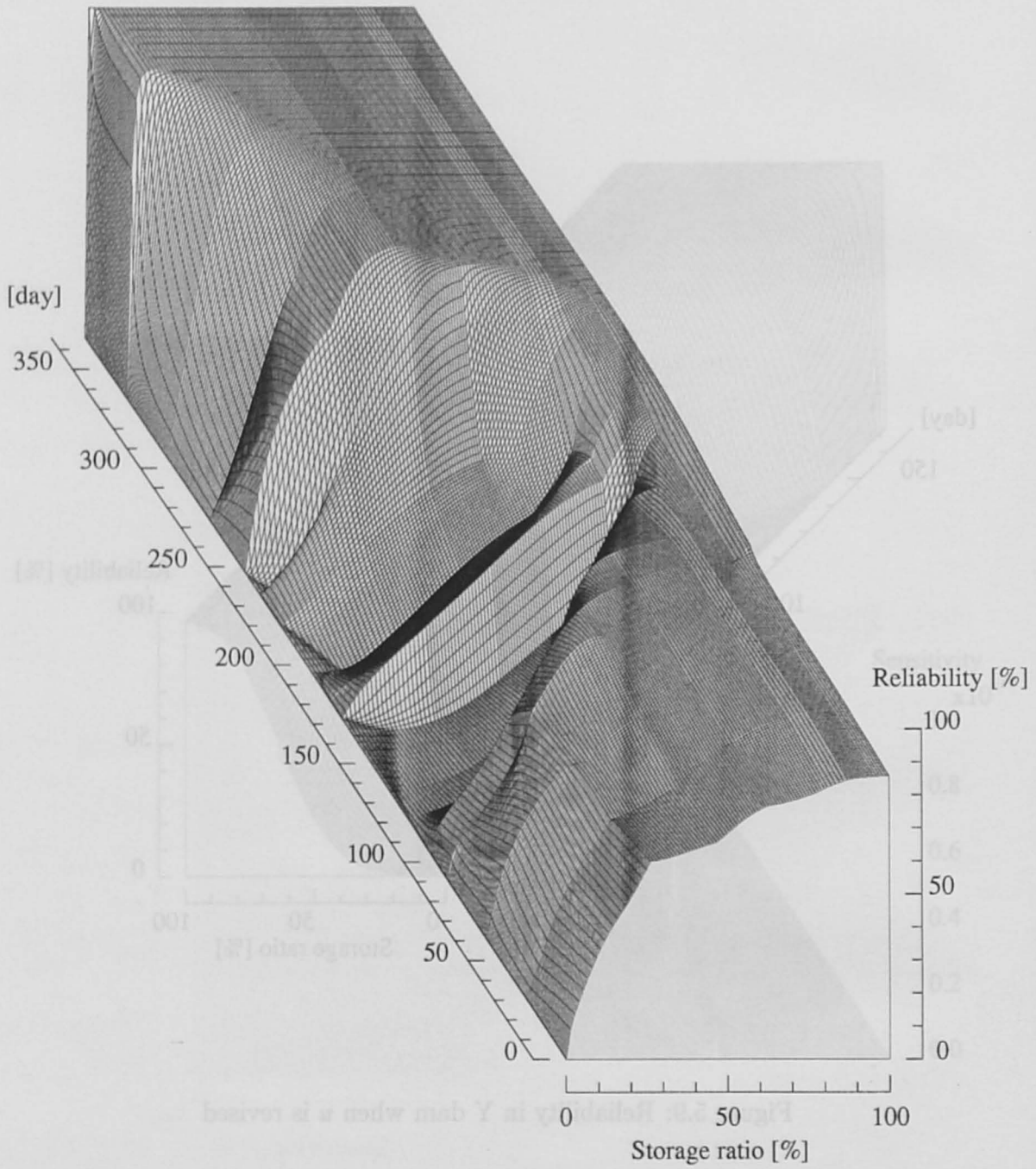

Figure 5.10: Reliability in K dam when u is revised

Chapter 6

Robust Control of Water Storages

6.1 Introduction

Automatic regulation of water resources system is a key subject to achieving its flexible and efficient management. In this chapter, the linear control theory is applied to a water storage model which describes reservoirs as well as open channel networks so that controllable hydraulic structures are automatically regulated (Nakanishi *et al.* [70]; Unami and Kawachi [87]).

Application of the linear control theory to mathematical open channel flow models such as in Corriga *et al.* [21] is frequently discussed. Buyalski and Falvey [16] utilize the transient-response method and the frequency-response method to determine control parameters in a proportional integral system for canal check gates. These methods require unsteady flow simulations by the method of characteristics in advance. Classical linear control theory is investigated by many authors (Buyalski [13]; Buyalski [15]; Buyalski [14]; Clemmens and Replogle [19]; Schuurmans *et al.* [84]; Hancu and Dan [33]; Rodellar *et al.* [80]; Clemmens *et al.* [20]; Molina and Miles [67]; Schuurmans *et al.* [83]). Balogun *et al.* [7] apply the linear quadratic regulator theory, which minimizes a performance index in the time domain, to a linearized and discretized hydrodynamical unsteady flow model. Further developments of the linear quadratic regulator in open channel flows are found in Reddy [76], Reddy *et al.* [78], and Reddy [77], where a Kalman filter is introduced into the system to handle canals subjected to external disturbances.

The control system presented here essentially differs from the earlier works in the following three respects. In the first sense, derived from the global continuity equations, a water storage model gives a linear dynamical system model of flows in the open channel network which consists of several interacting pools connected with each other by regulating the controllable hydraulic structures. Thus, the system model does not involve any hydrodynamical equation of motion and is applicable to reservoirs. In the second sense,

the control errors are taken into account to prevent wind-up phenomena, or awkward expansion of a control variable. And in the third sense, the external disturbances are related to observable references by a generator, which is also represented by a linear dynamical model and may include modeling errors. In this context, three controllers are designed; one is a feed-forward controller to cancel out the external disturbances assuming that there is no modeling error in the generator, one is a controller for anti wind-up, and the other one is a feed-back controller to stabilize the control system under observation errors and to bound variations in storage volumes of the pools. Thus, the system is an extension of the two-degree-of freedom system which consists of a feed-back controller and a feed-back controller (Horowitz [35]; Unami *et al.* [92]). The robust control theory, which rigorously deals with the modeling errors as well as the external disturbances, is applied to designing the feed-back controller. The controllers designed are first tested in a reservoir operation problem and then incorporated into the hydrodynamical numerical simulation model of unsteady flows to demonstrate applicability to open channel networks.

6.2 Water storage model

Throughout the mathematical description of the control system, the same notation is used for representing a variable both in the time and the frequency domains. The frequency is denoted by s.

A storage network that consists of n_s pools and m_s controllable hydraulic structures is modeled as the linear system which is described by the state equation

$$\frac{d\mathbf{X}}{d\tau} = B\boldsymbol{u} + \boldsymbol{q} \tag{6.1}$$

with the observation equation

$$\boldsymbol{y} = \mathbf{X} \tag{6.2}$$

where τ = scaled time, $\mathbf{X}$ = n_s-dimensional state variable vector which represents the scaled storage volume deviations of the pools, $\boldsymbol{u}$ = m_s-dimensional control variable vector which represents the discharge deviations of controllable hydraulic structures, $\boldsymbol{q}$ = external disturbance vector, and $\boldsymbol{y}$ = observation output vector. The incidence matrix B is of $n_s \times m_s$ in size.

The external disturbance vector $\boldsymbol{q}$, which is the external inflow discharges into the pools, is assumed to be generated by a generator G from an observable n_s–dimensional reference vector $\boldsymbol{r}$. In practice, the generator G and the reference vector $\boldsymbol{r}$ may be a runoff

model and precipitation data.

6.3 Errors in the model

The modeling error in the generator G and the control error are taken into account in the controller design.

The generator G, whose definite expression is hardly obtained, is perturbed from a nominal generator G_0, which is written as

$$G_0 = \mathrm{diag}\left[\frac{k_i}{s+a_i}\right] \tag{6.3}$$

where $k_i = i-$th load coefficient, and $a_i = i-$th decay coefficient. In the true generator G, k_i and a_i are assumed to deviate as $k_i + \Delta_i^k$ and $a_i + \Delta_i^a$ with deviation parameters Δ_i^k and Δ_i^a whose maximum absolute values are prescribed. Then, the generator G as the transfer function from $\boldsymbol{r}$ to $\boldsymbol{q}$ is expressed as the block diagram shown in Figure 6.1.

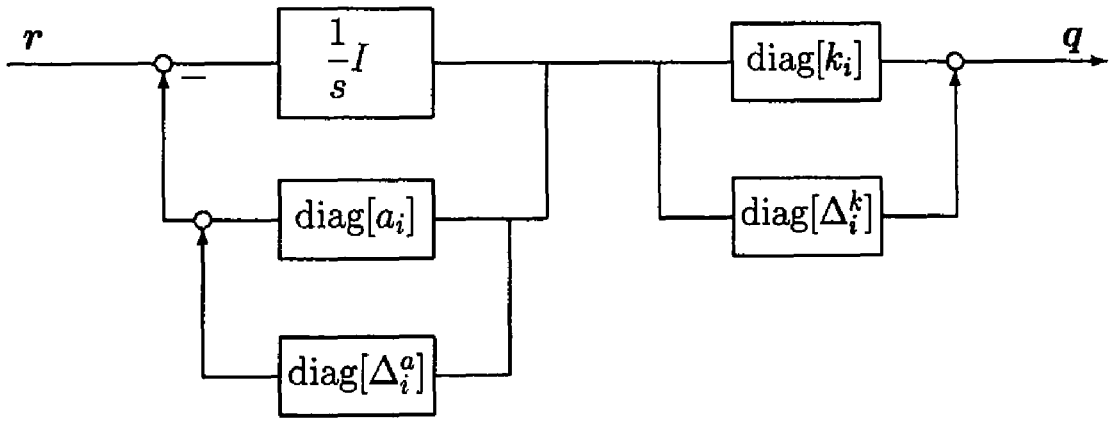

Figure 6.1: Block diagram of gengerator G

The control error is mostly due to the saturation of control variables. If a gate is fully open, the discharge cannot be controlled. Discharges given as boundary conditions are constrained. Thus, the control variable vector $\boldsymbol{u}$ is assumed to be multiplicatively perturbed from a nominal control variable vector $\boldsymbol{u}_1$ as

$$\boldsymbol{u} = (I + \mathrm{diag}[\Delta_i^u])\,\boldsymbol{u}_1 \tag{6.4}$$

where $I = n_s$-dimensional unit matrix, and $\Delta_i^u =$ deviation parameter for the $i-$th com-

ponent of $\boldsymbol{u}$.

6.4 Design of controllers

The Doyle's notation (Doyle *et al.* [22]) is used for the system matrix. For example, $\left[\begin{array}{c|c} G_{11} & G_{12} \\ \hline G_{21} & G_{22} \end{array}\right]$ denotes the transfer matrix $G_{21}\,(sI - G_{11})^{-1}\,G_{12} + G_{22}$ for matrices G_{ij} $(i, j = 1, 2)$ of compatible dimensions.

Let the reference vector $\boldsymbol{r}$, the actual control variable vector $\boldsymbol{u}$, and the observation output vector $\boldsymbol{y}$ be known. In the control system whose block diagram is shown in Figure 6.2, controllers K_G, K_C, and K_R are designed to determine the nominal control variable vector $\boldsymbol{u}_1$ which stabilizes the entire system.

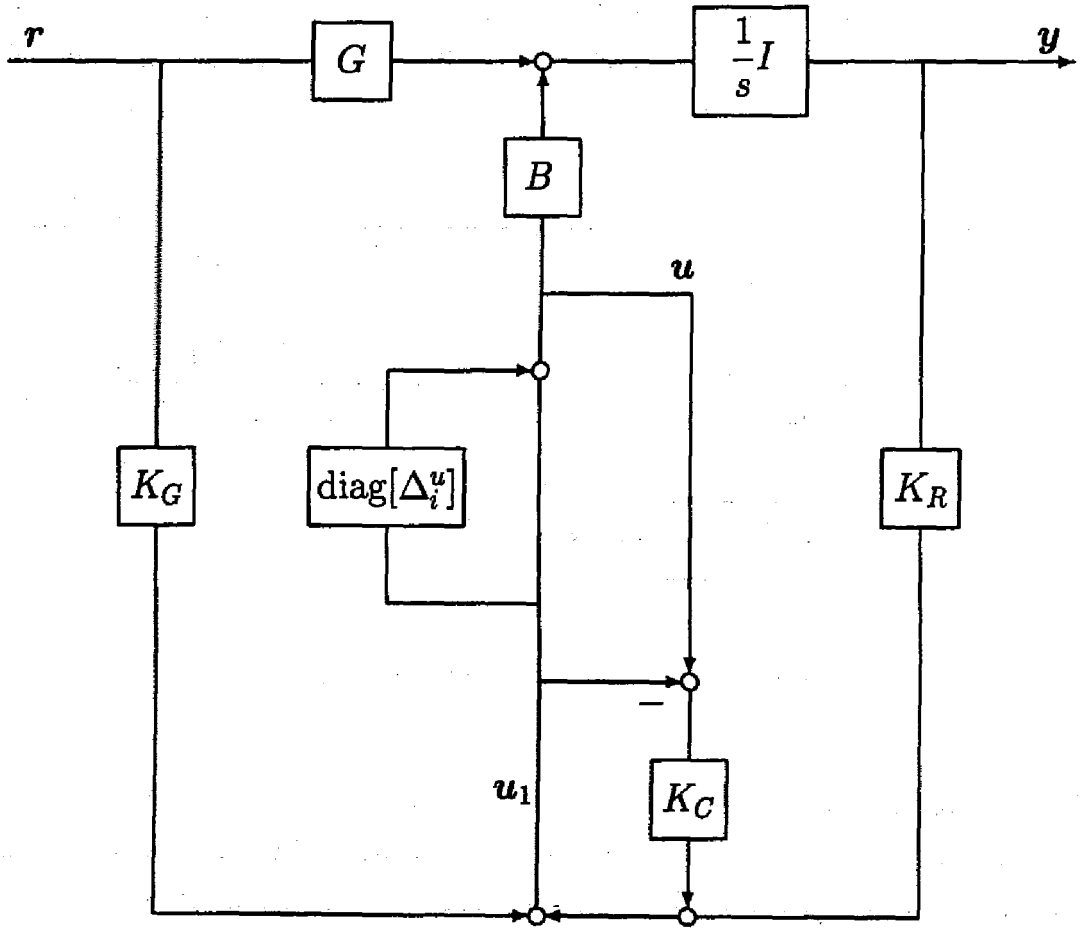

Figure 6.2: Block diagram of control system

6.4.1 Controller K_G

The controller K_G is chosen as

$$K_G = -B_F\,(BB_F)^{-1}\,G_0 \stackrel{s}{=} \left[\begin{array}{c|c} -\mathrm{diag}[a_i] & I \\ \hline -B_F\,(BB_F)^{-1}\,\mathrm{diag}[k_i] & 0 \end{array}\right] \tag{6.5}$$

where $B_F = m_s \times n_s$ matrix which can be taken as B^T, to cancel out the external disturbance if there is no error in the whole system.

6.4.2 Controller K_C

Extracting the control error characteristics as an H_∞ standard problem as shown in Figure 6.3, the controller K_C is determined to make the H_∞ norm of the closed-loop transfer function matrix, which is equal to $\mathrm{diag}[\Delta_i^u]$, less than unity. The class of such K_C is characterized by

$$K_C = \mathrm{diag}\left[\frac{1}{\Delta_i^u}\right] N(s) \tag{6.6}$$

where $N(s)$ = any stable transfer function matrix whose H_∞ norm is less than unity.

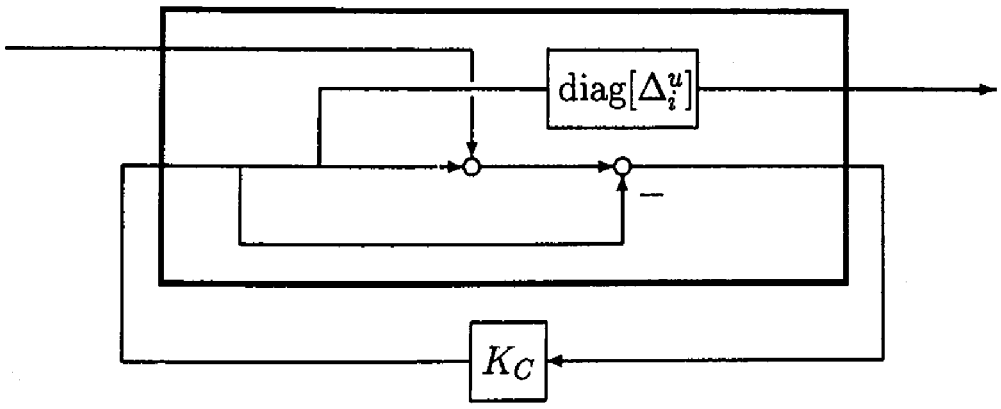

Figure 6.3: H_∞ standard plant for K_C

6.4.3 Controller K_R

The algebraic design method is employed to obtain the controller K_R. An H_∞ standard problem is formulated as expressed in Figure 6.4 to bound the H_∞ norm of the closed-

loop transfer function from an input disturbance vector $\begin{bmatrix} \boldsymbol{w}_1 \\ \boldsymbol{w}_2 \\ \boldsymbol{w}_3 \end{bmatrix}$ to an error signal vector $\begin{bmatrix} \boldsymbol{z}_1 \\ \boldsymbol{z}_2 \\ \boldsymbol{z}_3 \end{bmatrix}$ taking the reference vector $\boldsymbol{r}$ as the input disturbance $\boldsymbol{w}_1$ and using $w_i^y (i = 1 \sim n_s)$, constant weights to scale the observation output vector $\boldsymbol{y}$ as the error signal $\boldsymbol{z}_3$. A state space representation of the generalized plant in the H_∞ standard problem is obtained as

$$\begin{bmatrix} \mathrm{diag}\left[\frac{\Delta_i^a}{s+a_i}\right] & -\mathrm{diag}\left[\frac{\Delta_i^a}{s+a_i}\right] & 0 & 0 \\ \mathrm{diag}\left[\frac{\Delta_i^k}{s+k_i}\right] & -\mathrm{diag}\left[\frac{\Delta_i^k}{s+k_i}\right] & 0 & 0 \\ 0 & -\frac{1}{s}\mathrm{diag}\left[\frac{w_i^y \Delta_i^k}{s+a_i}\right] & \frac{1}{s}\mathrm{diag}\left[w_i^y\right] & -\frac{1}{s}\mathrm{diag}\left[w_i^y\right] B \\ 0 & -\frac{1}{s}\mathrm{diag}\left[\frac{\Delta_i^k}{s+a_i}\right] & \frac{1}{s} I & \frac{1}{s} B \end{bmatrix} \overset{s}{=} \left[\begin{array}{c|cc} A_0 & B_1 & B_2 \\ \hline C_1 & [0] & [0] \\ C_2 & [0] & [0] \end{array}\right]$$

$$= \left[\begin{array}{cc|ccc} \begin{bmatrix} -\mathrm{diag}[a_i] & 0 & 0 & 0 \\ 0 & -\mathrm{diag}[a_i] & 0 & 0 \\ 0 & 0 & 0 & \mathrm{diag}[k_i] \\ 0 & 0 & 0 & -\mathrm{diag}[a_i] \end{bmatrix} & & \begin{bmatrix} I & -I & 0 \\ I & -I & 0 \\ 0 & 0 & I \\ 0 & -I & 0 \end{bmatrix} & \begin{bmatrix} 0 \\ 0 \\ B \\ 0 \end{bmatrix} \\ \hline \begin{bmatrix} \mathrm{diag}[\Delta_i^a] & 0 & 0 & 0 \\ 0 & \mathrm{diag}\left[\Delta_i^k\right] & 0 & 0 \\ 0 & 0 & \mathrm{diag}[w_i^y] & 0 \end{bmatrix} & & \begin{bmatrix} 0 \end{bmatrix} & \begin{bmatrix} 0 \end{bmatrix} \\ \begin{bmatrix} 0 & 0 & I & 0 \end{bmatrix} & & \begin{bmatrix} 0 \end{bmatrix} & \begin{bmatrix} 0 \end{bmatrix} \end{array}\right] \tag{6.7}$$

where $A_0 = 4n_s \times 4n_s$ state matrix, $B_1 = 4n_s \times 3n_s$ disturbance distribution matrix, $B_2 = 4n_s \times m_s$ control distribution matrix, $C_1 = 3n_s \times 4n_s$ error output matrix, and $C_2 = n_s \times 3n_s$ observation output matrix.

Since all the components are zero matrix in the 2-2 block of the system matrix in Eqn. 6.7, the class of all stabilizing controllers cannot be identified as in Glover and Doyle [31]. However, Sampei *et al.* [82] deduce an existence theorem and take an algebraic approach similar to Zhou and Khargonekar [98] as follows.

A strictly proper controller stabilizes the system and makes the H_∞ norm of the closed-loop transfer function less than unity if and only if the following conditions are satisfied.

1. There exists F such that there exists a positive definite solution X_∞ to the algebraic

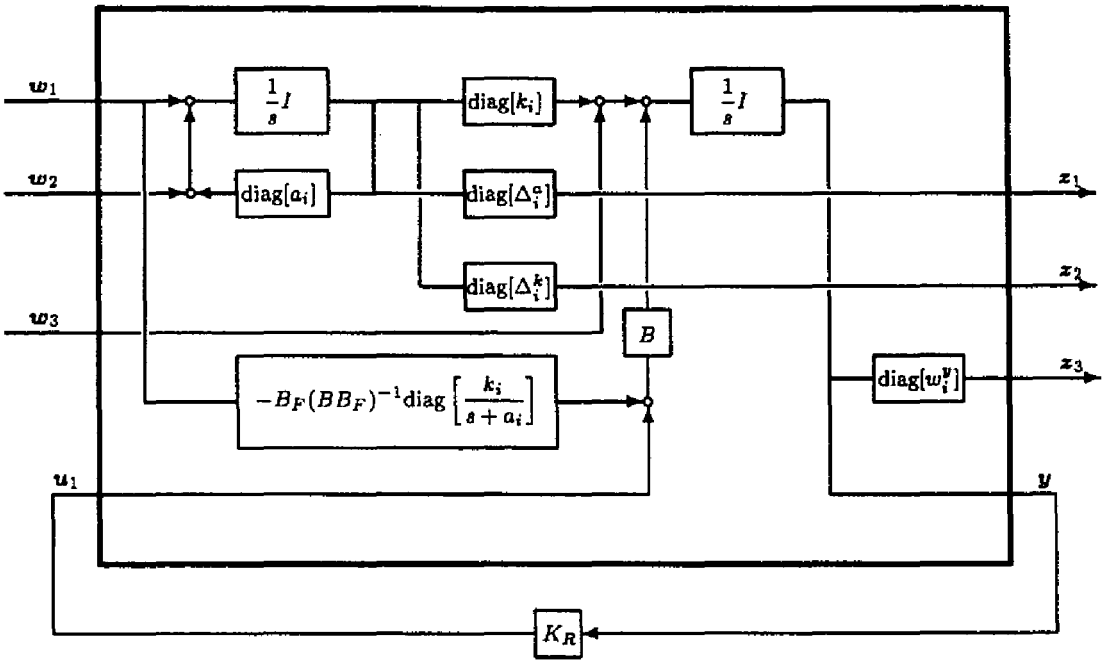

Figure 6.4: H_∞ standard plant for K_R

Riccati inequality

$$X_\infty A_X + A_X^T X_\infty + C_1^T C_1 + X_\infty B_1 B_1^T X_\infty < 0 \tag{6.8}$$

where $A_X = A_0 + B_2 F$.

2. There exists L such that there exists a positive definite solution Y_∞ to the algebraic Riccati inequality

$$Y_\infty A_Y^T + A_Y Y_\infty + B_1 B_1^T + Y_\infty C_1^T C_1 Y_\infty < 0 \tag{6.9}$$

where $A_Y = A_0 + L C_2$.

3. The maximum singular value of $(X_\infty Y_\infty)$ is less than unity.

Moreover, one of such strictly proper controller is given by

$$K_R = \left[\begin{array}{c|c} \hat{A} & \hat{B} \\ \hline \hat{C} & 0 \end{array}\right] = \left[\begin{array}{c|c} A_X + B_1 B_1^T X_\infty - Z\left(E + F^T B_2^T X_\infty - Y_\infty^{-1} L C_2\right) & -Z Y_\infty^{-1} L \\ \hline F & 0 \end{array}\right] \tag{6.10}$$

where $Z = (Y_\infty^{-1} - X_\infty)^{-1}$, and $E = -\left(X_\infty A_X + A_X^T X_\infty + C_1^T C_1 + X_\infty B_1 B_1^T X_\infty\right)$. A proof is given in Appendix D. Numerical solutions of the Riccati equations

$$X_\infty A_X + A_X^T X_\infty + C_1^T C_1 + X_\infty B_1 B_1^T X_\infty + \varepsilon I = 0 \tag{6.11}$$

and

$$Y_\infty A_Y + A_Y^T Y_\infty + B_1 B_1^T + Y_\infty C_1^T C_1 Y_\infty + \varepsilon I = 0 \tag{6.12}$$

determine X_∞ and Y_∞, respectively, in practical design.

6.5 Applications

6.5.1 Reservoir operation in flood

The controllers are applied to determining the release discharge of a single reservoir, where $n_s = m_s = 1$ and $B = [1]$, when a flood wave enters into it. Two sets of data D-1 and D-2 are observed at Y dam as summarized in Tables 6.1 and 6.2 and used for identifying the runoff model. Identification procedures using the least square method yield the runoff models $\frac{0.2012}{s+6.899}$ and $\frac{0.0885}{s+3.506}$ for D-1 and D-2, respectively. Then, the nominal generator G_0 is taken as $\frac{0.15}{s+5}$ with the deviation parameters $\Delta_i^k = 0.10$ and Δ_i^a =3.4. Setting $\varepsilon = 10^{-2}$, $F = \begin{bmatrix} 0 & 0 & -5 & 0 \end{bmatrix}$, and $L = \begin{bmatrix} 0 \\ 0 \\ -1 \\ -1 \end{bmatrix}$, the controller K_R is obtained from Eqn.(6.10).

Simulation runs are executed for 5 cases which include different combination of controllers as shown in Table 6.3. Results for flood data D-1 and D-2 are depicted in Figures 6.5 and 6.6, respectively, and show that the controller K_C is necessary for settling the storage volume after the saturation of the control variable occurs. The role of the controller K_R is not dominant.

6.5.2 Open channel network

When controllable hydraulic structures such as gate or pump are installed in an open channel network to separate it into water pools, the network is regarded as a storage network no matter how is the flow dynamics in the pools. Applicability of the control system to such an open channel network is tested in the WB model. However, 4 gates

Table 6.1: Flood data D-1

Time[hour]	Precipitation[m/day]	Inflow discharge [10^6m/day]
1	0.168	0.51
2	0.360	0.70
3	0.480	1.35
4	0.360	1.82
5	0.648	3.12
6	0.300	4.85
7	0.420	5.76
8	0.096	6.34
9	0.000	4.97
10	0.012	4.24
11	0.060	3.73
12	0.048	3.34
13	0.024	2.83
14	0.012	2.38
15	0.000	2.25
16	0.000	2.01
17	0.000	2.25

other than the one in the previous chapters are installed across the channel as shown in Figure 6.7, and drops are removed as shown in Figure 6.9. The gates G-1 through 5 and the boundaries Γ_1 and Γ_2 are handled as the controllable hydraulic structures to separate the channel network into 4 pools. Thus, the open channel network is regarded as a storage network of 4 pools with 7 controllable hydraulic structures, as shown in Figure 6.8, and the 4×7 matrix

$$B = \begin{bmatrix} 1 & -1 & -1 & 0 & 0 & 0 & 0 \\ 0 & 1 & 0 & -1 & -1 & 0 & 0 \\ 0 & 0 & 1 & 1 & 0 & -1 & 0 \\ 0 & 0 & 0 & 0 & 1 & 1 & -1 \end{bmatrix} \tag{6.13}$$

becomes the incidence matrix B in Eqn.(6.1).

The coefficients, deviation parameters, and weights are prepared as shown in Table 6.4 to be used for designing controllers K_G and K_R. The deviation parameter Δ_i^u is supposed 0.5 for every controllable hydraulic structure, and the free transfer function matrix $N(s)$ in Eqn.(6.6) is specified as the 7×7 matrix diag$[s+1]$ to establish the controller K_C.

Table 6.2: Flood data D-2

Time[hour]	Precipitation[m/day]	Inflow discharge [10^6m/day]
1	0.288	0.81
2	0.720	1.98
3	0.540	7.34
4	0.192	7.59
5	0.036	5.40
6	0.072	4.37
7	0.336	4.44
8	0.060	5.18
9	0.012	4.32
10	0.120	3.77
11	0.984	4.04
12	1.524	7.89
13	1.476	20.07
14	1.512	23.96
15	0.624	28.68
16	0.204	19.01
17	0.156	12.42
18	0.084	12.82
19	0.144	12.92
20	0.120	10.57
21	0.048	8.52
22	0.012	8.39
23	0.000	7.91
24	0.000	6.26
25	0.012	5.22
26	0.000	5.72
27	0.012	5.43
28	0.000	4.33
29	0.000	4.42
30	0.000	4.17
31	0.000	3.64
32	0.000	3.32

Setting $\varepsilon = 10^{-2}$, $F = \begin{bmatrix} 0 & 0 & -150B^T & 0 \end{bmatrix}$, and $L = \begin{bmatrix} 0 \\ 0 \\ -150I \\ 0 \end{bmatrix}$, the controller K_R is obtained from Eqn.(6.10).

The controllers are incorporated into the open channel flow model. The storage volumes of the pools are evaluated from the water depths at the boundary nodes and those at the

nodes which bound the gates. All components of the reference $\boldsymbol{r}$ are equally taken, and the discharges which are actually withdrawn from the turnouts in the pools are different from those which are expected from the reference $\boldsymbol{r}$ with the nominal generator G_0, as shown in Figure 6.10.

Simulation runs are executed for 4 cases which include different combination of controllers as shown in Table 6.5. The scaled storage volumes of pools are calculated as in Figure 6.11. Nominal and actual discharge deviations of controllable hydraulic structures are depicted in Figure 6.12. The system drastically becomes stable in Case 4 where all the controllers are used, even though significant differences exist between the nominal and the actual discharge deviations. However, in contrast with the case of reservoir, contribution of the controller K_R is more significant than that of the controller K_C. Indeed, removing the controller K_C from Case 4 results in minor change in system performance.

6.6 Conclusions

The robust control system which considers a generator and has three controllers is designed. Robustness when the generator includes the modeling errors, robustness under the control errors, and bounded variations in storage volumes are guaranteed in the sense of the H_∞ control problem and verified in the simulations. The system is applied to the reservoir, where the generator is the runoff model from precipitation to inflow into it, and then to the open channel network. The simulation results demonstrate excellent regulation performance in both cases. The observation errors are not explicitly evaluated but scarcely affects stability of the system.

Table 6.3: Combination of controllers for reservoir operation

Case 1	No controller
Case 2	K_G
Case 3	K_G and K_C
Case 4	K_G and K_R
Case 5	K_G, K_C, and K_R

Table 6.4: Design data for controllers

i	k_i	Δ_i^k	a_i	Δ_i^a	w_i^y
1	15	10	25	10	50
2	20	10	50	20	50
3	25	10	75	30	50
4	30	10	100	40	50

Table 6.5: Combination of controllers for open channel network operation

Case 1	No controller
Case 2	K_C
Case 3	K_G
Case 4	K_G, K_C, and K_R

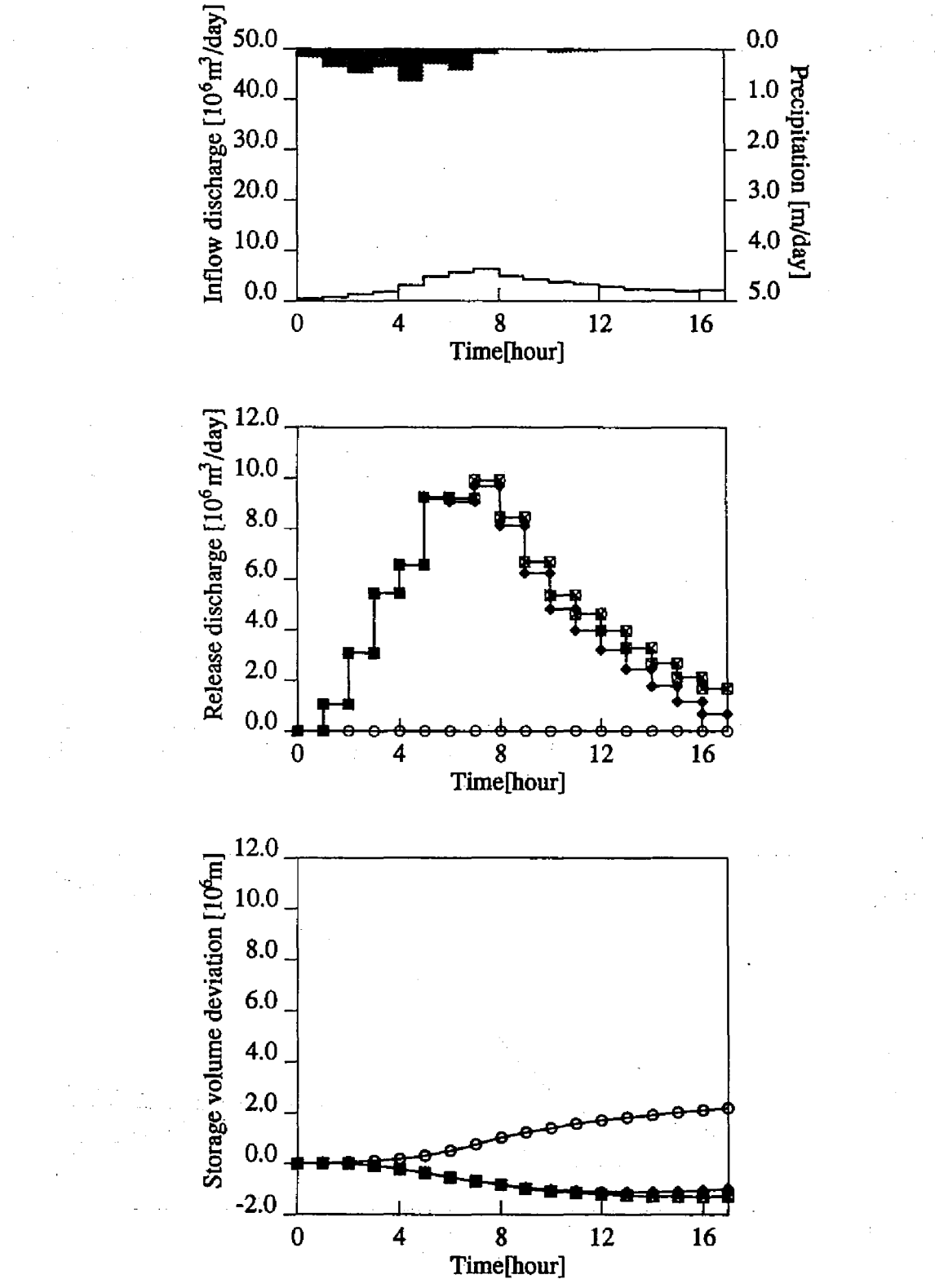

Figure 6.5: Simulation results for flood data D-1

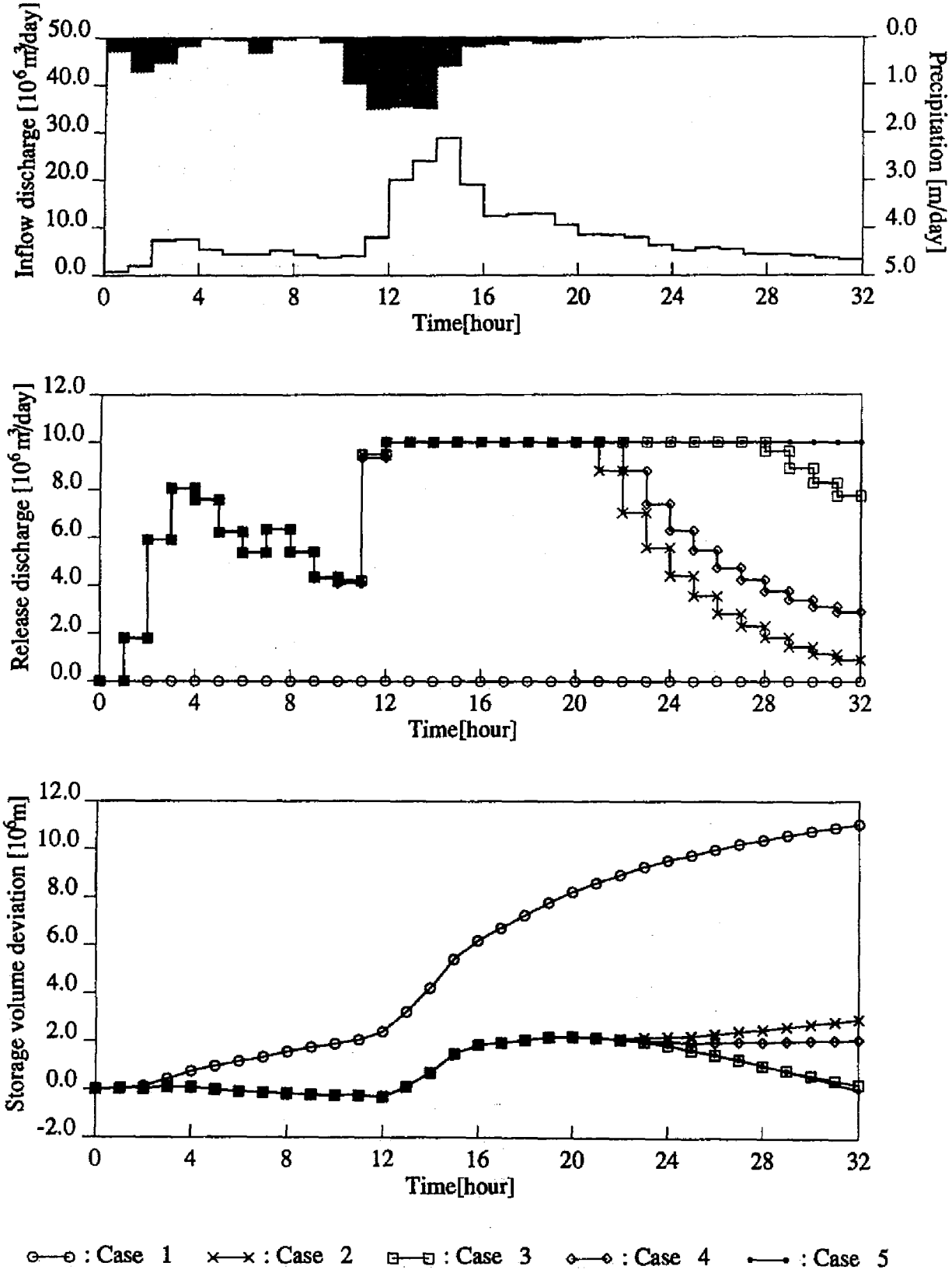

Figure 6.6: Simulation results for flood data D-2

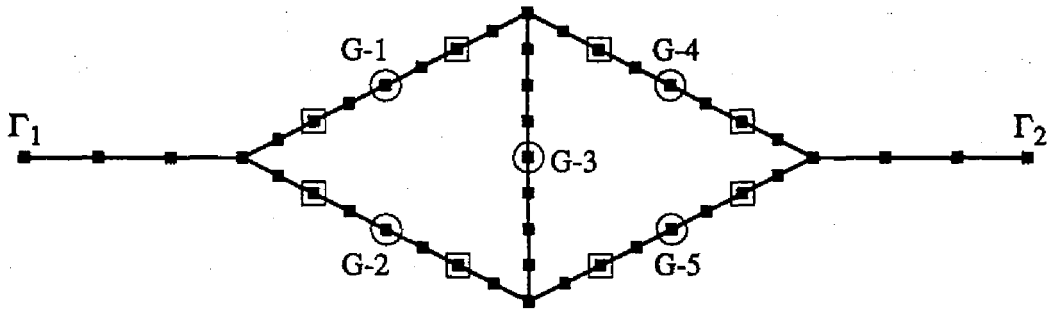

■ : node ○ : gate □ : turnout

Figure 6.7: Open channel network of Wheatstone bridge type

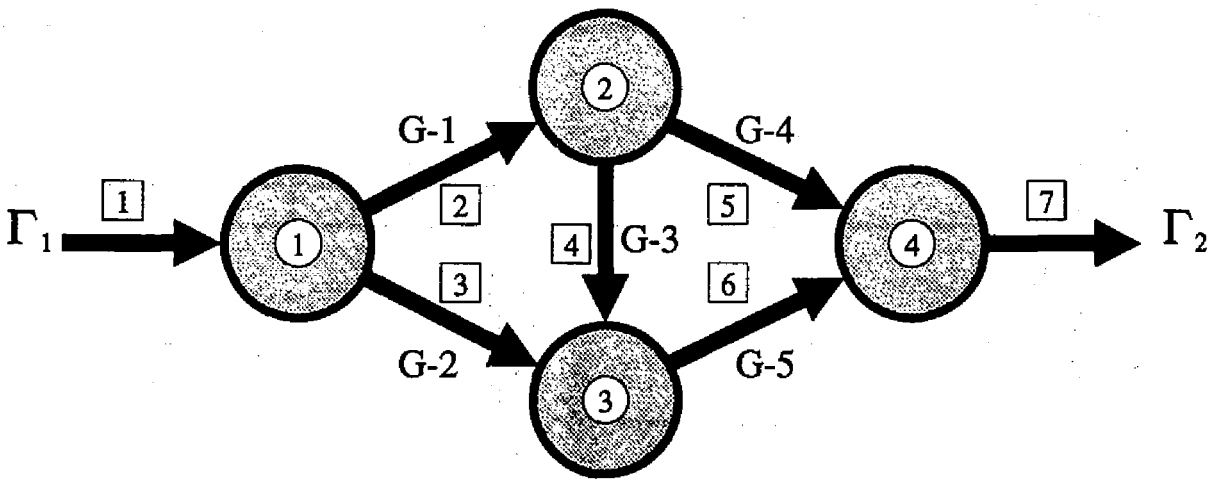

$\boxed{i}$: i−th controllable hydraulic structure $\textcircled{i}$: i−th pool

Figure 6.8: Storage network

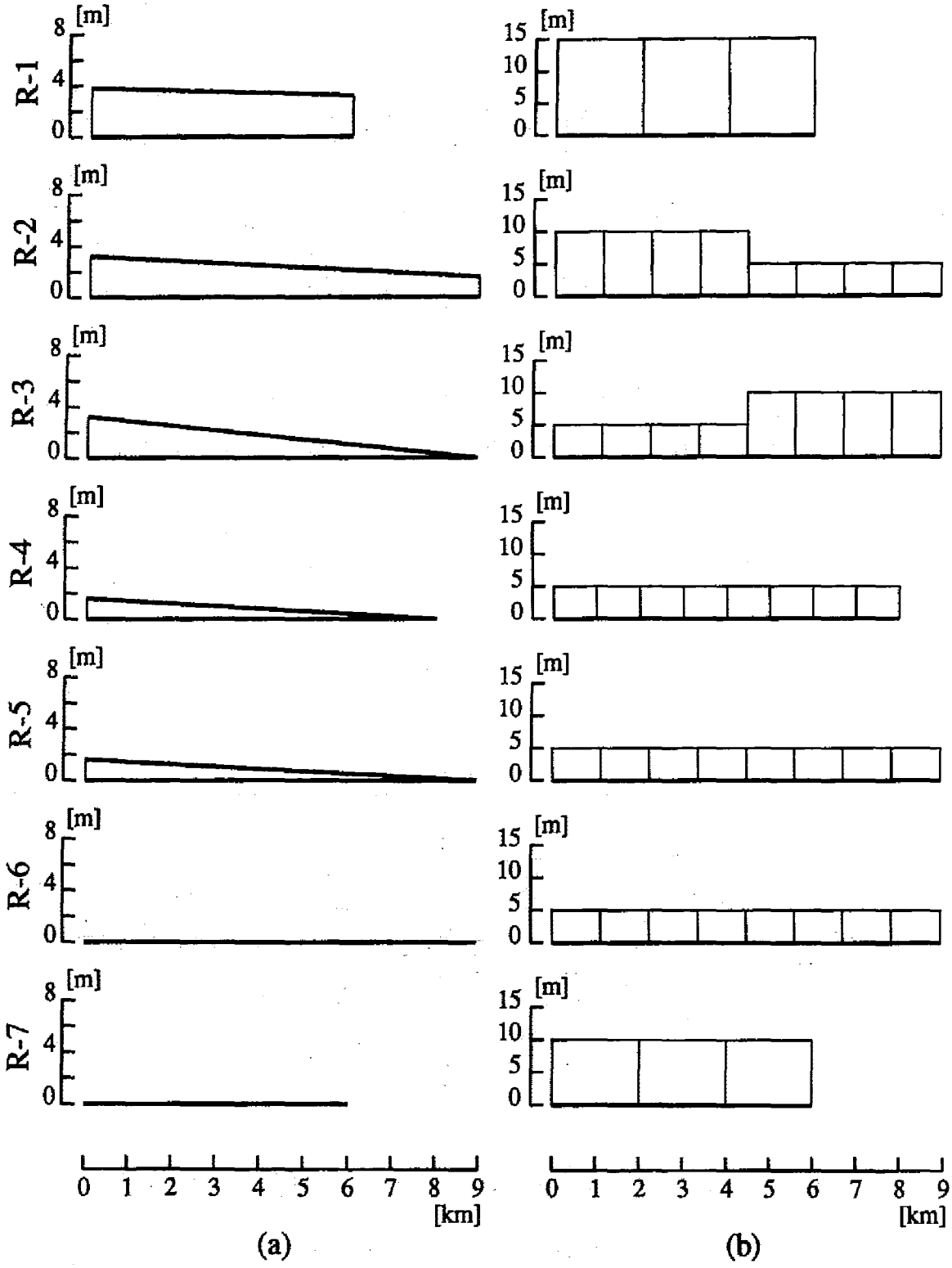

Figure 6.9: Channel geometry: (a) Bed elevation; (b) Section width

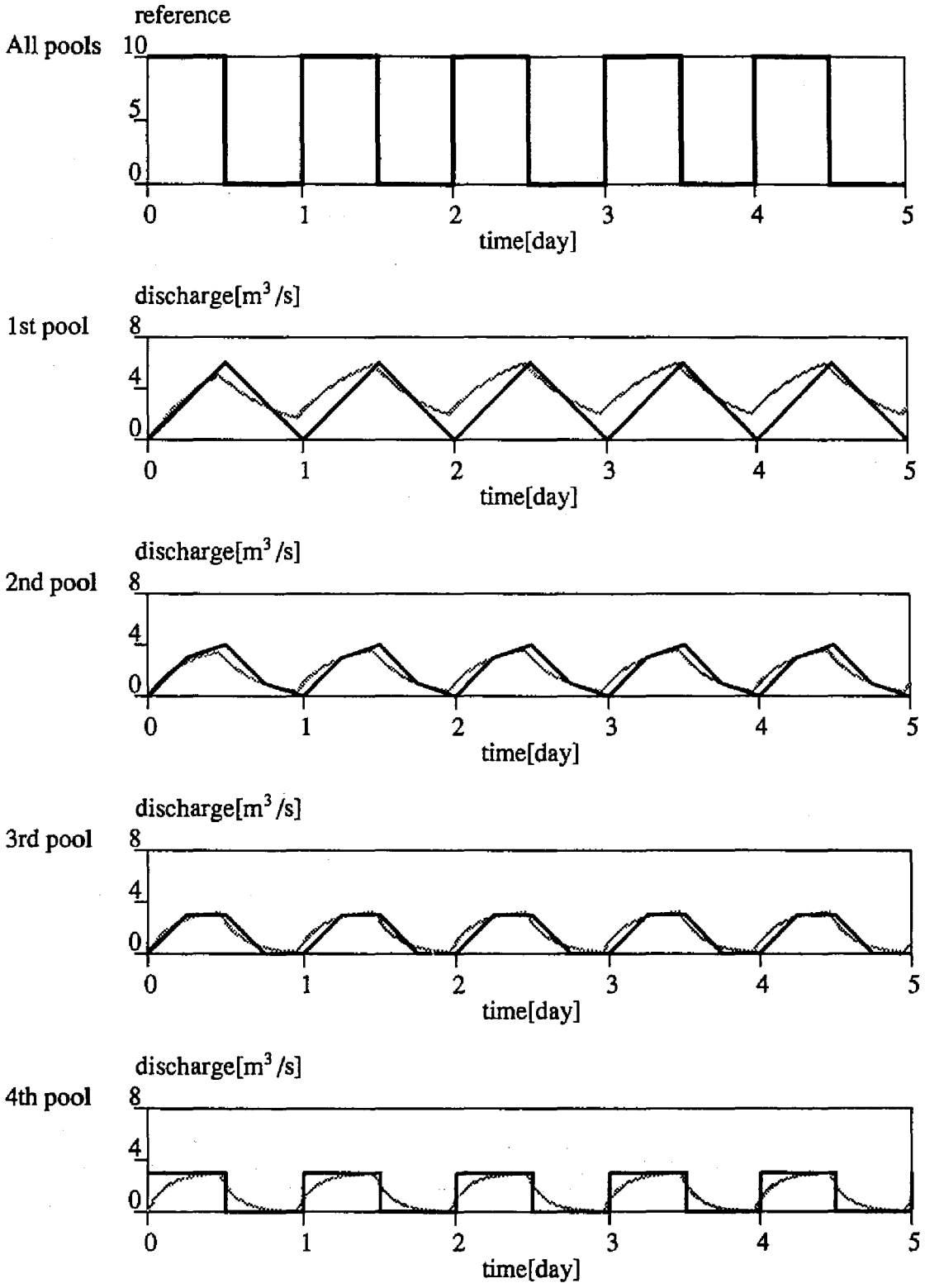

Figure 6.10: Reference and external disturbances

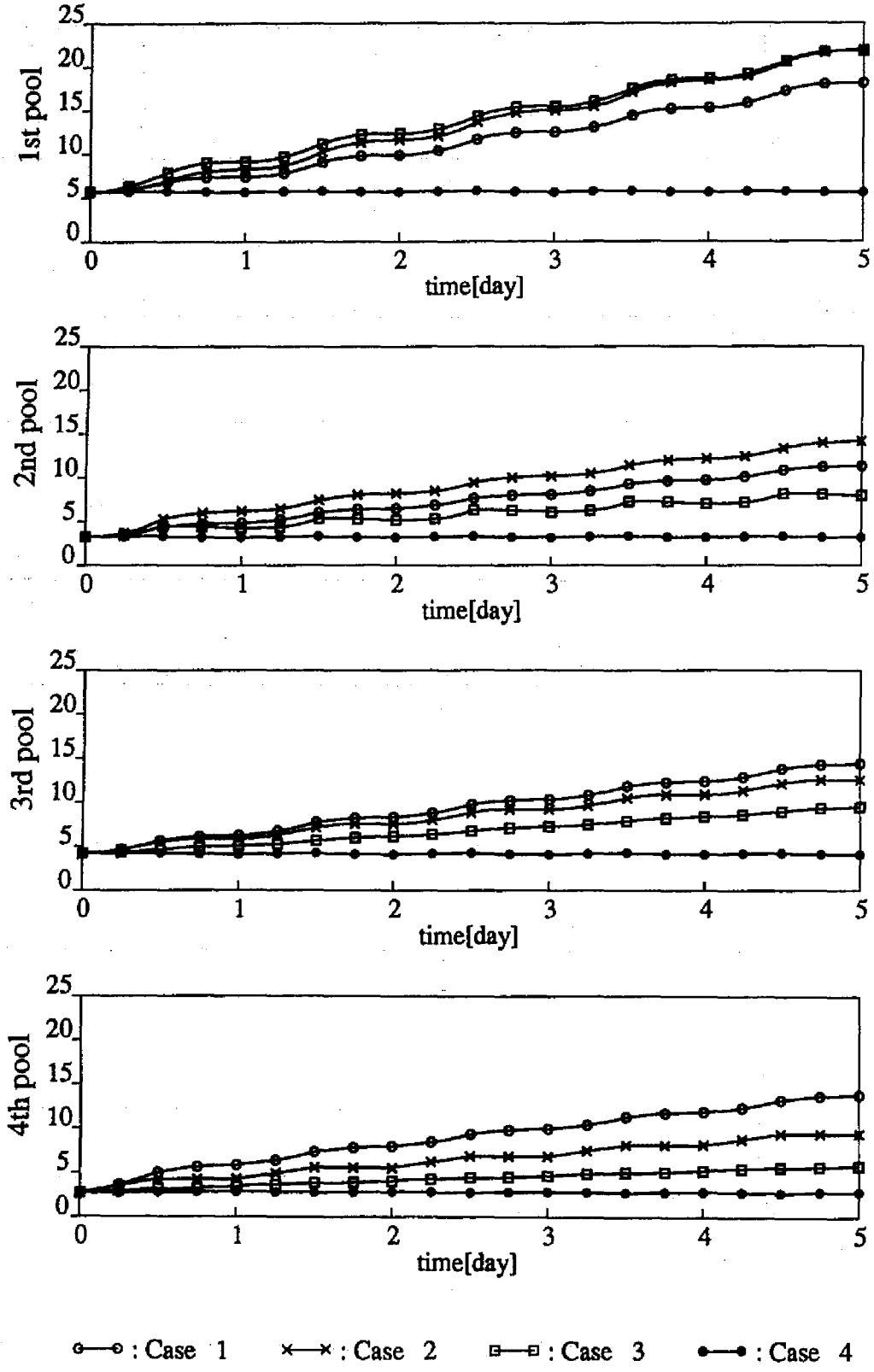

Figure 6.11: Scaled storage volumes of pools

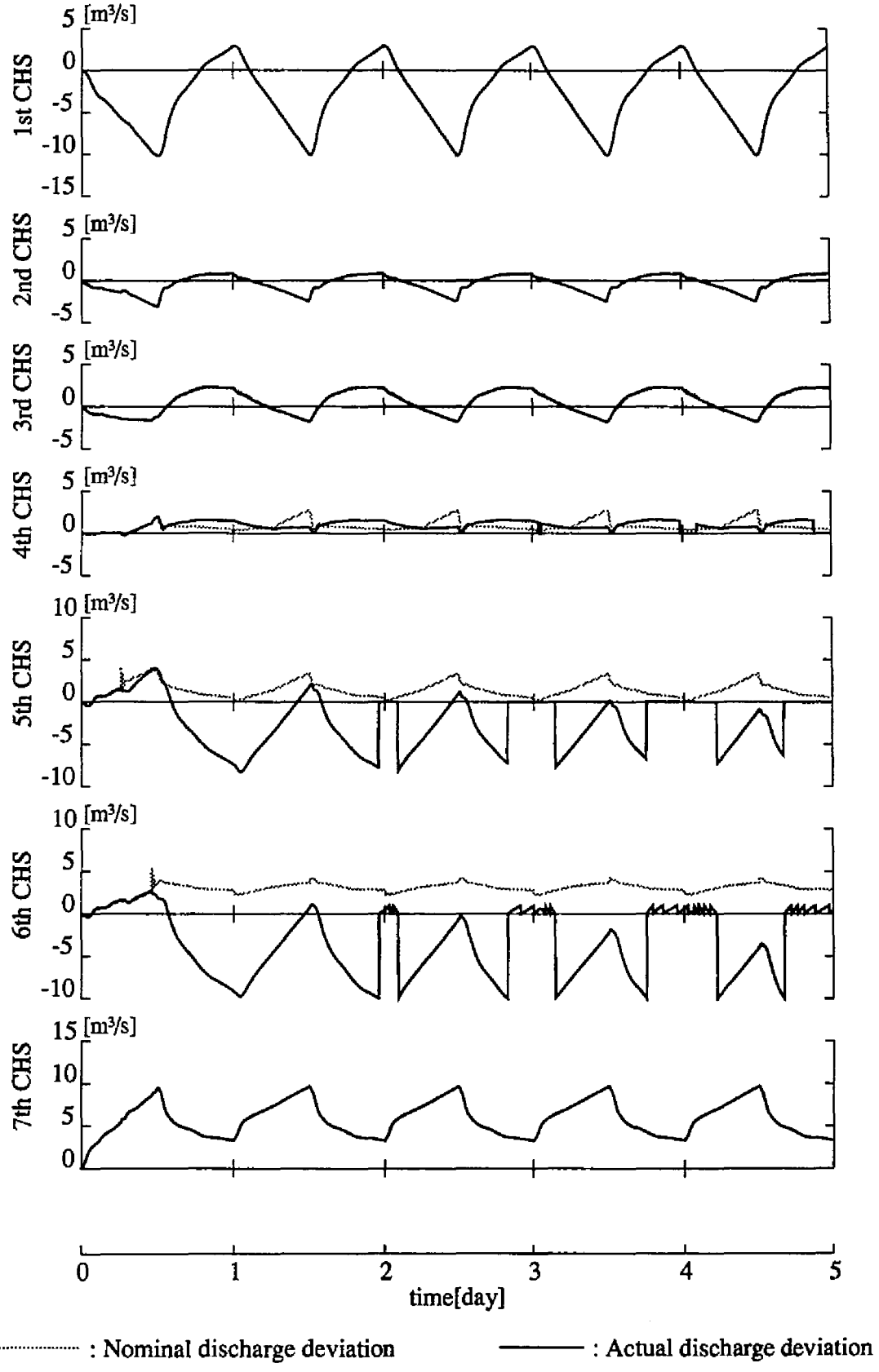

Figure 6.12: Discharge deviations of controllable hydraulic structures (CHSs)

Chapter 7

Conclusions

In this thesis, optimization and control problems in water conveyance and water storage systems are studied as part of comprehensive synthesis of water resources management.

The mathematical and numerical modeling techniques are prepared in Chapter 2 and used for examining applicability of optimization theories in the succeeding chapters by computer. The WB model, which is a model for a multiply connected open channel network, is consistently investigated in Chapters 2, 3, 4, and 6, where open channel network flows are considered.

The optimal control problems are formulated in the framework of the variational calculus for open channel unsteady flows and for reservoir reliability in Chapters 3 and 5, respectively. The minimum principle given in Chapter 3 comprehends all combination of observation and control, but only the boundary observation boundary control, the mixed observation domain control, and the terminal time observation domain control problems are demonstratively solved. An important practical example which is not discussed is a calibration problem of key parameters of channels such as roughness from measured water level data, which shall be a boundary observation domain control problem. The decision support model developed in Chapter 5 is an application of the terminal time (physically initial time) observation domain control problem formulation. A systematic optimization algorithm is not used except for the terminal time observation domain control problem in Chapter 3, where the iteration procedure yields the good convergent result. However, information obtained from the adjoint variables serves as a powerful tool to revise the control variables even by the manual procedures.

The Markov process models are discussed in Chapters 4 and 5 using the FPPDEs. Allowing for spatial distribution of possible variation in free surface enables a tight design of an open channel. The FPPDE and its adjoint system are numerical solved in Chapter 5 using the upwind discretization scheme developed for parabolic PDEs which may be of convection dominant in Chapter 2. The demonstrative examples use data observed at the

existing reservoirs. The determination of the coefficients in the FPPDE shall be further investigated especially when a certain event can be anticipated in advance.

Possibility of real time automatic control is discussed in Chapter 6. Open channels and reservoirs are inclusively investigated using the water storage model. The modern control theory is employed to design robust control systems. Since four zero components appear in the 2-2 block of the generalized plant, identification of the class of all stabilizing controllers cannot be given for the time being. However, the stabilizing strictly proper controller obtained by the algebraic method proves excellent robust performance in example simulations.

Computational efficiency is scarcely discussed throughout this thesis. The nonlinear equations are mostly solved by the Newton-Raphson method using numerical derivatives, which consume a huge amount of computational time. The Riccati equations in the design of the robust controllers are obtained by a primitive numerical integration method. Sophistication of the computational algorithms is necessary for application to more complicated cases.

References

[1] Abbott, M.B. and D.R. Basco. *Computational Fluid Dynamics: An Introduction for Engineers.* Longman, 1989. pp.259–264.

[2] Afif, M. *Analyse numŕique de quelques problèmes hyperboliques issus de la modélisation des crues de rivières.* PhD thesis, L'Université de Saint-Etienne, 1986. (in French).

[3] Alam, M.M. and M.A. Bhuiyan. Collocation finite-element simulation of dam-break flows. *Journal of Hydraulic Engineering, ASCE*, 121(2), 118–128, 1995.

[4] Alshaikh, A. and S. Taher. Optimal desigh of irrigation canal network under uncertainty using reponse surface method. *Water International*, 20, 155–162, 1995.

[5] Altman, T. and P.F. Boulos. Solving flow-constrained networks: Inverse problem. *Journal of Hydraulic Engineering, ASCE*, 121(5), 427–431, 1995.

[6] Anastasiadou-Partheniou, L. and G. Terzidis. A dissipative finite element model for discontinuous unsteady flow in open channel. *Agricultural Water Management*, 13, 157–168, 1988.

[7] Balogun, O.S., M. Hubbard and J.J. DeVries. Automatic control of canal flow using linear quadratic regulator theory. *Journal of Hydraulic Engineering, ASCE*, 114(1), 75–102, 1988.

[8] Bautista, E., A.J. Clemmens and T. Strelkoff. Comparison of numerical procedures for gate stroking. *Journal of Irrigation and Drainage Engineering, ASCE*, 123(2), 129–136, 1997.

[9] Beffa, C. Backwater computation for transcritical river flows. *Journal of Hydraulic Engineering, ASCE*, 122(12), 745–748, 1996.

[10] Blandford, G.E. and L.E. Ormsbee. A diffusion wave finite element model for channel networks. *Journal of Hydrology*, 142, 99–120, 1993.

[11] Buchberger, S.G. and D.R. Maidment. Diffusion approximation for equilibrium distribution of reservoir storage. *Water Resources Research*, 25(7), 1643–1652, 1989.

[12] Burt, C.M. and G. Gartrell. Irrigation-canal – simulation model usage. *Journal of Irrigation and Drainage Engineering, ASCE*, 119(4), 631–636, 1993.

[13] Buyalski, C.P. Automatic downstream control of the Corning canal check gates. *Symposium for U.S./U.S.S.R. Cooperative Program – "Automation and Remote Control of Water Resource Systems"*, 1979.

[14] Buyalski, C.P. Automatic downstream control system for canal headworks pumping plants. *8th Technical Conference, U.S. Committee on Irrigation, Drainage, and Flood Control*, Phonix, Arizona, USA, 1979. ICID.

[15] Buyalski, C.P. Automatic upstream control system for canals. *8th Technical Conference, U.S. Committee on Irrigation, Drainage, and Flood Control*, Phonix, Arizona, USA, 1979. ICID.

[16] Buyalski, C.P. and H.T. Falvey. Stability of automatic canal systems utilizing the frequency response method. *Symposium on Fluid Motion Stability in Hydraulic Systems with Automatic Regulators*, Bucharest, Romania, 1976. IAHR.

[17] Choi, G.W. and A. Molinas. Simultaneous solution algorithm for channel network modeling. *Water Resources Research*, 29(2), 321–328, 1993.

[18] Choi, S.-U. and M.H. Garcìa. Modeling of one-dimensional turbidity currents with a dissipative-Galerkin finite element method. *Journal of Hydraulic Research*, 33(5), 623–648, 1995.

[19] Clemmens, A.J. and J.A. Replogle. Control of irrigation canal networks. *Journal of Irrigation and Drainage Engineering, ASCE*, 115(1), 96–110, 1989.

[20] Clemmens, A.J., G. Sloan and J. Schuurmans. Canal-control needs: Example. *Journal of Irrigation and Drainage Engineering, ASCE*, 120(6), 1067–1085, 1994.

[21] Corriga, G., F. Patta, S. Sanna and G. Usai. A mathematical model for open-channel networks. *Applied Mathematical Modelling*, 3, 51–54, 1979.

[22] Doyle, J.C., K. Glover, P.P. Khargonekar and B.A. Francis. State-space solutions to standard H_2 and H_∞ control problems. *Transactions on Automatic Control, IEEE*, 34(8), 831–847, 1989.

[23] Easa, S.M. Probabilistic design of open drainage channels. *Journal of Irrigation and Drainage Engineering, ASCE*, 118(6), 868–881, 1992.

[24] Easa, S.M. Reliability analysis of open drainage channels under mutiple failure modes. *Journal of Irrigation and Drainage Engineering, ASCE*, 120(6), 1007–1024, 1994.

[25] Falvey, H.T. and P.C. Luning. Gate stroking. Technical Report REC-ERC-79-7, Engineering and Research Center, Bureau of Reclamation, USA, 1979.

[26] Fujihara, M. and T. Kawachi. Kinematic eddy viscosity coefficients in residual current equations with tidal stress. *Transactions JSIDRE*, 176, 113–120, 1995.

[27] García-Navarro, P., F. Alcrudo and J.M. Savirón. 1-D open-channel flow simulation using TVD-McCormack scheme. *Journal of Hydraulic Engineering, ASCE*, 118(10), 1359–1372, 1992.

[28] Gates, T.K. and M.A. Al-Zaharani. Spatiotemporal stochastic open-channel flow. I: Model and its parameter dada. *Journal of Irrigation and Drainage Engineering, ASCE*, 122(11), 641–651, 1996.

[29] Gates, T.K. and M.A. Al-Zaharani. Spatiotemporal stochastic open-channel flow. II: Simulation experiments. *Journal of Irrigation and Drainage Engineering, ASCE*, 122(11), 652–661, 1996.

[30] Gates, T.K., A.A. Alshaikh, S.I. Ahmed and D.J. Molden. Optimal irrigation delivery system design under uncertainty. *Journal of Irrigation and Drainage Engineering, ASCE*, 118(3), 433–449, 1992.

[31] Glover, K. and J.C. Doyle. State-space formulae for all stabilizing controllers that satisfy an $H_\infty-$norm bound and relations to risk sensitivity. *Systems & Control Letters*, 11, 167–172, 1988.

[32] Gupta, R. and P.R. Bhave. Reliability analysis of water-distribution systems. *Journal of Irrigation and Drainage Engineering, ASCE*, 120(2), 447–460, 1994.

[33] Hancu, S. and P. Dan. Wave-motion stability in canals with automatic controllers. *Journal of Hydraulic Engineering, ASCE*, 118(12), 1621–1638, 1992.

[34] Hicks, F.E. and P.M. Steffler. Characteristic dissipative Galerkin scheme for open-channel flow. *Journal of Hydraulic Engineering, ASCE*, 118(2), 337–352, 1992.

[35] Horowitz, I.M. *Synthesis of Feedback Systems.* Academic Press, 1963. pp.246–298.

[36] Husain, T., W.A. Abderrahman, H.U. Khan, S.M. Khan, A.U. Khan and B.S. Eqnaibi. Flow simulation using channel network model. *Journal of Irrigation and Drainage Engineering, ASCE*, 114(3), 424–441, 1988.

[37] Ito, K. *Theory of Probability.* Iwanami Pub. Co., 1953. pp. 330–333, (in Japanese).

[38] Jha, A.K., J. Akiyama and M. Ura. Modeling unsteady open-channel flows – modification to Beam and Warming scheme. *Journal of Hydraulic Engineering, ASCE*, 120(4), 461–476, 1994.

[39] Jha, A.K., J. Akiyama and M. Ura. First- and second-order flux difference splitting schemes for dam-break problem. *Journal of Hydraulic Engineering, ASCE*, 121(12), 877–884, 1995.

[40] Jin, M. and D.L. Fread. Dynamic flood routing with explicit and implicit numerical solution schemes. *Journal of Hydraulic Engineering, ASCE*, 123(3), 166–173, 1997.

[41] Joliffe, I.B. Computation of dynamic waves in channel networks. *Journal of Hydraulic Engineering, ASCE*, 110(10), 1358–1370, 1984.

[42] Karamouz, M. and H.V. Vasiliadis. Bayesian stochastic optimization of reservoir operation using uncertain forecasts. *Water Resources Research*, 28(5), 1221–1232, 1992.

[43] Kawachi, T., B.-J. Cho, I. Minami and K.-S. Yoon. Finite element long-term analysis of the salt water exclusion process in an estuarine reservoir. *Irrigation Engineering and Rural Planning*, 20, 18–32, 1991.

[44] Kawachi, T., I. Fujimura and I. Minami. Finite element solutions of backwater profiles in open channel networks. *Transactions JSIDRE*, 150, 19–25, 1990.

[45] Kawachi, T. and H. Itagaki. An iterative finite-element model for simulating unsteady flow in open channel networks with flow-control structures. *Proc. of 24th IAHR Congress*, D301–D310. IAHR, 1991.

[46] Kawachi, T., K. Unami, T. Hasegawa and M. Yangyuoru. Optimum control of discharge alterations in irrigation canals using the Pontryagin principle of maximum. *Transactions JSIDRE*, 172, 17–27, 1994.

[47] Kawachi, T., K. Unami and K. Kawakatsu. Reliability prediction of the storage of an irrigation tank using a Markov process model. *Proc. of 2nd Japan International Rainwater Catchment Systems Association*, 52–57, 1994. (in Japanese).

[48] Kawachi, T., M. Yangyuoru, K. Hiramatsu, K. Unami and T. Hasegawa. A finite element model of steady regulated flow in open channel networks. *Transactions JSIDRE*, 173, 59–69, 1994.

[49] Kawachi, T., M. Yangyuoru, K. Unami and Itagaki H. Modelling steady flow in open channel networks with sudden transition. *Transactions JSIDRE*, 185, 93–98, 1996.

[50] Kawakatsu, K. Analysis of reservoir reliability using Markov process model. Master's thesis, Kyoto University, 1996. pp.47–68.

[51] Komatsu, T., K. Ohguchi and K. Asai. Refined numerical scheme for advective transport in diffusion simulation. *Journal of Hydraulic Engineering, ASCE*, 123(1), 41–50, 1997.

[52] Kutija, V. A generalized method for the solution of flows in networks. *Journal of Hydraulic Research*, 33(4), 535–554, 1995.

[53] Lax, P. and B. Wendroff. System of conservation laws. *Communications on Pure and Applied Mathematics*, 13, 217–237, 1960.

[54] Lax, P. D. and N. Milgram. Parabolic equations. *Contributions to the Theory of Partial Differential Equations, Annals of Mathematical Studies*, 33, 167–190, 1954.

[55] Lee, D.J., R.E. Howitt and M.A. Mariño. A stochastic model of river water quality: Application to salinity in the Colorado river. *Water Resources Research*, 29(12), 3917–3923, 1993.

[56] Liggett, J.A. and L.-C. Chen. Inverse transient analysis in pipe networks. *Journal of Hydraulic Engineering, ASCE*, 120(8), 934–955, 1994.

[57] Lions, J. L. *Contrôl Optimal de Systèmes Gouvernés par des Équations aux Dérivées Partielles.* Dunod, Paris, 1968. pp.vii–viii, (in French).

[58] *Ibid.* pp.114–147.

[59] *Ibid.* pp.289–376.

[60] Liu, F., J. Feyen and J. Berlamont. Computation method for regulating unsteady flow in open channels. *Journal of Irrigation and Drainage Engineering, ASCE*, 118(10), 674–689, 1992.

[61] Liu, F., J. Feyen and J. Berlamont. Downstream control algoriyhm for irrigation canals. *Journal of Irrigation and Drainage Engineering, ASCE*, 120(3), 468–482, 1994.

[62] Liu, F., J. Feyen and J. Berlamont. Downstream control of multireach canal systems. *Journal of Irrigation and Drainage Engineering, ASCE*, 121(2), 179–190, 1995.

[63] Meselhe, E.A. and F.M. Holly Jr. Invalidity of Preissmann scheme for transcritical flow. *Journal of Hydraulic Engineering, ASCE*, 123(7), 652–655, 1997.

[64] Meselhe, E.A., F. Sotiropoulos and F.M. Holly Jr. Numerical simulation of transcritical flow in open channels. *Journal of Hydraulic Engineering, ASCE*, 123(9), 774–783, 1997.

[65] Mishchenko, E.F. and L.S. Pontryagin. A statistical problem of optimal control. *Doklady Akademii Nauk*, 128(15), 890–892, 1959. (in Russian).

[66] Misra, R., K. Sridharan and M.S.M. Kumar. Transients in canal network. *Journal of Irrigation and Drainage Engineering, ASCE*, 118(5), 690–706, 1992.

[67] Molina, L.S. and J.P. Miles. Control of an irrigation canal. *Journal of Hydraulic Engineering, ASCE*, 122(7), 403–410, 1996.

[68] Muñoz-Carpena, R., C.T. Miller and J.E. Parsons. A quadratic Petrov-Galerkin solution for kinematic wave overland flow. *Water Resources Research*, 29(8), 2615–2627, 1993.

[69] Naidu, B.J., S.M. Bhallamudi and S. Narasimhan. GVF computation in tree-type channel networks. *Journal of Hydraulic Engineering, ASCE*, 123(8), 700–708, 1997.

[70] Nakanishi, S., K. Unami and T. Kawachi. Automatic reservoir management using precipitation data. *Proc. of 5th Japan International Rainwater Catchment Systems Association*, 11–16, 1997.

[71] Nardini, A., C. Piccardi and R. Soncini-Sessa. On the integration of risk aversion and average-performance optimization in reservoir control. *Water Resources Research*, 28(2), 487–497, 1992.

[72] Nguyen, Q.K. and H. Kawano. Simultaneous solution for flood routing in channel networks. *Journal of Hydraulic Engineering, ASCE*, 121(10), 744–750, 1995.

[73] Nguyen, Q.K. and H. Kawano. Fast solution for implicit flood routing in channel networks of general configuration. *Transactions JSIDRE*, 193, 51–59, 1998.

[74] Pegram, G.G.S. On reservoir reliability. *Journal of Hydrology*, 47, 269–296, 1980.

[75] Petrovsky, I.G. *Lectures on Partial Differential Equations.* Interscience, New York and London, 1954. pp.62–65, (translated by A. Shenitzer).

[76] Reddy, J.M. Design of a combined observer-controller for irrigation canals. *Water resources management*, 5, 217–231, 1991.

[77] Reddy, J.M. Design of global control algorithm for irrigation canals. *Journal of Hydraulic Engineering, ASCE*, 122(9), 503–511, 1996.

[78] Reddy, J.M., A. Dia and A. Oussou. Design of control algorithm for operation of irrigation canals. *Journal of Irrigation and Drainage Engineering, ASCE*, 118(6), 852–867, 1992.

[79] Risken, H. *The Fokker-Planck Equation.* Springer-Verlag, Berlin, 1989. pp.81–86.

[80] Rodellar, J., M. Gómez and L. Bonet. Control method for on-demand operation of open-channel flow. *Journal of Irrigation and Drainage Engineering, ASCE*, 119(2), 225–241, 1993.

[81] Saaty, T.L. and J. Bram. *Nonlinear Mathematics.* Dover, New York, 1981. pp.56–70.

[82] Sampei, M., T. Mita and M. Nakamichi. An algebraic approach to H_∞ output feedback control problems. *Systems & Control Letters*, 14, 13–24, 1990.

[83] Schuurmans, J., W. Schuurmans, M. Berger, M. Meulenberg and R. Brouwer. Control of water levels in the Meuse river. *Journal of Irrigation and Drainage Engineering, ASCE*, 123(3), 180–184, 1997.

[84] Schuurmans, W., R. Brouwer and P. Wonink. Identification of control system for canal with night storage. *Journal of Irrigation and Drainage Engineering, ASCE*, 118(3), 360–369, 1992.

[85] Swain, E.D. and D.A. Chin. Model of flow in regulated open-channel networks. *Journal of Irrigation and Drainage Engineering, ASCE*, 116(4), 537–556, 1990.

[86] Szymkiewicz, R. Method to solve 1D unsteady transport and flow equations. *Journal of Hydraulic Engineering, ASCE*, 121(5), 396–403, 1995.

[87] Unami, K. and T. Kawachi. Rainwater conveyance in channel systems. *Proc. of 5th Japan International Rainwater Catchment Systems Association*, 91–92, 1997.

[88] Unami, K., T. Kawachi and K. Kawakatsu. Analysis of reservoir reliability using Markov process model. *Journal of Japanese Society of Hydrology and Water Resources*, 9(4), 315–319, 1996. (in Japanese).

[89] Unami, K., T. Kawachi, K. Kawakatsu and T. Maruyama. Analytical approach to maximization of reservoir reliabiity. *Transactions JSIDRE*, 185, 81–86, 1996.

[90] Unami, K., T. Kawachi, K. Kawakatsu and T. Maruyama. A decision support model for reservoir management using the Fokker-Plank equations. *Proc. of the International Conference on Water Resources and Environmental Research: Volume II*, 191–198. Water Resources Research Center, Kyoto University, 1996.

[91] Unami, K., T. Kawachi, H. Okumura and K. Hiramatsu. Numerical model of pseudo steady flows in estuarine open channel networks using finite volume and finite element methods. *FInite Volumes for Complex Applications*. Hermes, 1996. 563-570.

[92] Unami, K., T. Kawachi, H. Okumura and S. Nakanishi. Robust servo control of open channel network flows. *Computer Methods and Water Resources IV*. Computational Mechanics Inc., 1998. (in press).

[93] Unami, K., T. Kawachi and M. Yangyuoru. Adjoint problem of unsteady open channel flow. *Computer Methods and Water Resources III*, 41–48. Computational Mechanics Inc., 1996.

[94] Unami, K., T. Kawachi and M. Yangyuoru. Optimal control of open channel unsteady flow governed by partial differential equation. *Transactions JSIDRE*, 181, 49–56, 1996.

[95] Unami, K., T. Kawachi, M. Yangyuoru and T. Hasegawa. Reliability of steady surface profile in irrigation canal. *Journal of Irrigation and Drainage Engineering, ASCE*, 123(1), 13–18, 1997.

[96] Wylie, E.B. Control of transient free surface flow. *Journal of the Hydraulics Division, ASCE*, 95(1), 347–361, 1969.

[97] Yeh, W. W.-G. Reservoir management and operations models: A state-of-the-art review. *Water Resources Research*, 21(12), 1797–1818, 1985.

[98] Zhou, K. and P.P. Khargonekar. An algebraic Riccati equation approach to H_∞ optimization. *Systems & Control Letters*, 11, 85–91, 1988.

[99] Zoppou, C. and K.S. Li. New point estimate method for water resources modeling. *Journal of Irrigation and Drainage Engineering, ASCE*, 119(11), 1300–1307, 1993.

Appendix A

Newton-Raphson Method

The Newton-Raphson method is an iterative procedure by successively calculating points that yields improved approximations to the solution to a system of $n-$algebraic equations for $n-$variables $\boldsymbol{f}(\boldsymbol{x}) = \mathbf{0}$. The formula to obtain $k-$th approximated point $\boldsymbol{x}^{(k)}$ from $\boldsymbol{x}^{(k-1)}$ is

$$\boldsymbol{x}^{(k)} = \boldsymbol{x}^{(k-1)} - \mathcal{J}_{k-1}^{-1}\boldsymbol{f}(\boldsymbol{x}^{(k-1)})$$

where $k = 1, 2, 3, \ldots$, and $\mathcal{J}_k$ = Jacobian matrix defined by $\left.\dfrac{\partial \boldsymbol{f}}{\partial \boldsymbol{x}}\right|_{\boldsymbol{x}=\boldsymbol{x}^{(k)}}$. The necessary and sufficient condition of convergence to the solution from an initial approximation $\boldsymbol{x}^{(0)}$ is as follows (Saaty and Bram [81]).

- The matrix $\mathcal{J}_0$ has a nonvanishing determinant D
- There exist constants C_A and C_B such that

  $$\left|\boldsymbol{f}_k(\boldsymbol{x}^{(0)})\right| \leq C_A$$

  for $k = 1, 2, 3, \ldots$, and

  $$\max_i \frac{1}{\mathrm{D}} \sum_{j=1}^{n} |A_{ij}| \leq C_B$$

  where A_{ij} = the $ij-$cofactor of $\mathcal{J}_0$.
- There exists a constant C_C such that

  $$\left|\frac{\partial^2 \boldsymbol{f}_k}{\partial \boldsymbol{x}_i \partial \boldsymbol{x}_j}\right| \leq C_C$$

for $k = 1, 2, 3, \ldots$, and $i, j = 1, \ldots, n$, in the region

$$\left|x - x^{(0)}\right| \leq \frac{1 - \sqrt{1 - 2C_0}}{C_0} C_A C_B$$

where C_0 is defined by and satisfies $C_0 = n^2 C_A C_B^2 C_C \leq \frac{1}{2}$.

Appendix B

Weak Solution of Steady Solute Transport Equation

It is not self-evident that a weak solution to the solute transport equation in Chapter 2 uniquely exists in steady state. A sufficient condition to guarantee the uniqueness and the existence of the solution is given by the Lax-Milgram's theorem (Lax and Milgram [54]), in which the bilinear form is assumed to be bounded and coercive. In this Appendix, these assumptions are briefly examined.

Let C_0^∞ be the class of all infinite times continuously differentiable functions which have compact support in the domain Ω. Completing C_0^∞ in H^1, a function space is obtained and denoted by H_0^1. The function space H_0^1 is equipped with a norm $\| \ \|_{H_0^1}$ defined by

$$\|\psi\|_{H_0^1} = \left(\int_\Omega \left(\frac{\partial \psi}{\partial x} \right)^2 dx \right)^{\frac{1}{2}}$$

for $\psi \in H_0^1$ and an inner product $\int_\Omega \frac{\partial C}{\partial x} \frac{\partial \psi}{\partial x} dx$ for $C, \psi \in H_0^1$.

Supposing that $AD_x > 0$, the bilinear form β is equivalently normalized as

$$\beta'(C, \psi) = \int_\Omega \left(\frac{\partial C}{\partial x} \frac{\partial \psi}{\partial x} + \frac{Q}{AD_x} \frac{\partial C}{\partial x} \psi \right) dx$$

where β' = normalized version of the bilinear form β. The bilinear form β' is always bounded because of

$$|\beta'(C, \psi)| = \left| \int_\Omega \left(\frac{\partial C}{\partial x} \frac{\partial \psi}{\partial x} + \frac{Q}{AD_x} \frac{\partial C}{\partial x} \psi \right) dx \right| \leq \left| \int_\Omega \frac{\partial C}{\partial x} \frac{\partial \psi}{\partial x} dx \right| + \left| \int_\Omega \frac{Q}{AD_x} \frac{\partial C}{\partial x} \psi dx \right|$$

$$\leq \|C\|_{H_0^1}\|\psi\|_{H_0^1} + \left(\int_\Omega \left(\frac{Q}{AD_x}\right)^2 dx\right)^{\frac{1}{2}} \|C\|_{H_0^1} \left(\int_\Omega \psi^2 dx\right)^{\frac{1}{2}}$$

$$\leq \left(1 + \frac{1}{\hat{\lambda}}\left(\int_\Omega \left(\frac{Q}{AD_x}\right)^2 dx\right)^{\frac{1}{2}}\right) \|C\|_{H_0^1}\|\psi\|_{H_0^1} = M\|C\|_{H_0^1}\|\psi\|_{H_0^1}$$

where $\hat{\lambda}$ = a positive finite number which is equal to $\inf_{\psi\in H_0^1, \psi\neq 0} \frac{\|\psi\|_{H_0^1}}{(\int_\Omega \psi^2 dx)^{\frac{1}{2}}}$ according to the Poincaré's inequality, and the bound M is taken as $M = 1 + \frac{1}{\hat{\lambda}}\left(\int_\Omega \left(\frac{Q}{AD_x}\right)^2 dx\right)^{\frac{1}{2}}$.

A sufficient condition for the coerciveness of β' is given as follows.

1. There exists a decomposition $\frac{Q}{AD_x} = r_0 + r_1$ such that $\int_\Omega r_0 \frac{\partial \psi}{\partial x} dx = 0$ for all $\psi \in H_0^1$.
2. The decomposition $\frac{Q}{AD_x} = r_0 + r_1$ is supposed to be done so as to minimize $\left(\int_\Omega r_1^2 dx\right)^{\frac{1}{2}}$, and the bound μ defined by

$$\mu = 1 - \frac{1}{\hat{\lambda}}\left(\int_\Omega r_1^2 dx\right)^{\frac{1}{2}}$$

is positive.

Indeed, it is reduced that

$$\beta'(\psi,\psi) = \int_\Omega \left(\frac{\partial\psi}{\partial x}\frac{\partial\psi}{\partial x} + \frac{Q}{AD_x}\frac{\partial\psi}{\partial x}\psi\right) dx = \|\psi\|_{H_0^1}^2 + \int_\Omega r_0 \frac{\partial}{\partial x}\left(\frac{\psi^2}{2}\right) dx + \int_\Omega r_1 \psi \frac{\partial\psi}{\partial x} dx$$

$$= \|\psi\|_{H_0^1}^2 + \int_\Omega r_1 \psi \frac{\partial\psi}{\partial x} dx \geq \|\psi\|_{H_0^1}^2 - \left(\int_\Omega r_1^2 dx\right)^{\frac{1}{2}} \left(\int_\Omega \psi^2 dx\right)^{\frac{1}{2}} \|\psi\|_{H_0^1}$$

$$\geq \|\psi\|_{H_0^1}^2 - \frac{1}{\hat{\lambda}}\left(\int_\Omega r_1^2 dx\right)^{\frac{1}{2}} \|\psi\|_{H_0^1}^2 = \mu\|\psi\|_{H_0^1}^2$$

under this condition, which is satisfied if $\frac{Q}{AD_x}$ is nearly divergence free so that r_1 is small enough.

Appendix C

Eigenvalues and Eigenvectors of Symmetric Matrix

The eigenvalues and the eigenvectors of a $n \times n$ symmetric matrix S whose ij component is denoted by $s_{i,j}$ are obtained by the following procedure.

First, the Householder tridiagonalization is implemented. Let $S^{(0)}$ be S. Matrices $S^{(k)}$ for $k = 1, \ldots, n-2$ are transformed from $S^{(k-1)}$ as

$$S^{(k)} = Q^{(k)} S^{(k-1)} Q^{(k)}$$

using matrices $Q^{(k)}$ defined by

$$Q^{(k)} = I_n - \alpha_k \mathbf{s}_k \mathbf{s}_k^T$$

where $I_n = n-$dimensional unit matrix, and the scalar α_k and the vector $\mathbf{s}_k$ are chosen so as to eliminate all the ik components of $S^{(k)}$ for $i = k+2, \ldots, n$. Such α_k and $\mathbf{s}_k$ are given by

$$\alpha_k = \frac{1}{\sigma_k^2 + \sigma_k |s_{k+1,k}|}$$

and

$$\mathbf{s}_k = \begin{pmatrix} 0 \\ \vdots \\ 0 \\ s_{k+1,k} + \mathrm{sign}(s_{k+1,k})\sigma_k \\ s_{k+2,k} \\ \vdots \\ s_{n,k} \end{pmatrix}$$

where $\sigma_k = \sqrt{\sum_{i=k+1}^{n} s_{i,k}^2}$. The matrices $Q^{(k)}$ are diagonal because

$$Q^{(k)^T} Q^{(k)} = (I_n - \alpha_k \mathbf{s}_k \mathbf{s}_k^T)(I_n - \alpha_k \mathbf{s}_k \mathbf{s}_k^T) = I_n - 2\alpha_k \mathbf{s}_k \mathbf{s}_k^T + \alpha_k^2 \mathbf{s}_k \mathbf{s}_k^T \mathbf{s}_k \mathbf{s}_k^T$$

$$= I_n - 2\alpha_k \mathbf{s}_k \mathbf{s}_k^T + \alpha_k^2 \mathbf{s}_k \left((s_{k+1,k} + \mathrm{sign}(s_{k+1,k})\sigma_k)^2 + \sum_{i=k+2}^{n} s_{i,k}^2 \right) \mathbf{s}_k^T$$

$$= I_n - 2\alpha_k \mathbf{s}_k \mathbf{s}_k^T + \alpha_k^2 \mathbf{s}_k \left(2\mathrm{sign}(s_{k+1,k})\sigma_k s_{k+1,k} + \sigma_k^2 + \sum_{i=k+1}^{n} s_{i,k}^2 \right) \mathbf{s}_k^T$$

$$= I_n - 2\alpha_k \mathbf{s}_k \mathbf{s}_k^T + 2\alpha_k^2 \mathbf{s}_k \left(\sigma_k^2 + \sigma_k |s_{k+1,k}| \right) \mathbf{s}_k^T = I_n$$

and thus the eigenvectors of $S^{(k)}$ are unchanged by the transformation. Therefore, the resulting matrix $S^{(n-2)}$ is a tridiagonal matrix which is written as

$$S^{(n-2)} = \begin{pmatrix} \delta_1 & \beta_1 & & & 0 \\ \beta_1 & \delta_2 & \beta_2 & & \\ & \ddots & \ddots & \ddots & \\ & & \beta_{n-2} & \delta_{n-1} & \beta_{n-1} \\ 0 & & & \beta_{n-1} & \delta_n \end{pmatrix}$$

and has the same eigenvalues as S.

Next, the eigenvalues of the tridiagonal matrix $S^{(n-2)}$ are separated by the bisection method. The Sturm's theorem asserts that the number of the eigenvalues exceeding any real number λ' is equal to the number of sign variation in the Sturm sequence

$$\begin{cases} \phi_0 &= 1 \\ \phi_1 &= \lambda' - \delta_1 \\ \phi_i &= (\lambda' - \delta_i)\phi_{i-1} - \beta_{i-1}^2 \phi_{i-2} \quad (\text{for } 1 < i \leq n) \end{cases}$$

which are pricipal minors of the matrix $\lambda' I_n - S^{(n-2)}$. Indeed, there exists an orthogonal matrix U_k such that

$$\Lambda_k(\lambda') = U_k \left(\lambda' I_k - \begin{pmatrix} \delta_1 & \beta_1 & & & 0 \\ \beta_1 & \delta_2 & \beta_2 & & \\ & \ddots & \ddots & \ddots & \\ & & \beta_{k-2} & \delta_{k-1} & \beta_{k-1} \\ 0 & & & \beta_{k-1} & \delta_k \end{pmatrix} \right) U_k^{-1}$$

is a diagonal matrix for every $k = 1, \ldots n$, and thus the number of sign variation in the Sturm sequence is equal to the number of negative components of the diagonal matrix

$\Lambda_n(\lambda')$, which conserves the numbers of negative components of $\lambda' - S^{(n-2)}$ according to the well known Sylvester's law of inertia. Therefore, an interval $[l_i, r_i]$ which includes the $i-$th eigenvalue is determined by repeatedly dividing a test interval in half and then checking which half the $i-$th eigenvalue belongs to.

Finally, the $i-$th eigenvalue and the corresponding eigenvector are approximately calculated by the inverse iteration method. The $k-$th estimate $\mathbf{v}_i^{(k)}$ of the eigenvector is recursively given by

$$\mathbf{v}_i^{(k)} = \left(S^{(n-2)} - \frac{l_i + r_i}{2} I_n \right)^{-1} \frac{\mathbf{v}_i^{(k-1)}}{\left\| \mathbf{v}_i^{(k-1)} \right\|}$$

starting with an initial guess $\mathbf{v}_i^{(0)}$. This method for the matrix $S^{(n-2)} - \frac{l_i + r_i}{2} I_n$ yields a sequence which converges to the eigenvector corresponding to the eigenvalue closest to zero. Thus, the $i-$th eigenvalue and the corresponding normalized eigenvector for the matrix $S^{(n-2)}$ are approximated by $\frac{1}{\left\| \mathbf{v}_i^{(k)} \right\|} + \frac{l_i + r_i}{2}$ and $\frac{\mathbf{v}_i^{(k)}}{\left\| \mathbf{v}_i^{(k)} \right\|}$, respectively, when the difference between $\mathbf{v}_i^{(k-1)}$ and $\mathbf{v}_i^{(k)}$ is small enough.

This procedure is used for decomposing the diffusion tensor D in Chapter 4 as well as for checking the conditions imposed on the solutions of the algebraic Riccati equations in Chapter 6.

Appendix D

Existence Theorem of Controller

The controller

$$K_R = \left[\begin{array}{c|c} \hat{A} & \hat{B} \\ \hline \hat{C} & 0 \end{array}\right]$$

used in Chapter 6 for the linear system

$$\left[\begin{array}{c|cc} A_0 & B_1 & B_2 \\ \hline C_1 & 0 & 0 \\ C_2 & 0 & 0 \end{array}\right]$$

is to stabilize the closed-loop system

$$G_c = \left[\begin{array}{c|c} A_c & B_c \\ \hline C_c & 0 \end{array}\right] = \left[\begin{array}{c|c} \left[\begin{array}{cc} A_0 & B_2\hat{C} \\ \hat{B}C_2 & \hat{A} \end{array}\right] & \left[\begin{array}{c} B_1 \\ 0 \end{array}\right] \\ \hline \left[\begin{array}{cc} C_1 & 0 \end{array}\right] & 0 \end{array}\right]$$

and to satisfy $||G_c||_\infty < 1$. All matrices are of compatible dimensions. Assuming that (A_0, B_2) is stabilizable and that (C_2, A_0) is detectable, the following Theorem and Corollary by Sampei *et al.* [82] guarantee the existence of such a controller.

Theorem. *There exists a strictly proper controller K_R which stabilizes the system and satisfies $||G_c||_\infty < 1$ if and only if the following conditions are satisfied.*

1. There exists F_∞ such that there exists a positive definite solution X_∞ to the algebraic Riccati inequality

$$X_\infty A_X + A_X^T X_\infty + C_1^T C_1 + X_\infty B_1 B_1^T X_\infty < 0$$

where $A_X = A_0 + B_2 F_\infty$.

2. There exists K_∞ such that there exists a positive definite solution Y_∞ to the algebraic Riccati inequality

$$Y_\infty A_Y^T + A_Y Y_\infty + B_1 B_1^T + Y_\infty C_1^T C_1 Y_\infty < 0$$

where $A_Y = A_0 + K_\infty C_2$.

3. The maximum singular value of $(X_\infty Y_\infty)$ is less than unity.

Corollary. *Assume that the conditions of Theorem are satisfied. Then, one of such strictly proper controllers can be obtained by using X_∞, Y_∞, F_∞, and K_∞ in Theorem as*

$$\left[\begin{array}{c|c} \hat{A} & \hat{B} \\ \hline \hat{C} & 0 \end{array}\right] = \left[\begin{array}{c|c} A_X + B_1 B_1^T X_\infty - Z\left(E + F_\infty^T B_2^T X_\infty - Y_\infty^{-1} K_\infty C_2\right) & -Z Y_\infty^{-1} K_\infty \\ \hline F_\infty & 0 \end{array}\right]$$

where $Z = (Y_\infty^{-1} - X_\infty)^{-1}$, *and* $E = -\left(X_\infty A_X + A_X^T X_\infty + C_1^T C_1 + X_\infty B_1 B_1^T X_\infty\right)$.
Note that E is positive definite if the first condition of Theorem is satisfied.

Proof of the necessity

The bounded real theorem by Zhou and Khargonekar [98] states that the existence of a positive definite matrix X_c which satisfies the Riccati inequality

$$X_c A_c + A_c^T X_c + C_c^T C_c + X_c B_c B_c^T X_c < 0$$

is equivalent to the existence of such a K_R as stated in the theorem. Decomposing X_c as

$$X_c = \left[\begin{array}{cc} X_{11} & X_{12} \\ X_{12}^T & X_{22} \end{array}\right]$$

where the dimension of X_{11} is the same as that of A_0, a state coordinate transformation matrix T_X is defined by

$$T_X = \left[\begin{array}{cc} I & 0 \\ E_X & I \end{array}\right]$$

where $E_X = -X_{22}^{-1}X_{12}^T$. Pre-multiplied by T_X^T and post-multiplied by T_X, the Riccati inequality in the Theorem is reduced to an inequality whose (1,1) block matrix satisfies

$$X_1 A_X + A_X^T X_1 + C_1^T C_1 + X_1 B_1 B_1^T X_1 < 0$$

where $X_1 = X_{11} - X_{12}X_{22}^{-1}X_{12}^T$, and $A_X = A_0 + B_2\hat{C}E_X$. Since

$$T_X^T X_c T_X = \begin{bmatrix} X_1 & 0 \\ 0 & X_{22} \end{bmatrix}$$

is positive definite, X_1 is also positive definite. Thus, the first condition of the theorem is satisfied when $F_\infty = \hat{C}E_X$ and $X_\infty = X_1$. Moreover, $X_\infty = (1-\varepsilon)X_1$ also satisfies the Riccati inequality in the Theorem for sufficiently small ε because its left hand side becomes continuous with respect to ε.

Another state coordinate transformation matrix T_Y is defined by

$$T_Y = \begin{bmatrix} I & -E_Y \\ 0 & I \end{bmatrix}$$

where $E_Y = X_{11}^{-1}X_{12}$. Pre-multiplied by T_Y^T and post-multiplied by T_Y, the Riccati inequality in the Theorem is reduced to an inequality whose (1,1) block matrix satisfies

$$X_{11} A_Y + A_Y^T X_{11} + C_1^T C_1 + X_{11} B_1 B_1^T X_{11} < 0$$

where $A_Y = A_0 + E_Y\hat{B}C_2$. Since $X_{11} > 0$ and thus $X_{11}^{-1} > 0$,

$$X_{11}^{-1} A_Y^T + A_Y X_{11}^{-1} + B_1 B_1^T + X_{11}^{-1} C_1^T C_1 X_{11}^{-1} < 0$$

holds. Thus, the second condition of the theorem is satisfied when $K_\infty = E_Y\hat{B}$ and $Y_\infty = X_{11}^{-1}$.

From the above X_1, X_∞, and Y_∞,

$$Y_\infty^{-1} - X_\infty > Y_\infty^{-1} - X_1 = X_{11} - \left(X_{11} - X_{12}X_{22}^{-1}X_{12}^T\right) = X_{12}X_{22}^{-1}X_{12}^T \geq 0$$

is obtained, and the third condition of the theorem is satisfied.

Proof of the sufficiency

It is enough to show that the matrix S defined by

$$S = X_c A_c + A_c^T X_c + C_c^T C_c + X_c B_c B_c^T X_c$$

is negative definite for the controller in Corollary with a suitable X_c. Considering the definitions of X_∞ and Y_∞ in the proof of the necessity, X_c is defined as

$$X_c = \begin{bmatrix} Y_\infty^{-1} & -(Y_\infty^{-1} - X_\infty) \\ -(Y_\infty^{-1} - X_\infty) & Y_\infty^{-1} - X_\infty \end{bmatrix}$$

and the coordinate transformation matrix

$$T_X = \begin{bmatrix} I & 0 \\ I & I \end{bmatrix}$$

is introduced. Transforming X_c as

$$T_X^T X_c T_X = \begin{bmatrix} X_\infty & 0 \\ 0 & Y_\infty^{-1} - X_\infty \end{bmatrix}$$

shows that X_c is positive definite because of the first and the third conditions of Theorem.

Obviously, S is negative definite if and only if $S_T = T_X^T S T_X$ is negative definite. Using

$$T_X^{-1} A_c T_X = \begin{bmatrix} A_0 + B_2\hat{C} & B_2\hat{C} \\ \hat{A} + \hat{B}C_2 - A_0 - B_2\hat{C} & \hat{A} - B_2\hat{C} \end{bmatrix}$$

and

$$T_X^{-1} B_c = \begin{bmatrix} B_2 \\ -B_2 \end{bmatrix}$$

this S_T is expanded as

$$S_T = \begin{bmatrix} X_\infty A_X & X_\infty B_2 F_\infty \\ Z_{-1} B_1 B_1^T X_\infty - F_\infty^T B_2^T X_\infty - E & Z^{-1}\hat{A} - Z^{-1} B_2 F_\infty \end{bmatrix}$$

$$+ \begin{bmatrix} A_X^T X_\infty & X_\infty B_1^T B_1 Z_{-1} - X_\infty B_2 F_\infty - E \\ F_\infty^T B_2^T X_\infty & \hat{A}^T Z^{-1} - F_\infty^T B_2^T Z^{-1} \end{bmatrix} + \begin{bmatrix} C_1^T C_1 & 0 \\ 0 & 0 \end{bmatrix}$$

$$+ \begin{bmatrix} X_\infty B_1 B_1^T X_\infty & -X_\infty B_1 B_1^T Z^{-1} \\ -Z^{-1} B_1 B_1^T X_\infty & Z^{-1} B_1 B_1^T Z^{-1} \end{bmatrix} = \begin{bmatrix} -E & -E \\ -E & S_{22} \end{bmatrix}$$

where

$$S_{22} = Z^{-1}\left(A_0 + B_1 B_1^T X_\infty\right) + \left(A_0^T + X_\infty B_1^T B_1\right) Z^{-1} + Z^{-1} B_1 B_1^T Z^{-1} - 2E$$
$$- \left(X_\infty B_1 F_\infty + F_\infty^T B_1^T X_\infty - Y_\infty^{-1} K_\infty C_2 - C_2^T K_\infty^T Y_\infty^{-1}\right)$$
$$= -2E - Y_\infty^{-1}\left(Y_\infty A_Y^T + A_Y Y_\infty + B_1 B_1^T + Y_\infty C_1^T C_1 Y_\infty\right) Y_\infty^{-1}$$
$$- \left(X_\infty A_X + A_X^T X_\infty + C_1^T C_1 + X_\infty B_1 B_1^T X_\infty\right)$$
$$= -E - Y_\infty^{-1}\left(Y_\infty A_Y^T + A_Y Y_\infty + B_1 B_1^T + Y_\infty C_1^T C_1 Y_\infty\right) Y_\infty^{-1}$$

for A_X and A_Y in Theorem. Transforming the coordinate as

$$\begin{bmatrix} I & 0 \\ -I & I \end{bmatrix} S_T \begin{bmatrix} I & -I \\ 0 & I \end{bmatrix} = \begin{bmatrix} -E & 0 \\ 0 & Y_\infty^{-1}\left(Y_\infty A_Y^T + A_Y Y_\infty + B_1 B_1^T + Y_\infty C_1^T C_1 Y_\infty\right) Y_\infty^{-1} \end{bmatrix}$$

S_T is found to be negative definite because of the second condition of Theorem. Thus, $S < 0$.